Control of sex myoblast migration in *C. elegans*

Sihui Zhang

Dissertation submitted to the faculty of the Virginia Polytechnic Institute and State University in partial fulfillment of the requirements for the degree of

Doctor of Philosophy

In

Biological Sciences

Jeffrey R. Kuhn

Diya Banerjee

Daniela Cimini

William R. Huckle

June 20, 2013

Blacksburg, VA

Keywords: cell migration; actin; Rho GTPase; *C. elegans*; sex myoblast

Copyright 2013 Sihui Zhang

Control of sex myoblast migration in *C. elegans*

Sihui Zhang

Abstract

Cell migration is critical in generating complex animal forms during development; misregulation of migration contributes to pathological conditions such as cancer metastasis. Thanks to its easily traceable cell lineages in a transparent body and a compact genome accessible to a wealth of genetic manipulations, the use of the nematode *C. elegans* as a model system has greatly advanced our understanding of mechanisms governing cell migration conserved through higher organisms. Among several migration processes in *C. elegans*, sex myoblast (SM) migration is an attractive system that has a simple and well-defined migratory route along the ventral side from the posterior to the precise center of the gonad. A multitude of guidance mechanisms control SM migration, many of which are likely to be conserved in other migratory processes.

Similar to vertebrate systems, *C. elegans* uses Rho family small GTPases to regulate the engine of cell motility, the actin cytoskeleton, in response to guidance cues. The differential utilizations of Rho GTPases in distinct processes *in vivo* remain a central question in the study of Rho GTPases. I investigated how Rho GTPases regulate different aspects of SM migration, and found that Cdc-42/CDC42 functions in the anteroposterior migration, whereas MIG-2/RhoG and CED-10/Rac1 control ventral restriction independently of FGF and SLIT/Robo signaling. The

relative difficulty in perturbing SM migration using constitutively active Rho GTPases compared to other migration processes illustrates the robustness of the mechanisms that control SM migration.

On a technical aspect, I established a nematode larval cell culture system that allows access to postembryonic cells. Compared to the flourishing genetic researches in *C. elegans*, there are few studies of molecules that also extend to the subcellular level in postembryonic development, mainly due to the lack of a larval cell culture system. I developed a novel method combining SDS-DTT presensitization of larval cuticles and subsequent pronase E digestion. My method efficiently isolates both low- and high-abundance cell types from all larval stages. This technical advance will not only facilitate studies such as regulation of actin dynamics with high-resolution microscopy, but is beginning to be used by researchers to tackle cell-type specific questions through profiling methods as gene expression analysis.

Dedication

Dedicated to my family, for the joy and unconditional love

Acknowledgements

I would like to express my deep appreciation to my advisor, Dr. Jeffery Kuhn, for introducing me to the world of scientific research, for inspiring me to think outside the box, and for always being patient and supportive. Without his guidance and encouragement, this dissertation would not have been possible.

I am grateful to my committee members Drs. Diya Banerjee, Daniela Cimini and William Huckle for devoting their precious time to helping me improve my work. Their expertise in diverse fields has been invaluable to my graduate career. My special thanks to Dr. Diya Banerjee, for teaching me the biology of *C. elegans*.

I am indebted to my dear friends and colleagues in the lab for their valuable discussion with me. Without them it would not have been so much fun. I will always remember the good time with you – Nimisha Khanduja, Ying Li, Xiaohua Hu, Brent Bowden, Romy Romy Fajardo, Alexandra Douglass, and Emily Thornton.

I would also like to thank the faculty and staff in the Department of Biological Sciences for providing me the resources during my study, and the Institute for Critical Technology and Applied Sciences for providing me with 4-year financial support.

TABLE OF CONTENTS

LIST OF FIGURES

LIST OF TABLES

Chapter 1 Literature Review

OVERVIEW

The formation of complex multicellular organisms depends critically on the ability of cells to move. Long-range cell migration has to occur at the right time, in the proper place, in the correct direction, and at reasonable speeds. Motile cells must stop at their correct destination before assuming their developmental fates. Examples of such migration include the dissemination of neural crest cells to various parts of an embryo to give rise to a diverse array of cell lineages, and the migration of primordial germ cell to populate the developing gonad. Like other developmental programs, the migration of cells is largely determined genetically. When cancer cells hijack migratory schemes, they metastasize to other parts of the body and initiate new, malignant tumors.

The fascinating process of cell migration and its potential therapeutic relevance have attracted increasing interest since the initial observation of the dynamic structure called lamellipodium in cultured motile cells [2]. We now know that regulated actin polymerization and depolymerization in lamellipodium and other actin-based cellular structures drives cell motility, and some 60 classes of actin binding proteins (ABPs) have been discovered [3] to remodel these structures. In order to guide the motility machinery towards its target, a large set of extracellular matrix (ECM) proteins, cell adhesion molecules (CAM), anchored and diffusible morphogens and growth factors are utilized [4]. These extracellular signals bind to specific cell surface receptors and then trigger coordinated and localized activation or inactivation of appropriate

ABPs through numerous signal transduction mediators. To illustrate the potential complexity of this process, vertebrates encode 18 members of Rho family small GTPases [5], a major class of proteins that regulate actin cytoskeleton, with 85 activating Guanine-nucleotide exchange factors (GEFs), 70 inhibitory GTPase activating proteins (GAPs) [6], and ~100 downstream effectors [5]. Further increasing the complexity is the fact that some of the signals induce changes in gene expression to alter a cell's ability to respond to migratory cues. The list of molecules that are involved in cell migration is likely to grow longer. Clearly, to understand cell migration we need tools that allow us to probe into different aspects of the phenomenon and develop an integrated view from data generated from biochemical, cellular and genetic studies. In this review, I focus on the genetic studies in the simple model organism *C. elegans*, using sex myoblast as an example, summarize our current understanding of its cell migration and raise questions that need to be answered.

CELL MOTILITY AND GUIDANCE

The motility machinery

Cell migration can be conceptually viewed as a four-step cyclic process that involves spatial and temporal coordination of actin-based structures from the front to the back of a cell [7]. (Step 1) A cell first extends a broad, sheet-like structure called lamellipodium in the direction of movement [8]. This lamellar actin network is assembled at the forward cell membrane and is forced backwards toward the cell body in a dynamic process of retrograde flow. In certain types of cells and axon growth cones, finger-like structures called filopodia emanate from the periphery of the lamellipodium and dynamically protrude and retract to probe the environment

[4]. (Step 2) Focal adhesions form under the lamellipodium to stabilize the protrusion by attaching the cell to the substratum [9]. (Step 3) Myosin in the cell body contracts the actin network and pulls the rear of the cell forward. Focal adhesions then disassemble to detach the cell from the substratum, allowing the next cycle of protrusion – attachment – contraction – detachment to advance the cell [10].

The actin cytoskeleton forms the basis for all of the structures involved in the migration process. Actin monomers polymerize to form actin filaments, which are intrinsically polarized with a fast-growing barbed end and a slow-growing pointed end [3]. At equilibrium, actin monomers disassemble from the pointed end to continuously feed new assembly at the barbed end. Simultaneous assembly and disassembly of actin filaments is known as "treadmilling" and results in the net growth at filament barbed ends [11]. In the lamellipodium, actin filaments form a branched network, with barbed ends pointing toward the cell membrane [3]. Actin monomers are added between the barbed end and the membrane to provide the force that deforms the membrane in the direction of movement. At rest, forces generated by actin polymerization are balanced by membrane tension and actomyosin contraction at the back, leading to the net movement of the actin network centripedally towards the nucleus. This movement appears as retrograde flow when a cell is not attached to a substrate. However, when this retrograde-flowing actin network is coupled to the extracellular matrix through focal adhesions, the added stiffness of the actin network supports a protrusive force at the leading edge, and the cell membrane is pushed forward. Surprisingly, focal adhesions do not migrate at the same speed as the retrograde-flowing actin network. Instead, a cascade of integrin and actin binding proteins provides a "clutch" mechanism that loosely couples the fixed substratum anchors to the flowing actin

cytoskeleton. Through this step-down mechanism, the cell can "leverage" or couple the distributed power provided by the fast-flowing actin cytoskeleton into slower membrane protrusions that can provide remarkable force to push through interstitial spaces and tissue boundaries [10].

Persistent cell migration towards one direction is the result of localized actin polymerization in the lamellipodium. Spontaneous, or *de novo*, actin polymerization from monomers is very inefficient and is prevented from occurring by monomer sequestering proteins such as profilin and thymosin β4 in the cytoplasm [3]. In the lamellipodium, fast and controlled actin polymerization is primarily mediated by actin nucleators such as formin family proteins and the Arp2/3 complex. Arp2/3 binds to an existing actin mother filament at 70° angle and mimics a pointed-end actin nucleus to induce the formation of a new actin daughter filament [12] such that both mother and daughter filaments have their barbed ends oriented towards the cell membrane. This repetitive mother-daughter branched or "dendritic" filament pattern forms the actin network in the lamellipodium [13] and the filament crosslinking provided by branches gives the network tensile strength. In the absence of factors that balance nucleation, actin polymerization generates long filaments that are inefficient force generators. Rapid filament lengthening also depletes the actin monomer pool quickly. Thus, soon after actin filaments are formed, capping proteins bind to their barbed ends and prevent further elongation. As a result, branched actin network in the lamellipodium is composed of short filaments capped at their barbed ends with elongation occurring mainly at newly form filament ends. The combination of branching and capping leads to a network of short, crosslinked filaments with more tensile strength than a network of long, unbranched filaments. Further away from the leading edge, ADF/Cofilin severs actin filaments

and promotes their disassembly from the pointed ends to replenish the pool of actin monomers [13]. Actin monomers are then recharged with ATP by profilin to be ready for the next round of polymerization.

In contrast to branched network in lamellipodia, filopodia feature long actin filaments. Formin nucleates linear actin filaments and processively assembles actin monomers at the barbed end. Enabled (Ena)/VASP binds to filament barbed ends and prevents them from being capped. These actin filaments are bundled by fascin [14]. Thus, lamellipodia and filopodia utilize different suites of proteins to induce the formation of distinct actin-based load-bearing structures.

Guidance cues

Directionality of cell migration is conveyed by a myriad of extracellular chemoattractants. These cues can induce attractive or repulsive reaction, and can work within short- or long-ranges [4]. Canonical guidance cues include Netrin, Slit, Ephrin, and Semaphorin [15]. These canonical guidance cues have conserved functions from worms to mice and are best characterized by their roles in axonal guidance. Besides the canonical guidance cues, other molecules such as morphogens (Wnt, Sonic Hedgehog, TGF-β, etc.), growth factors (fibroblast growth factor/FGF, neuregulin, stem cell factor, etc.) and cell adhesion molecules (Ig CAM) can also function as guidance cues [15]. Guidance cues bind to cell surface receptors and induce changes in gene expression or cytoskeleton reorganization. Ligand-bound receptors initiate downstream signaling pathways such as kinase cascades and Rho family GTPase activation.

Rho family GTPases

Rho family GTPases form a branch of Ras superfamily small GTPases. Like Ras GTPase, Rho family GTPases cycle between a GTP-bound active form and a GDP-bound inactive form [6] (Figure 1.1). The two activity states allow Rho family GTPases to work as molecular switches to turn on and off downstream targets. The switch is on all the time when mutations render GTPases unable to hydrolyze GTP, and this type of mutation is termed constitutively active (CA) mutation [16].

The most prominent effectors of Rho family GTPases are directly linked to the actin cytoskeleton [5]. Early biochemical studies found that introducing CA versions of three subfamilies of Rho GTPases (Cdc42, Rac1 and RhoA) into fibroblasts induces the formation of filopodia, lamellipodia, or stress fibers, respectively [17-19]. This established the major roles of Rho family GTPases in regulating actin cytoskeleton. In mammalian systems, Rac1 and Cdc42 can activate Arp2/3 activators WAVE and WASP, respectively [20], inducing the formation of branched lamellipodial network. These GTPases can also activate the formin, mDia2, to promote the formation of unbranched actin filaments. In contrast, RhoA mainly functions in actomyosin contraction. RhoA can both induce unbranched actin filament formation by activating formin and can promote actin network contraction by activating myosin II through the myosin activator, Rho Kinase (ROCK) [21].

The distinct and sometimes overlapping roles of members of Rho family GTPases are carefully regulated by localized activation through guanine nucleotide exchange factors (GEFs). GEFs induce the exchange of GDP for GTP on GTPases, thus increasing the ratio of GTP-bound

to GDP-bound GTPases [22]. A class of proteins called GAPs for GTPase activating proteins has the opposite effect, and promotes GTP hydrolysis to inactivate GTPases. There are two- to three-fold more GEFs than Rho family GTPases [6], and their tissue specific expression and activation patterns underlie the complexity of the regulation of Rho family GTPase [16].

CELL MIGRATION IN *C. ELEGANS*

Our understanding of the functions of ABPs and Rho GTPases in cell migration has primarily come from vertebrate cell culture systems. An ultimate goal of studying these proteins is to understand how they regulate directed cell movement *in vivo*. Originally developed to facilitate the study of the development of the nervous system, *C. elegans* has proved to be an excellent model organism to study axonal guidance as well as cell migration. *C. elegans* is a small transparent nematode, which makes tracking cells in live animals relatively easy. It has a fully-mapped cell lineage with invariant cell migratory path among individuals, which facilitates phenotypic analysis of mutant animals. *C. elegans* also have a remarkably compact and fully sequenced genome that can be targeted with RNA interference and genetic mutations. Mutants can easily be made homozygous or crossed in the presence of both hermaphrodites and males – methods that are crucial for convenient genetic dissection of signaling pathways. These advantages have already been used to elucidate some of the mechanisms underlying various cell migrations.

Several cells undergo long-range migration during *C. elegans* embryogenesis and larval development [23, 24]. According to the direction of movement, these cells can be categorized as anteriorly directed or posteriorly directed. Posteriorly directed cells include the QL neuroblast

and its descendants (QL.a and QL.ap/PQR), ALM neurons, CAN neurons, coelomocytes, M cell, muIntR cell, and somatic gonadal cells (Z1 and Z4). Cells moving anteriorly are the QR neuroblast and its descendants (QR.a, QR.ap/AQR, QR.p and QR.pa), HSN neurons, and sex myoblasts (SMs) [23, 24]. An exception to this classification is the migration of the two distal tip cells (DTCs), which start out moving to the opposite directions from the center of the worm, then change direction and move dorsally and finally turn again towards the center [25]. Additionally, P cells and vulval cells adjust their position with short-range motility and can be affected by gene mutations that also disrupt long-range cell migration. Finally, the guidance of neuronal axons can occur anterior-posteriorly or dorsoventrally, and their guidance shares many similar mechanisms with those in directed cell migration [26].

Several features of *C. elegans* benefit the study of these migration processes *in vivo*. Forward and reverse genetic screens have identified hundreds of genes that directly affect migration, and mutation analyses are ordering these genes into pathways. Our knowledge of the invariant cell lineages and migratory paths [27, 28], combined with the worm's transparent body, allows direct cell tracking and detailed phenotyping. Recent development of *in vivo* live imaging techniques makes kinetic characterization of cell migration at the cellular level a reality [29]. These experiments have provided us with great insight into the mechanisms controlling cell migration.

Q lineage neuroblast and DTC migration

Cells migrate for different distances, at different speeds, and toward different directions in these migration systems. Genetic analyses of several cell migration processes in *C. elegans*

revealed similarities as well as distinctively specified aspects of their underlying mechanisms [30]. A well-studied example is the migration of the Q neuroblast cells, QL and QR, and their descendants (Figure 1.2). QL and QR are born on the left and right sides of the worm. Despite the apparent bilateral symmetry in their initial positions, QL migrates towards the posterior, whereas QR towards the anterior. During their migrations, QL and QR each divide and produce Q descendant cells (QL.d and QR.d) that continue migrating in the same direction as their ancestors [28].

The Wnt family of signaling proteins helps to determine left-right asymmetric responses of the QL branch and the QR branch in the otherwise symmetric environment, though Wnt-independent pathways are also involved [31]. Five Wnt ligands (EGL-20, LIN-44, MOM-2, CWN-1, and CWN-2) are predominantly expressed in the posterior region of the worm [32], and EGL-20 Wnt activates MAB-5 Hox transcription factor in the QL to specify the posterior migration of QL.d. EGL-20 and other Wnt proteins direct the anterior migration of QR.d through another, non-canonical Wnt pathway [33]. The establishment of the different sensitivities of QL and QR to the dosage of Wnt remained a mystery until Wnt-independent pathways were discovered that induce the initial asymmetric polarization of QL and QR. UNC-40/DCC netrin receptor [34] and two novel transmembrane proteins DPY-19 [35] and MIG-21 [34] properly polarize QL and QR to potentiate this sensitivity. Despite the involvement of the netrin receptor, the canonical netrin ligand is not involved in this process, suggesting that other ligands can signal through the UNC-40 netrin receptor. Downstream of these morphogens and cell surface proteins, UNC-73/GEF, CED-10/Rac1, and MIG-2/RhoG act in parallel with PIX-1/GEF and CED-10/Rac1 to directly enable the polarization response [36]. Interestingly, the level of MIG-

2/RhoG correlates with the migration speed and extent of Q descendants, whereas that of INA-1/integrin α subunit that presumably mediates cell-cell and cell-ECM interaction has an opposite relationship [37]. Moreover, the actin binding protein UNC-34/Enabled acts in a parallel pathway to the Rac pathways to control the migration of Q descendants [38].

Another interesting yet distinct system is the migration of the two distal tip cells (DTCs). The gonad in the adult worm has two U-shaped arms facing anterior and posterior of the gonad center. This morphology is formed from a simple straight primordial gonad tube through a three-phase guided migration of the leading DTC at either end of the gonadal arm (Figure 1.3). During the first phase, the two DTCs migrate in opposite directions along the ventral basement membrane away from the center. This phase requires the extracellular matrix metalloprotease GON-1/ADAMT to clear the passage for DTCs, and MIG-6/ADAMTSL may function cooperatively with GON-1/ADAMT [39]. An integrin heterodimer composed of INA-1/α subunit and PAT-3/β subunit is required in the DTCs for the motility [40]. In the second phase after migration away from the center, the DTCs turn 90° towards the dorsal side. This turning is mediated by repulsion from UNC-6/Netrin on the ventral side. Interestingly, UNC-129/TGF- β does not instruct DTCs directly, but rather has been proposed to sensitize DTCs to Netrin signaling [39]. Integrins are also involved in this process, but a second type (PAT-2/α subunit and PAT-3/ β subunit) is required for the turning as DTCs transition from the ventral muscle basement membrane to the hypodermis basement membrane [40]. Once DTCs reach the dorsal side, in the third phase of migration, they turn 90° again and move centripetally. DTCs in mutants of another metalloprotease MIG-17/ADAM cannot move further after the initial two phases of migration, and this may be due to the lack of access to guidance molecules [40].

Several intracellular signaling modules have been discovered mediating these guidance and adhesion signals. Both Rac-dependent and –independent PAK (P21 activated kinase) pathways act downstream of integrin signaling [41], and a novel signaling protein CACN-1/Cactin inhibits MIG-2/RhoG and acts in parallel with CED-10/Rac1 to control DTCs migration [42]. Since PAK and Rho GTPases are regulators of the actin cytoskeleton, these data could lead to future identification of actin binding proteins that act downstream of these mediators to directly modulate the actin cytoskeleton.

The success in identifying pathways that regulate Q lineage migration and DTC migration partly benefit from the fact that these two migration processes are susceptible to relatively simple genetic manipulations. For example, single gene knockdown through genome-wide RNAi identified 99 genes that strongly affect DTC migration [43]. In contrast, the migration of sex myoblast is controlled by a multitude of partially redundant pathways, and single gene mutations most often do not produce any migration defects. This complexity is itself an interesting phenomenon and warrants more careful analyses, and I devote the next part to describing the intriguing control mechanisms of sex myoblast migration.

Mechanisms of sex myoblast migration

Sex myoblast guidance has gonad-dependent and –independent components

The sex myoblast (SM) in *C. elegans* is the precursor of the vulval and uterine muscles. These 16 muscles contact the uterine cells located at the gonad in the mid-body of the worm to expel eggs during egg-laying. Interestingly, the sex muscle precursor SMs are not born at the gonad center. Instead, during L2 stage, the pair of SMs on either side of the worm migrate

anteriorly on the ventral muscle quadrants from the posterior to precisely flank the center of the gonad. Once at the gonad center, they stop and divide to give rise to the sex muscles (Figure 3.1) [44]. Defects in the formation of the neuronal circuits that control the muscles, in the muscle themselves, or in the migration of SMs can all lead to egg-laying defects (egl phenotype) [45]. Random mutagenesis screens identified dozens of genetic mutations that produce egl phenotype, but only two of these, namely *egl-15* and *egl-17*(see below) directly affect SM migration [46, 47]. Two decades of studies on SM migration revealed that these two genes are only part of the multiple mechanisms that control SM migration.

Since the gonad is the target of SM migration, it presumably attracts SM anteriorly. Indeed, an ectopic gonad in *dig-1* mutant that locates on the dorsal side of the worm is sufficient to attract SMs dorsally from their normal ventral localization. This apparent gonad-SM attraction is abolished when the gonad is laser-ablated, and as a result, SMs remain on the ventral side [44]. This migration toward the gonad center was designated as the gonad-dependent mechanism (GDM). However, in wild-type (WT) worms that are gonad-ablated, SMs can still migrate, albeit less precisely, to the approximate center region of the worm [44]. This coarse guidance does not directly require the presence of the gonad, and is thus termed the gonad-independent mechanism (GIM). GIM is proposed to lead SMs to their approximate final region and GDM then refines their migration to ensure that SMs stop precisely at the gonad center.

GDM is composed of two opposing instructions, an attractive cue and a repulsive cue. Mutations in egl-17 and egl-15, genes encoding the worm counterparts of fibroblast growth factor (FGF) and its receptor (FGFR), result in severely posteriorly displaced SMs [47]. EGL-

17/FGF is expressed in a subset of the somatic gonad cells and vulva precursor cells (VPCs) that are induced by the gonad [48], thus it is conceivable that FGF mediates gonad-dependent attraction (GDA) to attract SMs to the gonad center. However, the same subset of cells secreting FGF also express a hypothetical molecule that counteracts the attractive effect of FGF, since ablating gonad in *egl-17* or *egl-15* mutants relieves the posterior displacement of SMs [47]. Thus normally a GDR counter-balances the GDA to manifest the precise-targeting function of GDM.

GDM and GIM intimately collaborate during SM migration. Time-course analysis revealed that during SM migration, GIM acts early on to attract SMs from their birth position at the posterior end. As the attractive effect of GIM diminishes while SMs approach the gonad, GDM takes on the relay and finely positions SM to the gonad center [48]. In the absence of GIM, although SMs can still migrate anteriorly, they move at a slower speed. Only when both GIM and GDM are abolished, will SM be completely prevented from migrating [49]. Thus GIM and GDM act together to ensure the efficiency as well as precision of SM guidance.

Molecular composition of GDM and GIM

Elegant genetic screens identified a partial part list of the molecular components of GDA, GDR, and GIM (Table 1-2). This list encompasses conserved guidance molecules, intracellular signaling modules, cytoskeleton regulators, as well as proteins involved in other processes such as gene expression.

EGL-17/FGF, a fibroblast growth factor expressed at the gonad center [50] and EGL-15/FGFR, an FGF receptor expressed by SMs are the major mediators of gonad-SM interaction in GDA. EGL-15/FGFR is a receptor tyrosine kinase, and its chemoattractant effect on SM

migration is mediated by SEM-5/Grb-2, a SH2 domain and SH3 domain-containing adaptor protein [51]. This effect is partly mediated by a Ras-Raf-MEK-MAPK pathway, as mutations in any of the components of this pathway reduce GDA [52]. However, this Ras pathway is unlikely the sole mediator of the FGF signaling, as activated LET-60/Ras can only partially rescue SM defects in EGL-15 mutants [52]. On the other hand, the Ras pathway may also participate in SM guidance mechanism other than GDA, as mutants of this pathway do not exactly phenocopy *egl-15* or *egl-17* phenotypes [53].

Candidate gene screen of genes known for their role in axon guidance identified several molecules that are also important for mediating GDR. Netrin and Semaphorin, but not Slit/ROBO, are implicated in GDR [48]. In *C. elegans* and vertebrate systems, UNC-6/Netrin can mediate repulsion as well as attraction, depending on the receptor that is present, with UNC-40/DCC mediating attraction and UNC-5 mediating repulsion. Netrin is found on the ventral side of the worm and normally mediates circumferential axon guidance and dorsoventral migration [54]. *Unc-6* only weakly compromises GDR and mutations in either receptor have no GDR defects. However, mutations in *unc-51* and *unc-14* that normally localize UNC-5/Netrin receptor in neurons strongly compromise GDR [48]. Thus, whether Netrin is involved in GDR remains to be further tested. Mutations in MAB-20/Semaphorin, another guidance cue that is involved in axon guidance, and its intracellular signaling mediator UNC-33/CRMP-2, also lead to defective GDR [48]. In addition to the possible involvement of these guidance cues, cytoskeleton structural and regulatory proteins such as anti-capping factor UNC-34/Enabled and linker protein UNC-44/Ankyrin that connects cell membrane to the actin cytoskeleton were also identified in GDR [48].

Genetic screen in worms with compromised GDM revealed the roles of UNC-53/Neuron Navigator (NAV), UNC-73/Rac GEF, and the metalloprotease UNC-71/ADAM in GIM [49]. Although other matrix metalloproteases "clear the way" in front of invading cells, the metalloprotease domain of UNC-71/ADAM is inactive. Consequently UNC-71/ADAM has been proposed to interact with a receptor or alter the distribution of a ligand, consistent with its functions with integrin and Netrin in motor axon guidance [55]. While UNC-71/ADAM functions non-cell-autonomously, both UNC-73/Rac GEF and UNC-53/NAV are mediators of signals to the actin cytoskeleton. UNC-53/NAV physically interacts with SEM-5/Grb2 and ABI-1 [56], the latter is a subunit of the pentameric WAVE complex that activates Arp2/3 complex, the branched actin network nucleator. Since UNC-71/ADAM, UNC-73/Rac GEF, and UNC-53/NAV seem to act in a single pathway [55], it would be interesting to see whether this module mediates a still unidentified instructive cue in guiding SMs in parallel to the FGF pathway.

In addition to anteroposterior axis migration defects, a few dorsoventral localization defects have been observed with SMs. SMs are normally maintained on the ventral side. The strongest dorsal misplacement was observed in double mutant of *egl-17* and *sax-3* [48]. SAX-3/Robo is the receptor for the guidance molecule SLT-1/SLIT that normally mediates repulsion, and the dorsal expression of SLT-1/SLIT in *C. elegans* [57] is consistent with its potential role in restricting SMs to the ventral side. Thus, in addition to guiding SMs anteriorly, EGL-17/FGF cooperates with SAX-3 to maintain SMs on the ventral muscle quadrants. A candidate intracellular mediator of ventral localization signal to the actin cytoskeleton is UNC-34/Enabled, which confers intermediate level of dorsal localization when combined with *egl-17* [48]. Additionally, in single mutants of the Ras-Raf-MEK-MAPK pathway, a small percentage of SMs

localizes to the dorsal side [52]. Dorsal localization was also observed when a gain-of-function allele of *let-60/Ras* was combined with *egl-15*. Since *egl-15* alone does not confer dorsally localized SM, the Ras pathway may have roles in dorsoventral guidance independent of EGL-15/FGFR [52]. Interestingly, in the most severely affected worms among these mutants, only half of SMs are on the dorsal side. Thus, it is plausible that other guidance cues exist to provide additional ventral restriction.

The diversity of the molecules that control postembryonic SM migration indicates that multiple pathways act in parallel to converge on the precise targeting of SMs. Many of the molecules that have been identified appear to represent isolated points along canonical signaling pathways rather than complete signaling modules in a potentially complex signaling network. Because actin-based motility is required for proper embryonic development, mutants in actin pathway genes often prove embryonically lethal. Unidentified genes with embryonic lethality would thus likely have been missed in postembryonic screens for SM migration defects. For example, some alleles of let-60/Ras are lethal, which prevented the use of these alleles to study SM migration [52]. On the other hand, there are likely important but less essential pathways involved in SM guidance – the identification of which would only be possible when the majority of other redundant mechanisms are compromised. This could be further complicated when the mutations used are not null alleles, and the residual activity of the gene product would suffice for near-WT phenotype. Sometimes a particular mutation may only disrupt processes other than the one of interest, as in the case of several alleles of *egl-15* that result in scrawny worms or lethality but confer no SM migration defects, although other alleles of *egl-15* do affect SM migration [53]. Finally, when considering the convergence of upstream guidance signals to the cytoskeleton, a

multitude of effectors may be involved, and redundant pathways in turn likely mediate their activities. This is the case for Rho family GTPases in other organisms, and a complex relationship among *C. elegans* Rho GTPase family members has also started to emerge.

Coupling guidance to the actin cytoskeleton – the role of Rho family GTPases

Spatial information from guidance cues eventually converge on the actin cytoskeleton to change cell shape in order to move in a certain direction. As introduced earlier, Rho family GTPases, whose activities can be modulated by signals through membrane receptors, are potent master regulators of the actin cytoskeleton. Among the seven *C. elegans* Rho family GTPases [58], genes of the Rac subfamily have been primarily implicated in cell migration. While RAC-2/Rac1 is possibly a nonfunctional pseudogene, CED-10/Rac1 and MIG-2/RhoG (a functional homologue of RhoG in the mammalian Rac subfamily) often have redundant roles in mediating cell migration and axon guidance [58]. For example, both Racs are required for DTC migration, vulva cell migration, amphid axon outgrowth, migration and/or axon guidance of CAN, DD, VD neurons [36, 59-62].

Racs regulate cell migration and axon guidance by controlling the formation of lamellipodia and filopodia (Figure 1.4). Downstream of UNC-40/DCC/Netrin receptor, and in parallel to UNC-34/Enabled pathway, CED-10/Rac1 and MIG-2/RhoG function to activate distinct actin regulatory proteins [63]. CED-10/Rac1 activates actin filament binding protein UNC-115/abLIM [64], and at the same time activates WVE-1/WAVE [65]. WVE-1/WAVE in turn promotes Arp2/3 activity. Similarly, MIG-2/RhoG mediates Arp2/3 activation through WSP-1/WASP [65].

CED-10/Rac1 also functions upstream of MIG-10/Lamellipodin [66], an adaptor protein that interacts with ABI-1, part of WAVE complex, to induce axon outgrowth.

In addition to acting in common cell migration pathways, Racs can be activated through shared Rac GEFs. For instance, in all cell migration and axon guidance processes examined to date, UNC-73, a DH-PH GEF, controls the activity of both CED-10/Rac1 and MIG-2/RhoG [36]. In Q neuroblast migration, PIX-1, a PIX class GEF can also activate CED-10 in addition to UNC-73 [36]. In CAN neuron and P cell migration, CED-5, a DOCK180 GEF, may function upstream of MIG-2 [62], whereas it could activate CED-10/Rac1 in DTC migration [62]. CED-5/DOCK180 GEF is mostly implicated in activating CED-10/Rac1 in phagocytosis [61]. It was later shown that MIG-2/RhoG can also activate CED-10/Rac1 through a novel interaction with CED-12/ELMO, which forms complex with CED-5/DOCK180 GEF to activate CED-10/Rac1 [67]. In vertebrates, the homologous MIG-2/RhoG-CED-10/Rac1 pathway promotes fibroblast migration *in vitro* [67]. Whether it also functions in *C. elegans* cell migration *in vivo* remains an open question.

Currently, the connection to Rac GTPases in SM migration comes from the involvement of UNC-73/GEF in gonad-independent attraction of SM [49]. Whether both CED-10/Rac1 and MIG-2/RhoG are involved in SM migration and how they might function in GDM and GIM is still unknown. Elucidating the role of Rho family GTPases is an important step to link upstream guidance cues to the actin cytoskeleton in SM migration.

CONCLUSION

Studies of cell migration in the model organism *C. elegans* have shaped our understanding of cell migration in general. Experiments on different migration systems reveal diverse mechanisms cells use to guide their migration. The particular sets of mechanisms cells adopt depend on their environments and their own reservoirs of responding molecules. Despite this diversity, we have observed common themes emerging from these studies. For example, although *C. elegans* have a more compact genome than vertebrates, redundancy of different degrees exists on the molecular level as cells use multiple proteins for the same purpose. C. elegans also use redundancy on the pathway level as parallel signaling modules are adopted to ensure the robustness of cellular guidance. The conservation of mechanisms extends well into higher organisms: the initial discovery of Netrin in *C. elegans* led to the subsequent identification of similar proteins in mammals that are crucial for the wiring of the brain [15], illustrating the importance of studying model organisms.

The success of using *C. elegans* to study cell migration benefits from a wealth of genetic tools. For example, to circumvent early lethality, RNA interference (RNAi) can be used to start gene knockdown at later stages. To tackle the problem of redundancy, compound mutants of several genes can be used, and genetic mutations can also be used in combination with RNAi when making compound mutants is difficult or results in lethality. Additionally, dominant negative and constitutively active mutations are particularly useful when the gene of interest has functional homologues that act redundantly, and this approach can be used for initial discovery of possible involvement of a gene. When used with lineage-specific promoters, transgenes of

such dominant negative or constitutively active mutations can elucidate stage-specific and cell-autonomous gene functions.

Despite the powerful genetic tools and the ability to track cells *in vivo*, opportunities to directly observe consequences of gene mutation on the cellular and subcellular levels in *C. elegans* are limited. This is especially crucial when many of the commonly studied migrations occur postembryonically, such as DTC migration and SM migration. In contrast, cell culture on 2D substrates in vertebrate systems has provided invaluable insights into the mechanisms that remodel the actin cytoskeleton in response to altered environmental cues. In fact, most of our knowledge on how cells perceive signals and elicit response by changing its actin cytoskeleton as described in the earlier sections of this review comes from studies on cells in culture. The lack of larval cell culture system in *C. elegans* hindered our testing of the conservation of mechanisms that operate in vertebrate systems, as well as the discovery of new mechanisms that could also function in higher organisms. Thus, establishing larval cell culture in *C. elegans* would complement embryonic cell culture, and would have enormous impact on the study of cell motility, as well as other cell and developmental events that occur postembryonically.

As we develop novel tools to study cell migration, we would like to answer several important questions about SM migration and other cell migration processes: (1) what additional guidance cues cooperate with identified ones to guide cell migration? (2) How are these cues integrated to elicit coordinated cellular response? (3) What Rho family GTPases are used to transmit directional cues to the actin cytoskeleton, and how do they induce changes through actin regulatory proteins? The answers to these questions will fill in gaps in our understanding of how

cells coordinate their navigation system with their motility engine to direct themselves in a myriad of road signs. Insights into these important aspects will lead to a better understanding of the motility aspects in normal morphogenesis, immunity, and tissue repair, and will shed light onto understanding of aberrant migration in disease conditions such as autoimmune diseases, mental retardation, and cancer.

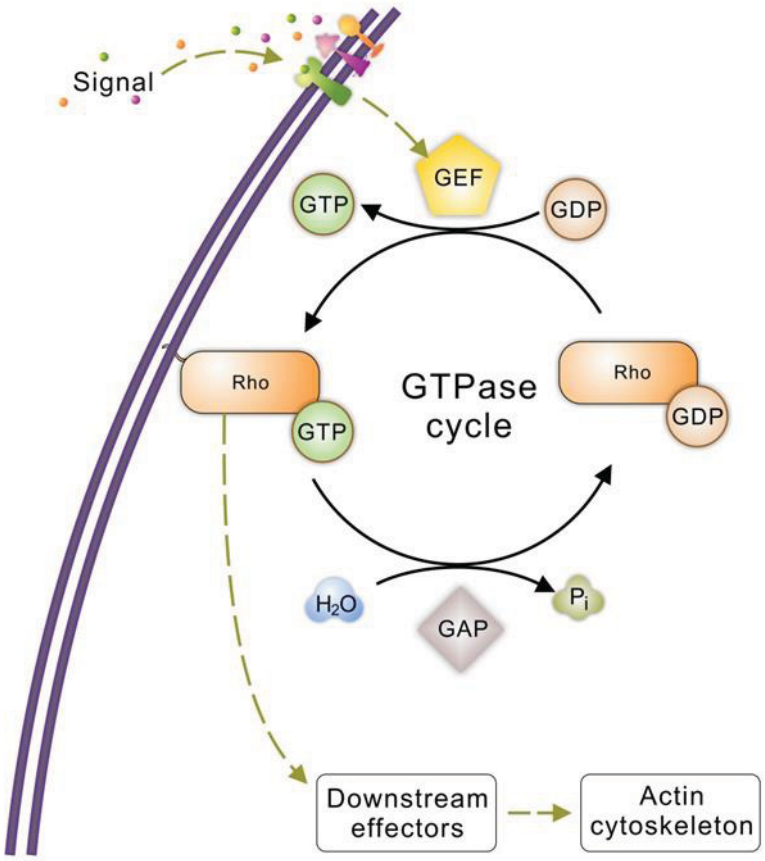

Figure 1.1 Rho GTPases as molecular switches in transducing signals to the actin cytoskeleton

During cell migration, upstream signals such as guidance cues bind to membrane receptors and activate guanine nucleotide exchange factor (GEF). GEF facilitates the conversion from "OFF" state, GDP-bound Rho GTPase to "ON" state, GTP-bound Rho GTPase. GTPase-activating protein (GAP) catalyzes the reverse reaction. Active "ON" state Rho GTPase then binds to and activates downstream effectors, many of which lead to remodeling of actin cytoskeleton.

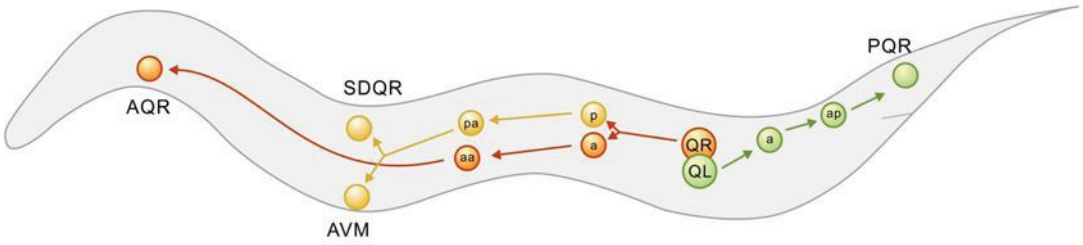

Figure 1.2 Schematic diagram of the migration of Q neuroblasts and their descendants

Two Q neuroblasts are born at symmetric left (QL, large green circle) and right (QR, large orange circle) lateral positions. QR and its descendants migrate anteriorly, and QL and its descendants migrate posteriorly. Arrow shows direction and extent of migration, and arrow branch point indicates a cell division. “a” stands for anterior daughter cell and “p” posterior daughter cell from a cell division. For example, QR.pa is the anterior daughter cell of QR.p, which is the posterior daughter cell of QR. The final products of the divisions are AQR, PQR ciliated sensory neurons, AVM touch sensory neuron, and SDQR interneuron, and they assume their final positions through the migration.

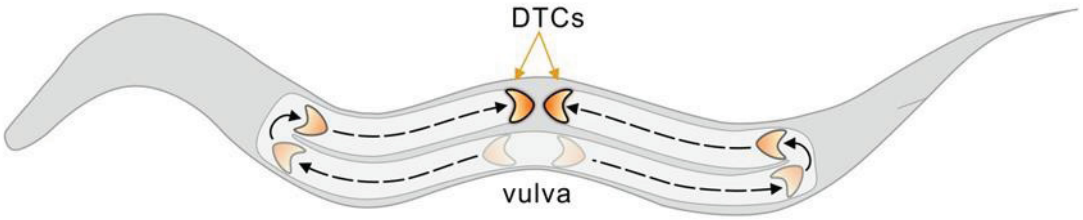

Figure 1.3 Schematic diagram of distal tip cell (DTC) migration

DTC migration generates the mirror images of U-shaped gonad (light grey). Two DTCs (orange; darker color indicates later stages) at either end of the gonad tube start migrating to the anterior or posterior from the middle body region (indicated by vulva), then turn dorsally and finally migrate to the center again but on the dorsal side. The trajectory (arrow) of migration reflects the U-shaped two gonad arms that are mirror images of each other.

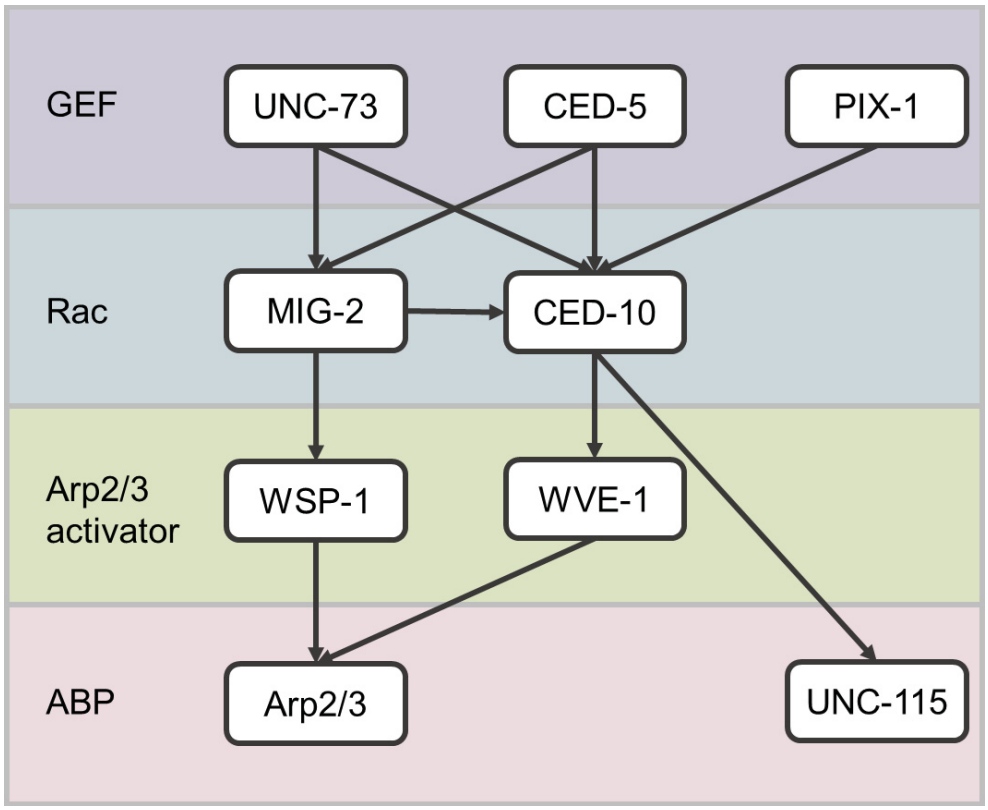

Figure 1.4 Signaling network that regulates actin binding proteins through controlling Rac activity

Rac GEFs UNC-73, CED-5, and PIX-1 activate MIG-2/RhoG and/or CED-10/Rac1. Arp2/3 activators WSP-1/WASP and WVE-1/WAVE are activated by MIG-2/RhoG and CED-10/Rac1, respectively. CED-10/Rac1 can also activate actin filament binding protein UNC-115/abLIM. Arp2/3 and UNC-115/abLIM induce remodeling the actin cytoskeleton that is fundamental to cell motility.

Table 1-1 A glance at selected migratory cells in *C. elegans*

Migrating cell/axon	Stage	Direction	Distance (μm)	Velocity (μm/h)
CAN neurons[1]	embryo	pos.	~22	NA
ALM neurons[1]	embryo	pos.	~15	NA
HSN neurons[1]	embryo	ant.	~23	NA
QL[2]	L1	pos.	~7	~3.5
QL.a	L1	pos.	~5	~2.5
QL.ap/PQR	L1	pos.	28.9 ± 5.2	16.8 ± 3.3
QR	L1	ant.	~7	~3.5
QR.a	L1	ant.	~25	11.2 ± 2.6
QR.ap/AQR	L1	ant.	~45	24.6 ± 4.2
QR.p	L1	ant.	~15	5.9 ± 2.2
QR.pa	L1	ant.	~20	10.8 ± 2.3
SM (left and right)[3]	L2	ant.	~50	~12
DTC[4]	L2-L3	ant. (ant. DTC), pos. (pos. DTC)	~54	6
	L3-L4	dorsal	NA	NA
	L4	pos. (ant. DTC), ant. (pos. DTC)	~60	10

Keys:

1. Migration distances for CAN, ALM, and HSN are estimated according to reports by [28, 68].

2. Migration distance and velocity for the Q lineage are adapted from [37].

3. Migration distance for SM is estimated according to the distance between Pn.p cells reported in [44] and the start and finish location reported in [48]. Velocity of SM is estimated according to the time for SM to finish migrating (4 hours, [48]).

4. Migration distance for DTC during L2 and L4 stages are estimated according to the velocity and duration of migration reported in [69].

Table 1-2 Summary of genes involved in mechanisms controlling SM migration

Protein	GIM[2] (early acting)	GDM (late acting)		Dorsoventral[1]
		GDA[2]	GDR[2]	
Growth factor/Morphogen/protease				
EGF pathway				
EGF/LIN-3			*	
EGFR/LET-23			*	
FGF pathway				
FGF/EGL-17				53% (*sax-3*)
FGFR/EGL-15				53% (*let-60(gf)*)
PTPRE/CLR-1				
Grb2/SEM-5				15% (*egl-15*)
ADAM				
ADAM/UNC-71				
netrin pathway				
netrin/UNC-6	x			
netrin receptor/UNC-40	x		x	
netrin receptor/UNC-5	x		x	
ULK/UNC-51	x			
RUN/UNC-14	x			
semaphorin pathway				
semaphorin/MAB-20				
Plexin B2/PLX-2				
CRMP-2/UNC-33	x			
Slit/Robo pathway				
Slit-1/SLT-1			x	
Roundabout/SAX-3			x	53% (*egl-17*)
Ras/Rho signaling				
Rho family GTPase signaling				
GEF/UNC-73				
Ras-Raf-MEK-MAPK				
RasGEF/SOS-1/LET-341				
Ras/LET-60				11% (*lf*); 53% (*gf; egl-15*)
KSR/KSR-1				3%
Raf/LIN-45				7% (*egl-15*)
MEK/MEK-2				6%
ERK/MAPK/SUR-1				
Actin regulatory/structural proteins				
NAV2/UNC-53				
Enabled/VASP/UNC-34	x			17% (*egl-17*)
Ankyrin/UNC-44	x			
Gene expression				
PITX1/UNC-30				
Other processes				
zeta-2/UNC-76	x			

Keys:

x: No effect.

*: Effects due to changes in VPC induction

1. Non-ventral SM observed in single or double mutants (allele in parentheses indicates mutation combined with); number indicates highest percentage in tested alleles.

2. Darker colors indicate stronger impact on SM migration, and lighter colors indicate weaker impact on SM migration.

Chapter 2 Isolation and culture of larval cells from *C. elegans*

Sihui Zhang, Diya Banerjee, and Jeffrey R. Kuhn

Chapter 2 used with permission of PLoS ONE

Zhang S, Banerjee D, Kuhn JR (2011) Isolation and Culture of Larval Cells from C. elegans. PLoS ONE 6(4): e19505. doi:10.1371/journal.pone.0019505

ABSTRACT

Cell culture is an essential tool in the study of cell function. In *C. elegans* the ability to isolate and culture cells has been limited to embryonically derived cells. However, cells or blastomeres isolated from mixed stage embryos terminally differentiate within 24 hours of culture, thus precluding post-embryonic stage cell culture. We have developed an efficient and technically simple method for large-scale isolation and primary culture of larval-stage cells. We have optimized the treatment to maximize cell number and minimize cell death for each of the four larval stages. We have obtained up to $7.8x10^4$ cells per microliter of packed larvae, and up to 97% of adherent cells isolated by this method were viable for at least 16 hours. Cultured larval cells showed stage-specific increases in both cell size and multinuclearity and expressed lineage- and cell type-specific reporters. The majority (81%) of larval cells isolated by our method were muscle cells that exhibited stage-specific phenotypes. L1 muscle cells developed 1 to 2 wide cytoplasmic processes, while L4 muscle cells developed 4 to 14 bifurcating processes of various thicknesses. L4 muscle cells developed bands of myosin heavy chain A thick filaments at the cell center that spontaneously contracted *ex vivo*. Neurons constituted less than 10% of the isolated cells and the majority of neurons developed one or more long, microtubule-rich protrusions that terminated in actin-rich growth cones. In addition to cells such as muscle and neuron that are high abundance *in vivo*, we were also able to isolate M-lineage cells that normally constitute less than 0.2% of cells *in vivo*. Our novel method of cell isolation extends *C. elegans* cell culture to larval developmental stages, and allows use of the wealth of cell culture tools, such as cell sorting, electrophysiology, co-culture, and high-resolution imaging of subcellular dynamics, in investigation of post-embryonic development and physiology.

INTRODUCTION

Caenorhabditis elegans is used widely as a genetic and developmental model organism because of its simple anatomy, invariant cell lineage, compact genome, and the wealth of genetic tools available for its study. However, high-throughput access to individual cells has been limited to embryonic lineages. Early work showed that embryonic cells from dissociated blastomeres could be cultured for short periods of time and were capable of partial differentiation in vitro [70-72]. Building upon this early work, Bloom systematically tested a variety of cell isolation techniques and conditions for larger scale embryonic cell culture [73]. Bloom's work was expanded and optimized upon by Strange and colleagues who introduced a method of embryonic cell culture to the wider *C. elegans* community [74-76]. Large-scale embryonic cell culture expanded the available experimental repertoire to include electrophysiological analysis of cultured neurons and muscles [74, 77], isolation of specific cell types by automated cell sorting [78, 79], cell type specific gene expression profiling [76, 80, 81], assessing the effect of environmental toxins on cultured cells [82, 83], dissecting cellular mechanisms of RNA interference [84, 85], and high-resolution total internal reflection fluorescence microscopy of subcellular events [86].

Although embryonic cell culture has allowed new advances in cell and tissue-specific studies in *C. elegans*, it is not without limitations. Embryonically derived cells differentiate within 24 hours to resemble L1 stage cells *in vitro* [74, 75]. Development of key tissue and organ systems, such as the reproductive system and neuro-epithelial tissues [87], occurs after hatching, and many cells do not gain their full functionalities until later larval stages [88]. These post-

embryonic developmental events, and the molecular mechanisms that control them, cannot be studied using cultured embryonic cells.

The ability to access and manipulate larval stage cells would greatly benefit cell and tissue specific studies of post-embryonic developmental events. However, there are no current reports of successful isolation of larval stage cells, and former attempts appear to have been hindered by the tough and relatively impermeable cuticle that encapsulates the worm and prevents access to cells and tissues [89]. An alternative approach to gaining access to larval cells and organs is dissection of individual animals [90-93]. However, dissection is both technically-demanding and can only be performed on a small scale. Tagging of mRNA is a molecular approach to cell-specific studies that can be carried out in whole worms without isolating cells, and has been used to profile gene expression in specific larval cell types [78, 94]. However, mRNA tagging suffers from several experimental constraints, such as the need for cell-specific promoters, and is limited to providing transcriptional information [78, 95]. To circumvent the limitations of using dissection and mRNA tagging to access *C. elegans* post-embryonic cells, we have developed a technically simple method for large-scale isolation of cells from *C. elegans* larvae. Large quantities of viable larval cells from synchronized L1 to L4 stage worms can be isolated using this method and used for cell and tissue specific studies of post-embryonic cellular phenomena.

Results

Effective disruption of the larval cuticle to release cells

The cuticle is the primary barrier to accessing cells and tissues in *C. elegans* larvae and adults. Larval and adult cuticles are composed primarily of collagens, highly cross-linked

cuticlins, and surface glycoproteins [96]. We tested the ability of a range of proteases, including elastase, pepsin, α-chymotrypsin, pronase, and a cocktail of collagenases to dissolve the cuticle and release cells. However, none of these reagents affected the integrity of the larval cuticle (not shown). We therefore sought a method that would break down the extensive disulfide bonds and di- and tri-tyrosine cross-links that strengthen the cuticle, and would thus make the cuticle more accessible to protease digestion. The anionic detergent sodium dodecyl sulfate (SDS) and reducing agents denature proteins and are known to weaken the cuticle. In studies where the aim was to solubilize and extract the cuticle, Cox and colleagues [97] showed that treatment with SDS and a 5% solution of the reducing agent ß-mercaptoethanol, along with sonication and heating, solubilized 69% of cuticle content. Austin and colleagues [98] employed a similar method, but with shorter and gentler treatment, using 0.25% SDS to dissolve the cuticle while preserving epithelial seam cell contacts. We found that incubation of nematodes in 0.25% SDS and 3% of the reducing agent dithiothreitol (DTT) for 2 to 4 minutes at room temperature altered the appearance of the cuticle without disrupting nematode body integrity (Figure 2.1). The anterior portion of the heads of SDS-DTT treated animals protruded rather than being smoothly linked to the more posterior part, and the cuticle wrinkled, indicating the disruption and loosening of cuticular structure (Figure 2.1(**C**)). Nematodes incubated in SDS-DTT swelled to resemble a "dumpy" phenotype and showed reduced mobility, traits that are associated with mutations that decrease cuticle integrity [99]. When animals were treated for longer times, the majority of worms became stiff and immobile and lacked wild type movement. Extensive SDS-DTT treatment eventually solubilized worms completely, leaving empty cuticles husks (Figure 2.1(**D**)). Although animals treated with SDS-DTT for short times were less active and lost

sinusoidal movement, they still twitched, indicating function of the nervous system and musculature.

To evaluate the effect of SDS-DTT treatment on animal survival, we determined survival rates over 9 minutes of SDS-DTT treatment (Figure 2.1(**I**)). We found that 94% of L1 worms survived after 2 minutes of SDS-DTT treatment, but that survival dropped rapidly to 58% at 3 minutes of exposure. In contrast, SDS-DTT treatment killed L2 through L4 worms more slowly. At 4 minutes, 90% of L2 to L4 worms remained alive and survival did not decrease below 50% until 7 to 8 minutes. The decreasing sensitivities to SDS-DTT treatment for L1 through L4 worms are consistent with changes in cuticle composition and structure over larval development. For example, L4 larvae are likely more resistant to SDS-DTT treatment because L4 cuticles are approximately 2.5 times thicker than L1 cuticles [100].

Having established a treatment that weakens the cuticle without causing extensive death, we sought to identify compounds that could disrupt the cuticle and release live cells from larval worms. Mechanical treatments of SDS-DTT treated worms, including repeated pipetting, were ineffective in releasing cells (Figure 2.1(**E**)). Treatment with either of the proteinases pepsin or α-chymotrypsin also did not release cells from SDS-DTT treated worms. However, it was previously demonstrated that the proteinase elastase can digest both basal and cortical cuticle layers of SDS-purified cuticles, and that the proteinase pronase can digest the basal cuticle layer and the pharyngeal cuticle [97]. We thus tested these two proteinases and found that while elastase digested only 10% of SDS-DTT treated worm, addition of 15 mg/ml pronase to SDS-DTT treated worms (Figure 2.1(**F**)) resulted in digestion of 70% (L1) to 96% (L4) of cuticles. When combined with mechanical disruption by pipetting, pronase and SDS-DTT treatment

dissociated tissues and released single cells very efficiently (Figure 2.1(**G-H**)). However, L2 to L4 nematodes required 2.5- to 3-fold longer incubation time in pronase compared to L1 nematodes for efficient digestion, reflecting the increased thickness of older larval cuticles. For both L1 and older larvae, pronase treatment alone was ineffective in digesting cuticles and pre-sensitization by SDS-DTT treatment was required for efficient pronase-mediated cuticular digestion (Figure 2.1(**B**)).

Primary culture of isolated larval cells

Cell yields: SDS-DTT-pronase treatment and mechanical disruption of L1 worms yielded $2.7 \pm 1.9 \times 10^4$ (mean ± S.D., n=3 independent isolations) cells in solution per microliter (µl) of packed nematodes. With approximately 1.1×10^4 packed L1 animals per µl (n=1) and typical yields of approximately 40 µl of packed worms from three to five 60 mm diameter feeding plates, we could obtain $1.1 \pm 0.8 \times 10^6$ cells during a typical L1 isolation. Cell isolation from L2 to L4 larvae was more efficient, yielding $7.8 \pm 1.7 \times 10^4$ cells per µl of packed nematodes (n=4).

An accurate comparison of the efficiencies of larval and embryonic cell isolation is difficult because of the large ranges in cell number and cell size among embryonic and different larval stages, and variability in the numbers of packed embryos or larvae in a given volume. Nevertheless, we provide a rough comparison of cell yields based on equivalent volumes of packed embryos and larvae. We used the method of Christensen et al [74, 75] to isolate embryonic cells, and obtained $6.1 \pm 2.9 \times 10^4$ pre-adhered cells per µl of packed eggs (n=3). At a density of 1.6×10^4 packed eggs per µl (n=1), embryonic cell isolation produced 3.8 ± 1.8 cells per egg. Approximately 40 µl of packed eggs yields $2.4 \pm 1.2 \times 10^6$ pre-adherent cells. Thus, our method of larval cell isolation ($2.7 \pm 1.9 \times 10^4$ to $7.8 \pm 1.7 \times 10^4$ pre-adhered cells per µl of packed

larvae) provides cell yields in the same order of magnitude as embryonic cells ($6.1 \pm 2.9 \times 10^4$ pre-adhered cells per µl of packed eggs) isolated by the method of Christensen et al [74, 75]. Both embryonic and larval cell isolation protocols provide cell yields that are sufficient for methods, such as cell sorting, that require large quantities of cells [78, 80]

Adherence to substrate: We tested a number of molecules, including laminin, poly-D-lysine, fibronectin, and collagen IV, which are commonly used in cell culture to enable adherence of cells to a substrate. The larval cells showed maximum adherence to glass surfaces plated with 0.5 mg/ml peanut lectin, which was subsequently used for all isolations. Cells adhered less well to poly-D-lysine and fibronectin, and did not adhere at all to laminin or collagen IV coated surfaces. Isolated larval cells were typically plated at a density of $5\text{-}6 \times 10^6$ cells/ml, and were maintained in commercially available L-15 culture medium supplemented with fetal bovine serum albumin at an osmolarity of 340 mOsm. The plating density and the culture conditions are similar to those optimized for maintenance of *C. elegans* embryonic cells [74, 75]. For example, cells were allowed to adhere overnight and non-adhered cells were washed away. A typical density of adherent cells isolated from L1 stage worms was $3.8 \pm 1.3 \times 10^3$ cells/mm^2 spread over a total area of 200 mm^2, yielding $7.8 \pm 2.4 \times 10^5$ total adherent cells, or approximately 70% of cells in solution before plating.

Survival in culture: The SDS-DTT-pronase treatment and culture conditions described did not significantly damage the isolated larval cells. We simultaneously monitored live and dead cells using a two-color fluorescence assay with Calcein acetoxymethyl ester (Calcein-AM), which measures the population of live cells, and ethidium homodimer, which measures the

population of dead cells [101]. These cytotoxicity/cytoviability assays showed that 80% to 97% of adherent larval cells were viable after 16 hrs in culture (Figure 2.1(**K**)).

Bacterial contamination: In our initial attempts at isolating and culturing larval cells, we grew *C. elegans* larval populations on bacterial lawns plated on solid media. While we obtained substantial yields of viable larval cells, the cell culture would frequently become contaminated with bacterial populations that overwhelmed the antibiotics in the culture medium. However, cells isolated from L1 larvae that were hatched and grown only in sterile M9 medium remained uncontaminated, indicating that the contaminating bacteria in older larval cell cultures were likely from the 'food' lawns and had survived the SDS-DTT-pronase treatment. To circumvent bacterial contamination, we grew synchronized larval populations under axenic conditions in sterile CeHR medium [102, 103], which prevented bacterial contamination of cultured cells (Figure 2.1(**L**)).

Cells can be isolated from both high and low abundance larval cell types

We used GFP reporter strains to identify some of the cell types isolated from larval worms using the SDS-DTT-pronase method. We observed expression of *myo-3*::GFP, which represents the expression of a body wall muscle cell specific myosin [104, 105], in approximately 81% of L1 derived cultured cells (Figure 2.2, Table 2-1). We also observed expression of *unc-119*::GFP, which is expressed primarily in neural cells and also a few muscle cells [106], in less than 10% of L1 derived cultured cells. In vivo, muscles constitute 15% (81/558) and neurons constitute 40% (222/558) of all cells in L1 larvae. Thus, our cell isolation method appears to enrich for muscle cells but not neural cells.

We tested whether our cell isolation method could extract larval cells that are present *in vivo* at a substantially lower density than muscle and neural cells types. *hlh8::*GFP is expressed in the M lineage mesodermal cells, which constitute only 0.18% (1/558) of the total cell population of L1 larvae [107] (Figure 2.2). We found that GFP positive cells constituted approximately 1% of the cells isolated and cultured from *hlh-8*::GFP larval populations, indicating the presence and enrichment of M lineage cells in larval cell culture (Figure 2.2). Therefore, our SDS-DTT-pronase method is capable of isolating viable cells from both high and low abundance cell types in larval *C. elegans*. However, it is unlikely that every larval cell type can be successfully isolated and our protocol will need to be tested and modified for isolation of specific cell lineages.

Isolated larval cells express cell type-specific morphologies and exhibit cellular activities *in vitro*

To evaluate whether isolated larval cells maintain cell type specific characteristics in vitro, we examined the GFP-positive cells from *unc-119*::GFP and *myo-3*::GFP strains for neural and muscle cell associated proteins and structures. Muscle cells are characterized by the presence of sarcomeres, contractile filament bundles that consist primarily of actin filaments and the motor protein myosin II. Myosins act by moving actin filaments over and past each other, thus generating changes in cell shape and effecting cellular contractions. *C. elegans* larvae express two isoforms of myosin II heavy chain (MHC) in body wall muscles [108-111]. MYO-3/MHC-A is found in the center of the A band of thick filaments, while the more abundant UNC-54/MHC-B isoform is found throughout the distal tips of the A band [112, 113]. We used a *myo-3*::GFP reporter strain to locate body wall muscle cells in vitro (Figure 2.3(**A**)). Antibody staining of

MHC-A in isolated *myo-3*::GFP larval muscle cells showed thin bands that were restricted to the center of the cell body, consistent with MYO-3/MHC-A localization to the center of the A band *in vivo*. These myosin structures in L4 isolated muscle cells functioned as sarcomeres as seven of the eight *myo-3*::GFP expressing L4 muscle cells showed spontaneous and repeated contractions over 30 minutes (Figure 2.3(**B**)). Observations of five *myo-3*::GFP expressing cells for 30 minutes each showed an average of 0.9 ± 0.3 contractions/min (mean ± SD, n=5), with each contraction lasting 11.5 ± 1.6 seconds, and intervals of 102 ± 63 seconds of relaxation between contractions.

We next examined microtubule and actin localization in GFP-positive neurons isolated from the *unc-119*::GFP strain. In *C. elegans,* neurons are born mainly during embryogenesis and neural generation is completed by the L2 stage [114]. However, many neurons undergo post-mitotic development during which the neural cell bodies, clustered in ganglia at the head and tail, generate long, thin dendrite- and axon-like processes. These processes show local swellings of vesicle clusters that form at synaptic regions. The dendrite- and axon-like processes and neurite branches are characterized by microtubule bundles. Actively migrating axons terminate in a growth cone consisting of a dense, peripheral actin network that excludes all but a few microtubules bundles [4, 115]. In L1 derived GFP-positive cells from the *unc-119*::GFP strain, we found that microtubules were present in both cell bodies and neuronal processes (Figure 2.4(**C**, **H** and **L**)), but that microtubules were excluded from the periphery of protrusions, where actin was highly expressed (Figure 2.4(**K-N**)), a cytoskeletal arrangement that is typical of the leading edges of motile cells. Cultured neurons varied in the number and size of projections, and some isolated GFP-positive cells developed wide protrusions with strong microtubule staining

(Figure 2.4(**E**, **J** and **N**)). Actin-rich protusions, which are reminiscent of motile cell lamellipodia, appeared at one or more points along the length of each neuronal process, and showed dynamic protrusive activity (Figure 2.4(**O**)). These actin rich structures were likely active growth cones of neuronal processes or active lamellipodia of neurons capable of motility. Although neuronal processes were not present in freshly isolated cells, we observed that cultured neurons from all larval stages were capable of forming long dendritic and axonal processes (Figure 2.5(**A**, arrowheads)). Because most neurons begin to form processes by stage L2, it is likely that isolated neurons can regenerate processes lost during isolation.

Isolated larval cells exhibit developmental stage specific morphologies and behavior

Nematodes actively regulate cell and organ size during postembryonic development [116]. L4 larvae are about 2-fold thicker and 2.4-fold longer than L1 despite the fact that somatic cells only increase 1.7-fold in number [87]. Thus, based on stage specific estimates of nematode volume [117] and number of nuclei [87], we estimate that average cell size increases roughly two-fold from L1 to L4. We measured cell body area in cells isolated from different larval stages and found that cells isolated from L4 stage larvae were on average 2.7-fold larger than L1 derived cells (Figure 2.5(**B**)). Cells from different larval stages also adopted distinct morphologies. For example, while the majority of L1 derived cells were spindle-shaped with single or double processes, many later stage cells had round cell bodies and extended wide cytoplasmic protrusions (Figure 2.5(**A**)). We further examined these developmental stage-specific phenotypes using L1 and L4 derived cells from the *myo-3*:: GFP strain that expresses GFP in the nucleus and mitochondria of body wall muscle cells. Similar to the overall increase in cell size, we found that L4 GFP-positive muscle cells were 2.6 times larger than L1 GFP-positive

muscle cells (Figure 2.5(**D**)). Furthermore, isolated L4 muscle cells developed more cellular processes than L1 derived muscle cells. Observations from 3 independent cell isolations showed that L1 muscle cells developed from 1 to 2 wide processes with an average of 1.48 ± 0.08 (n=301) processes per cell, while L4 muscle cells developed an average of 8.4 ± 1.0 (n=45) processes of various thicknesses per cell (Figure 2.5(**C**)). The developmental age of muscle cells *in vitro* correlated with muscle arm development. *In vivo*, L1 larvae muscle cells typically extend a maximum of 2 muscle arms, while older larval and adult muscle cells extend 3 to 5 muscle arms [118]. Therefore, our observations, that L4 derived cells increased muscle arm number 5.7-fold over L1 derived cells, are consistent with the *in vivo* temporal pattern of muscle differentiation [118]. We note that *in vitro* cultured muscle cells have an abnormally large number of muscle arms (4 to 14, n=45) compared to in vivo muscle cells of comparable developmental age (3 to 5) [118]. Dixon and colleagues [118] proposed that muscle arms extend passively as body wall muscles move away from the nerve cord during embryogenesis but switch to active extension during larval development. Because we observed active protrusion and retraction of muscle processes in culture (not shown), and larval muscle arm extension is highly regulated *in vivo*, it is possible that *in vitro* culture conditions induce ectopic muscle arm extension in L4 muscle cells due to the lack of late stage suppression that is normally found in vivo.

In addition to developmental stage specific muscle cell morphology, we observed large multinucleate cells in L4 cell culture, but rarely in cells isolated from younger nematodes (Figure 2.5(**E**)). Approximately one third of somatic nuclei in the adult are found in syncytia [119]. For example, the Hyp7 epithelial syncytium, the largest somatic syncytium in *C. elegans* consists of 133 adult nuclei and forms a contiguous epidermal tubes that encircles the entire nematode body

except for the extreme head and tail regions [28, 119, 120]. However, the multinucleate cells isolated from late larval stage worms are unlikely to be derived from the large Hyp7 syncytium, which would be broken apart on dissolution of the cuticle and mechanical disruption of cell contacts. The observed multinucleated cells may instead be derived from vulval, uterine and epithelial cell lineages that form syncytia of 4 to 16 nuclei during late larval development [69, 121]. During L4 stage, the vulval cells form tetra-nucleate and bi-nucleate syncytia that constitute the epithelial toroids of the vulva, while the uterine toroid cells form similar epithelial syncytia at the uterine lobes [69]. At the end of larval development, 16 seam cells terminally differentiate by fusing along their lateral axes to form the seam syncytium, which extends along the body length of the worm, and from which the adult alae structures are secreted [121]. The multinucleate cells observed in late larval sage cell isolations may thus be vulval, uterine or seam cell epithelial in origin.

Alternatively, developmentally older cells may have greater competence for cell fusion, an event that is normally restricted *in vivo* by active cellular mechanisms that are lost or absent in culture conditions, thus allowing older cells to form multinucleate cells *in vitro*. The rare L1 derived multinucleate cells may derive from a number of cell lineages that form syncytia during late embryogenesis and early larval development. For example, pharyngeal muscle cells form hexa-nucleate and bi-nucleate syncytia, and arcade cells of the anterior hypodermis form two epithelial syncytia that are part of the buccal cavity [122].

DISCUSSION

The investigation of cellular and subcellular processes in cultured cells is a mainstay experimental approach for the study of invertebrate and vertebrate model organisms. However, large scale cell culture in *C. elegans* has been limited to embryonically derived cells [74, 75]. Primary cultures of *C. elegans* embryonic cells terminally differentiate within 24 hours of isolation to resemble L1 stage cells [75], and thus post-embryonic cellular phenomena cannot be studied using these cells. We have developed a technically simple and efficient method for large-scale isolation and primary culture of cells from *C. elegans* larvae. Our method involves treatment of *C. elegans* larvae with a combination of detergent and reducing agent followed by protease digestion that effectively solubilizes the larval cuticle but does not kill cells. Large quantities of viable larval cells from synchronized L1 to L4 stage worms can be obtained using this method, and we have successfully isolated both high and low abundance larval cell types. Like embryonic cells that can be cultured for up to two weeks [74, 75], we have repeatedly cultured active larval cells for at least seven days. The isolated larval cells showed both cell type specific and developmental stage specific gene expression, morphologies and cell behaviors in vitro, indicating that isolated cells are normally differentiated and functional.

There are minor differences in the optimum attachment substrate for larval cells versus embryonic cells, but overall, the culture conditions, cell viability and cell yields of our larval cell isolation method are very similar to those of embryonic cell isolation as described by Strange and colleagues [74, 75]. Thus, *C. elegans* larval cells isolated according to our method should be amenable to the various cell biological techniques that have been used to study cultured embryonic cells, such as electrophysiology, RNAi, and fluorescence activated cell sorting (FACS)

[74]. However, using isolated larval cells have several advantages over using embryonically derived cells. Embryonic isolation yields cells that are primarily from pre-comma stage embryos [74]. Since cultured *C. elegans* embryonic cells terminally differentiate after one day in isolation, it is possible that cell differentiation is not entirely normal compared to cells in situ. For example, transmembrane receptors and membrane channels characteristic of a cell type may not be expressed or properly localized in isolated embryonic cells [123]. In contrast to using isolated *C. elegans* embryonic cells, the ability to isolate and culture larval stage cells enables the investigator to specify cell isolation from a developmental stage at which the cell type of interest is properly differentiated. In addition, a greater variety of differentiated cell types are available from *C. elegans* larvae compared to embryos. Larval cells isolated by our method show developmental-stage specific morphologies for at least 72 hours, indicating that they at least partially maintain their original differentiation state and do not terminally differentiate within this period of time. Thus, larval cell culture can be used to investigate differences in cell physiology and behavior, cell autonomy, or track temporal changes in expression patterns, during larval development of a particular cell type.

It may be possible to manipulate culture conditions to maintain the undifferentiated or partial differentiation state of isolated larval cells. Cell plating density and the use of 'feeder' cells are two parameters that have substantial influence on differentiation and proliferative capability of cultured mammalian cells [124-126]. For example, mouse and human progenitor cells and induced pluripotent stem cells can be maintained in a self-renewal state by growth on a layer of 'feeder' fibroblast cells and similar techniques could be adapted for *C. elegans* larva cell culture [124, 127]. For *C. elegans* cell lineages that divide during larval development but do not

terminally differentiate until the adult stage, such as the epidermal seam cells or the vulval cells, isolation of larval cells and culture in conditions that prevent terminal differentiation would be the basis of establishing both primary and transformed cell lines, a cell biology tool that is currently not available for *C. elegans* research.

C. elegans larva cell culture has the normal disadvantages of any culture system, such as the absence of extracellular signaling due to the lack of cell to cell and cell to extracellular matrix contacts. In addition, although we have shown that we can successfully isolate a low-abundance cell type that normally constitutes less that 1% of the in vivo cell population, our method may not be equally successful in isolating other low abundance cell types. However, in combination with embryonic cell culture, and a variety of existing experimental tools, including RNAi and FACS, our method to isolate and culture a variety of cell types from different post-embryonic developmental stages has the potential to substantially further the study of physiological, cellular, and molecular phenomena at the single cell and subcellular levels in *C. elegans.*

Materials and Methods

C. elegans strains and culture. The following *C. elegans* strains were used: N2 (wild type), DP132 [unc-119::gfp], PD4251 [myo-3::Ngfp-lacZ; myo-3::Mtgfp], NH3402 [hlh8::gfp-caax].

Standard Culture: For standard culture of *C. elegans* on solid medium, worms were maintained on NGM seeded with OP50 bacteria at either 15°C, 20°C, or 25°C.

Axenic culture. For axenic liquid culture, *C. elegans* were first grown at 25°C at a density of 20,000/plate on NEP plates seeded with NA22 bacteria [128]. Eggs were isolated from these worm cultures and grown in CeHR medium according to Szilagyi et al. and Nass and Hamza

[102, 103] with minor modifications. 40,000-80,000 freshly hatched sterile L1 were seeded in 10 ml CeHR medium without antibiotics in a T-25 flask and grown at 22°C at 70 rpm in a shaker. After each generation, gravid adults were pelleted as above, eggs isolated and hatched in sterile M9 buffer, and L1 larvae were seeded into fresh, sterile CeHR media and grown to adulthood or the desired isolation stage. The first generation of nematodes grows slowly on CeHR (7-10 days), while successive generations grow at similar rates (4 days) to those on solid media [103]. Nematodes were allowed to adapt to CeHR media for at least one full generation before use.

Larval cell isolation and culture. *Worm synchronization:* Eggs were released by lysing gravid adults with 0.5 M NaOH and 1.2% NaClO for 5 min, pelleted by centrifugation at 1 min in a clinical centrifuge, and washed 3 times with sterile ddH_2O. Eggs were hatched in sterile M9 and L1 were starved for 20-24 hrs at 20°C (22°C for CeHR culture).

L1 cell isolation. Synchronized L1 were pelleted by centrifugation at 1 min in a clinical centrifuge, and M9 was removed by washing the pellet once with sterile ddH_2O. Pelleted L1 were transferred to a 1.6 ml microfuge tubes and residual ddH_2O was removed by centrifugation at 13,000 rpm for 2 min in a microcentrifuge. 20-40 µl L1 pellet was used for cell isolation. Worms were incubated in 200 µl freshly thawed sterile SDS-DTT solution (200 mM DTT, 0.25% SDS, 20 mM HEPES, pH8.0, 3% sucrose, stored at -20°C) for 2 min at room temperature. Immediately after SDS-DTT treatment, 800 µl egg buffer (118 mM NaCl, 48 mM KCl, 2 mM $CaCl_2$, 2 mM $MgCl_2$, 25 mM HEPES, pH7.3, osmolarity adjusted to 340 mOsm with sucrose) was added to the reaction. Worms were pelleted at 13,000 rpm for 1 min, and washed 5 times with 1 ml egg buffer. Pelleted SDS-DTT treated worms were then digested with 100 µl of 15

mg/ml pronase (Sigma-Aldrich, St. Louis, MO) in egg buffer at room temperature for 7 to 9 min. Mechanical disruption was applied during pronase digestion by pipetting the reaction up and down 60 times with a 1-200 µl tip pushing against the bottom of the 1.6 ml microfuge tube. The reaction was stopped by adding 900 µl L-15 medium (Invitrogen, Carlsbad, CA) supplemented with 10% fetal bovine serum (Invitrogen, Carlsbad, CA), 50 U/ml penicillin, and 50 µg/ml streptomycin (Sigma-Aldrich, St. Louis, MO) and adjusted to 340 mOsm [74]. Cells were pelleted by centrifugation at 10,000 rpm for 5 min at 4°C, and washed 2 times with L-15/FBS. The pellet was resuspended with 1 ml L-15/FBS, settled on ice for 30 min. The top 800 µl cell suspension devoid of large worm debris was transferred to a new tube and pelleted by centrifugation at 10,000 rpm for 5 min at 4°C.

L2-L4 cell isolation. Worms grown in CeHR medium were harvested at approximately 26 hrs (L2), 34 hrs (L3) and 50 hrs (L4) post L1 seeding according to the growth rate reported by Szilagyi et al. [102]. Five ml CeHR culture was transferred each time from a T-25 flask into a 15 ml tube with 5 ml sterile ddH_2O and mixed. Worms were pelleted at low speed for 5 seconds in a clinical centrifuge. The same procedure was applied to the other 5 ml of CeHR culture. Worms were washed 2-3 times with 10 ml ddH_2O. In each wash, worms were pelleted for only 5 sec in a clinical centrifuge so that medium particles remained in the supernatant. The same procedure as L1 was followed subsequently for L2-L4 cell isolation, except that for L2-L4 cell isolation, worms were first treated with SDS-DTT for 4 min, and then digested in 15 mg/ml pronase for 20-25 min with 140-160 times pipetting.

Estimation of pelleted embryos or larvae. Eggs from gravid adults were prepared as above and either counted immediately or hatched overnight in sterile M9 and counted. To estimate the number of animals in suspension, we counted all animals from 5 µl of a 10 ml egg or L1 suspension on a dissecting microscope. Animals were concentrated in a clinical centrifuge, transferred to a 1.5 ml tube, and pelleted at 13,000 rpm for 1 min. The supernatant was removed, and centrifugation was repeated twice to remove any remaining supernatant. The pellet was marked and discarded. Animals per µl of packed pellet were estimated from the starting number of animals in suspension and the final pellet volume estimated by refilling to the mark with ddH_2O.

Culture of isolated cells. Cell pellet was resuspended with fresh L-15/FBS. Suspended cells were counted in a haemocytometer, diluted to 5 to $6x10^6$ cells/ml and 30 to 40 µl of cell suspension was plated onto the center of a glass bottom dish (MatTek, Ashland, MA) or an acid-washed coverslip coated with 0.5 mg/ml peanut lectin (Sigma-Aldrich, St. Louis, MO). Cells were allowed to adhere overnight in a 20°C incubator without CO_2 in Snapware plastic containers with a gas exchange hole and humidified with moist kimwipes. Unbound cells and worm debris were washed off with L-15 the next day and 2 ml fresh L-15/FBS was added to the dish.

Cell viability assay. Cells grown on peanut lectin-coated glass bottom dishes were washed five times with egg buffer. Cells were incubated in 150 µl egg buffer containing 1 µM calcein-AM (Biotium, Hayward, CA) and 0.1 µM ethidium homodimer (Biotium, Hayward, CA) for 30 min at room temperature, and live and dead cells were quantified by fluorescence microscopy.

Control cells were killed with 50% methanol in egg buffer and stained as above. No- or very weak-green staining and bright red nuclear staining were observed in control experiment.

Immunofluorescence. *Microtubule and myosin staining:* Cells were fixed with 1% paraformaldehyde in cytoskeleton buffer (10 mM MES, pH 6.1, 150 mM NaCl, 5 mM EGTA, 5 mM $MgCl_2$, and 5 mM glucose) at room temperature for 30 min and then cold methanol at -20°C for 2 min, blocked with 5% BSA in PBS for 30 min, and incubated with mouse anti-tubulin primary antibody (Thermo Fisher Scientific, Fremont, CA; clone DM1A) or mouse anti-MHC-A primary antibody (Developmental Studies Hybridoma Bank, Iowa City, IA; clone 5-6). Cells were then stained with DyLight594-conjugated goat anti-mouse secondary antibody (Jackson ImmunoResearch Laboratories, West Grove, PA) and DAPI [74, 129].

Actin and microtubule staining. Cells were fixed with 0.25% glutaraldehyde in cytoskeleton buffer for 15 min and permeabilized with 0.1% Triton X-100 in cytoskeleton buffer for 10 min. Autofluorescence was quenched 3 times with fresh 1 mg/ml sodium borohydride in cytoskeleton buffer. Cells were blocked with 5% BSA in PBS and stained with TRITC-phalloidin (Sigma-Aldrich, St. Louis, MO) for 20 min, incubated with mouse anti-tubulin primary antibody, and then stained with FITC goat anti-mouse secondary antibody (Jackson ImmunoResearch Laboratories, West Grove, PA) and DAPI [129].

Microscopy. DIC and epifluorescence images were taken using Olympus IX81 inverted microscope (Olympus, Center Valley, PA). Images were acquired with 60X objective (UPlanSApo, NA=1.40, Olympus) or 100X objective (Apo N, NA=1.49, Olympus). Phase

contrast images were taken with Olympus CKX41 tissue culture microscope (Olympus, Center Valley, PA) equipped with a 20X objective (LCAch N, NA=0.40, Olympus).

Acknowledgments

We wish to thank Michael J. Stern for the generous gift of strains NH3402, and the *C. elegans* Genetics Center (CGC) for access to other strains. This work was supported by Virginia Tech Institute for Critical Technology and Applied Science Doctoral Fellowship to SZ and Burroughs-Wellcome Career Award at the Scientific Interface to JRK.

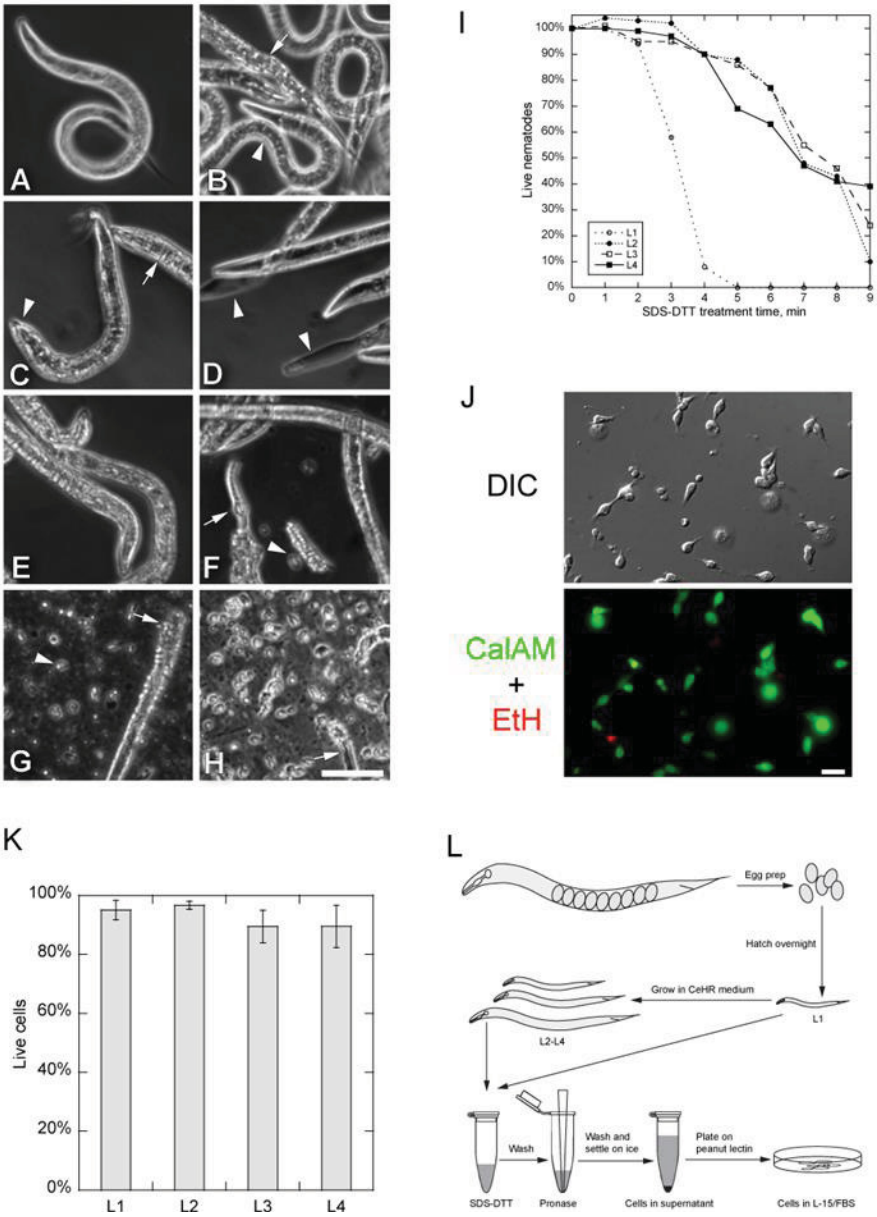

Figure 2.1 Larval cell isolation procedure

(**A-H**) Phase contrast micrographs of L3 nematodes during cell isolation. (**A**) Untreated L3 worms had smooth body outlines and normal bending motion. (**B**) Nematodes treated with 15 mg/ml pronase for 20 min did not dissociate during repeated pipetting. Most nematodes remained intact (arrowhead), but some developed a rougher cuticle (arrow). (**C**) Nematodes

treated with SDS-DTT for 4 min remained intact. Treated nematodes swelled slightly, especially at the head (arrowhead), and cuticle wrinkles appeared (arrow). However, nematodes continued to move. (D) Longer SDS-DTT treatment (8 min) killed nematodes. Some showed cuticle regions devoid of cells (arrowheads). (**E**) A short 4 min SDS-DTT treatment followed by repeated pipetting in egg buffer alone did not dissociate nematodes. (**F**) Adding pronase after a short SDS-DTT treatment (4 min) began to digest the cuticle. By 10 min, some nematodes lost cuticle integrity and released cells (arrowhead). Arrow points to an exposed pharynx in a partially digested worm. (**G**) Repeated pipetting during pronase digestion of SDS-DTT treated (4 min) nematodes over 20 min completely digested most worms. More cells were released (arrowhead) with pipetting than without. Some partially digested worms remained (arrow). (**H**) After digested worms were settled for 30 min on ice, the supernatant contained mostly cells and little nematode debris (arrow). Large worm debris but few cells settled into the pellet (not shown). Scale bar in A-H is 50 μm. (**I**) L2-L4 stage nematodes survived longer in SDS-DTT than did L1 nematodes. Nematodes were scored as dead if they were rigid without any bending activity or had dissolved leaving empty cuticles. Live/dead scores were normalized to worms incubated for 10 min in egg buffer (0 min). (**J**) DIC and fluorescence micrographs of live/dead cell assay of adherent larval cells one day after plating. Calcein-AM stains for live cells (green), and ethidium homodimer indicates dead cells (red). Scale bar: 10 μm. (**K**) Viability of adherent L1-L4 larval cells tested by Calcein-AM and ethidium homodimer staining one day after isolation. Error bar is SD of three observations (L1: n=819; L2: n=417; L3: n=485; L4: n=741). (**L**) Schematic diagram of larval cell isolation procedure. Eggs are isolated from gravid adults

and hatched overnight. L1 larval cells are isolated immediately, while larvae are grown in CeHR medium for L2 to L4 stage cell isolation. Nematodes are treated with SDS and DTT for 2-4 min, washed with egg buffer, and incubated with pronase for 8-20 min with gentle pipetting. Cells were separated from debris by settling on ice for 30 min, plated onto penut lectin coated glass substrates and maintained in L-15/fetal bovine serum medium.

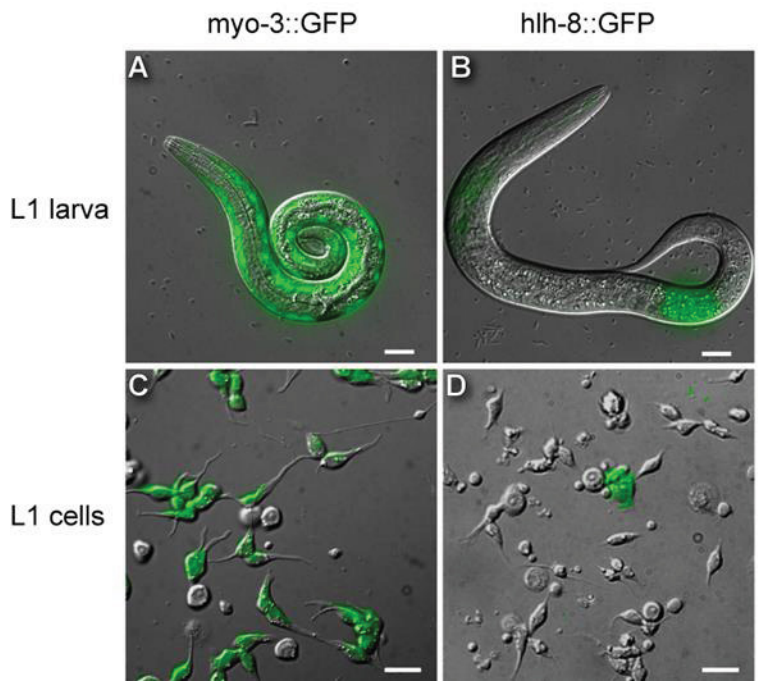

Figure 2.2 Fluorescent and DIC merge micrographs of muscle- or M-lineage-specific GFP expression in L1 larvae and L1 cell isolates

(**A**) L1 worm of strain PD4251/myo-3::GFP, which has nuclear and mitochondrial GFP expression (green) in body wall muscle cells. (**B**) L1 worm of strain NH3402/hlh-8::GFP, which expresses membrane-bound GFP (green) in the M cell (posterior) and a small number of neuron-like cells in the head (anterior). Both animal heads are positioned to the left. (**C**) One-day culture of cells from L1 PD4251/myo-3::GFP. Green shows GFP expression in mostly bipolar, spindle-shaped muscle cells. (**D**) One-day culture of cells from L1 NH3402/hlh-8::GFP. Green shows GFP expression in a squamous-shaped M cell. All scale bars are 10 μm.

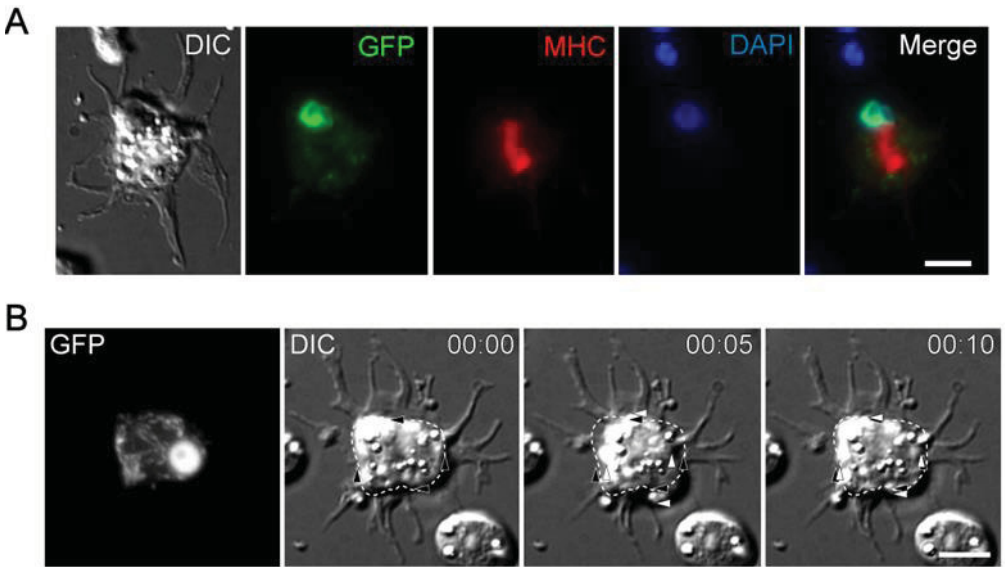

Figure 2.3 Muscle cells from L4 larvae express muscle-specific myosin and spontaneously contract *in vitro*

(**A**) DIC and fluorescence micrographs of fixed muscle cells isolated from L4 stage myo3::GFP worms, which expresses GFP in both nucleus and mitochondria of muscle cells. Cells were immunostained for myosin heavy chain A (MHC-A), and stained for nuclei (DAPI). A wide band of myosin was observed near the cell center. (**B**) Time-lapse DIC series of spontaneous contraction in a muscle cell from myo3::GFP reporter strain. GFP indicates muscle identity. Dotted outlines show cell body shape as at 0 second, and are static throughout the sequence. Arrowheads show edges of cell body. Black arrowheads indicate initial boundary and are static throughout the sequence. White arrowheads indicate the newest cell edge positions. The overall cell shape changes from near rectangular (0 sec) to oval (5 sec) and back to near rectangular (10 sec). Time is in min:sec. Scale bars are 5 µm.

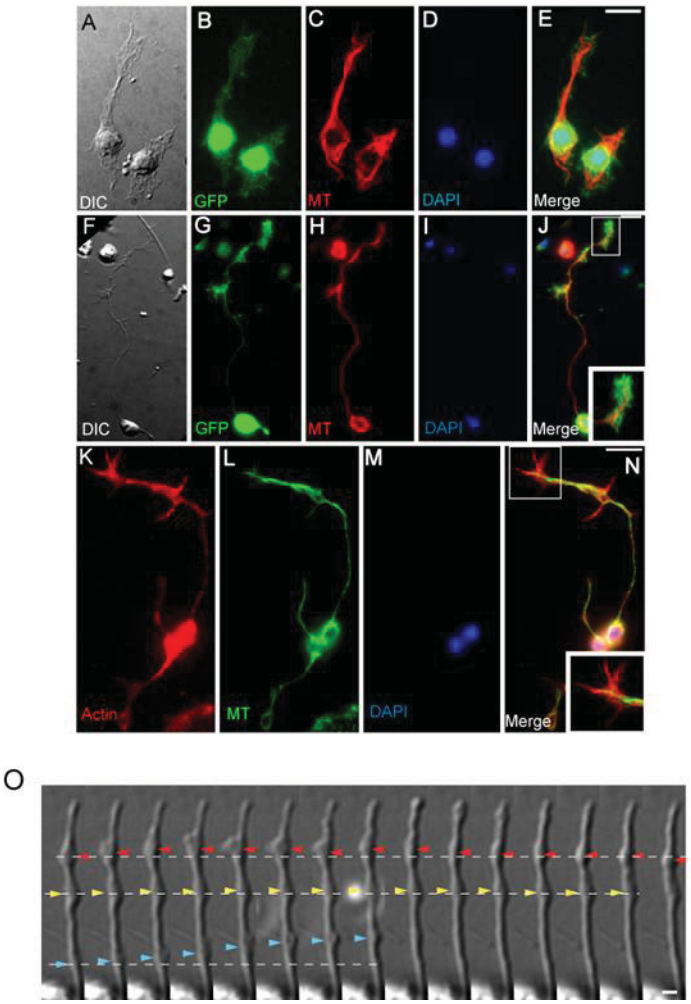

Figure 2.4 Cultured larval neurons extend projections and growth cones in vitro

(**A-E**) Microtubule network and cytoplasmic projections in GFP expressing cells isolated at L1 stage from an unc-119::GFP neuronal maker line. (**A**) DIC image of unc-119::GFP positive cells, (**B**) GFP expression in cell bodies (green), (**C**) anti-tubulin staining showing microtubules (red), (**D**) DAPI staining showing nuclei (blue), and (**E**) merged fluorescent images of fixed cells. (**F-J**) Microtubule network and cellular extensions in GFP expressing neurons after two days in culture. Staining as in A-E. (**J**) Enlarged inset shows a growth cone. (**K-N**) Actin and microtubule networks in neurons isolated from L1 stage N2/wildtype nematodes and fixed after

1 day. (**K**) Rhodamine-phalloidin staining for actin (red), (**L**) anti-tubulin staining for microtubules (green), (**M**) DAPI staining (blue), and (**N**) merged images. Enlarged inset in (**N**) shows actin enrichment in growth cone. Scale bars: 5 μm. (**O**) DIC time-lapse series of cellular activities in the dendrite-like extension process of a neuron isolated from L4 stage worms. Dotted lines represent baseline positions of each of three intracellular motilities. Red arrowheads: appearance and disappearance of a large protrusion. Yellow arrowheads: a relative static protrusion. Blue arrowheads: rapid forward movement of a protrusion. Interval between each frame is 5 sec. Scale bar: 1 μm.

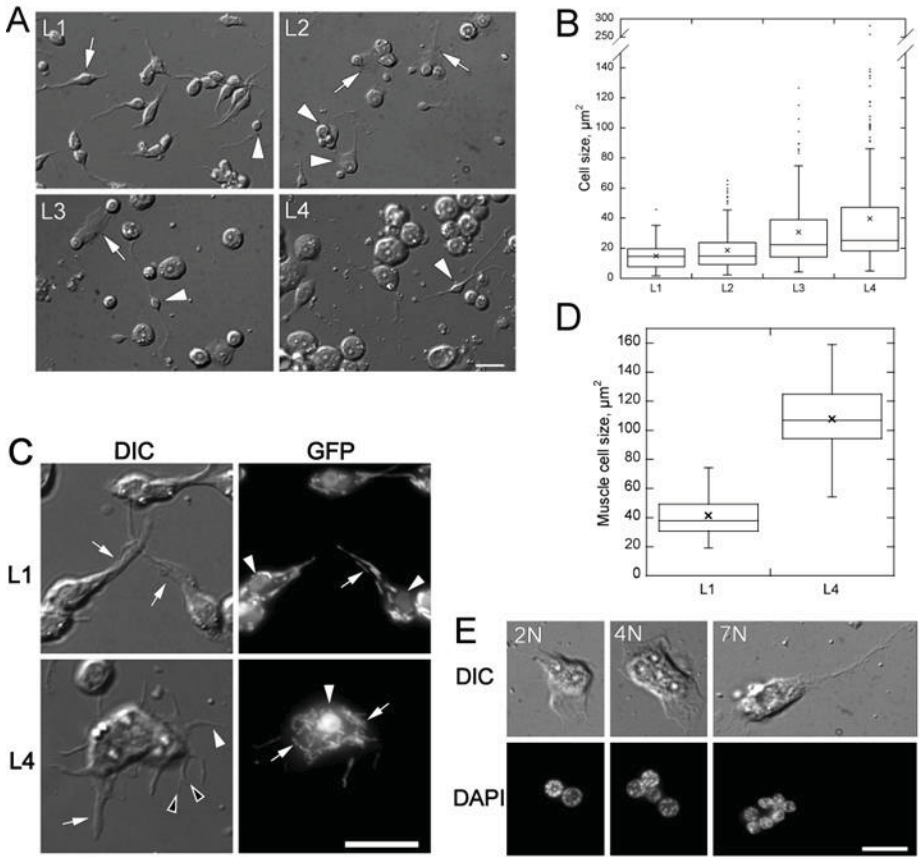

Figure 2.5 Cell sizes increase and cell morphologies vary with larval stage

(**A**) DIC micrographs of cells from L1-L4 worms one day after isolation (stage indicated in each panel). The fraction of large cells increases with larval stage at which they are isolated. Neurons (arrowheads) are found in cultures from all stages. Muscle is the major cell type in L1 isolates (arrow). Large cells from L2-L4 isolates are round with large flat protrusions (arrows). (**B**) Box and whisker plot of distribution of cell area of L1 (n=205), L2 (n=209), L3 (n=176) and L4 (n=238) cells one day after isolation. Central lines and boxes represent median and upper and lower quartiles of each distribution. Whiskers represent the robust range (quartiles ± 1.5x the interquartile distance). Means and outliers are show as crosses and dots. (**C**) DIC and

fluorescence micrographs of L1 and L4 stage GFP positive cells isolated from myo-3::GFP strain, which expresses GFP in the nuclei and mitochrondria of muscle cells. DIC: L1 muscle cells have either one (arrows) or two (not shown) cell processes. L4 muscle cells show multiple cell processes, including wide (arrow), thin (white arrowhead) and bifurcated (black arrowheads) processes. GFP: Cells isolated from L1 and L4 show GFP expression in both nucleus (arrowhead) and mitochondria (arrows). (**D**) Box and whisker plot of distribution of cell area of L1 and L4 muscle cells (L1: n=23; L4: n=19). (**E**) DIC and fluorescence micrographs of fixed multinucleate (DAPI) cells from L4 isolates. Examples of 2, 4, and 7 nuclei (left to right) per cell are shown. All scale bars are 10 μm.

Table 2-1 *In vivo* and *in vitro* frequencies of muscle cells and M lineage cells in L1 larvae

Strain	Marker	L1 Expression pattern	Frequency of cell type	
			in vivo[1]	*in vitro*[2]
PD4251	myo-3::NGFP-lacZ; myo-3::MtGFP	body wall muscles	15%	81 ± 5% (1128, 3)
NH3402	hlh-8::GFP-CAAX	M lineage cells and a subset of head neurons	0.18%	1.0 ± 0.1% (1152, 2)

[1]*In vivo* frequencies were calculated from Sulston and Horvitz [88] based on cell numbers at hatching.

[2]*In vitro* frequencies were measured by counting cells in 5 to 8 random fields of cells plated on peanut lectin one day after isolation. Values given as mean ± error (cells counted, no. of trials).

Chapter 3 Control of sex myoblast migration by Rho family GTPases

ABSTRACT

To migrate anteriorly and remain on the ventral side, *C. elegans* sex myoblast (SM) is controlled by multiple partially redundant signals on the anteroposterior (AP) and dorsoventral (DV) axis. Rho family GTPases transduce guidance signals and directly regulate actin cytoskeleton remodeling underlying directed cell migration. However, the roles of Rho-family GTPases in SM migration are unknown. Here we report a systematic study of three *C. elegans* Racs, MIG-2/RhoG, CED-10/Rac1, and Rac-2/Rac1, and the sole CDC-42/Cdc42 on the control of SM migration. We found that constitutively activating Rho-family GTPases in SMs affect different aspects of SM migration. MIG-2 undergoes fast turnover at SM leading edge during its migration, and activated MIG-2 increases the chance of SM dorsal localization. Dorsal SM mis-localization is enhanced by decreasing wild type (WT) CED-10, and is independent of FGF and SLIT/Robo signals. In contrast, activated CDC-42 anteriorly places SMs while changing the morphology of their ancestral M cell into a more elongated one. These results provide the first evidence of the possible involvement of Rho GTPases in SM migration. Rho GTPases affect actin cytoskeleton through regulating actin binding proteins, such as WASP, an activator of Arp2/3, a branched actin network nucleator. In these series of studies, we also piloted direct characterization of actin dynamics in isolated M cells treated with RNAi against arp-2 and wsp-1/wasp. High-resolution total internal reflection fluorescence (TIFR) microscopy revealed increased actin retrograde flow and reduced cell spreading in arp-2 or wsp-1 knockdown cells, consistent with their roles in actin polymerization observed in other organisms. We demonstrate

how culture and sub-cellular imaging of isolated *C. elegans* cells can be used to directly characterize the effects of actin binding proteins on actin dynamics.

INTRODUCTION

Cell migration is an essential process underlying fundamental events such as gastrulation, neural crest cell migration, and neutrophil chemotaxis. When deregulated, abnormal cell migration contributes to metastatic cancer, neurological disorders, and autoimmune diseases [130]. For a cell to move in a predefined direction, it must extend lamellipodia, the main engine of motility, in a highly coordinated fashion towards the direction conveyed by guidance cues [3, 8]. An important question in understanding cell migration is how cells integrate a variety of extracellular guidance cues to induce changes in actin-dynamics. A critical linker that bridges guidance cues and actin cytoskeleton is the family of Rho GTPases that can induce the formation of various actin-based structures [18, 19, 131].

Rho family GTPases are molecular switches that cycles between an active, GTP-bound form and an inactive, GDP-bound form. GTPase activating proteins (GAPs) inactivate Rho GTPases by promoting GTP hydrolysis, and guanine nucleotide exchange factors (GEFs) catalyze the exchange of GDP for GTP, increasing GTP-bound active Rho GTPases. Mutations that prevent GTP hydrolysis or GTP release increase the proportion of GTP-bound GTPases, leading to constitutively active (CA) Rho GTPases [5] (Figure 3.1 legend). Active Rho GTPases bind to and activate downstream effectors, a major class of which regulates the actin cytoskeleton. For example, two classic members of Rho family GTPases, Rac and Cdc-42, can activate WAVE

and WASP respectively, which then activate Arp2/3 complex to initiate formation of branched actin network in the lamellipodia [6, 131].

Biochemical and cell biology studies have elucidated how Rho GTPases induce the formation of actin-based structures in cultured cells, but their roles *in vivo* have remained unclear [16]. *C. elegans* has a compact genome, transparent body, and fully-mapped cell lineages, which make it an ideal model organism to study the function of Rho GTPases in cell migration. *C. elegans* encode one Cdc-42 Rho GTPase that is important for cell polarity and three Rac subfamily Rho GTPases (CED-10/Rac1, Rac-2/Rac1, and MIG-2/RhoG, a functional equivalent of Rac; Figure 3.1) that are critical in the regulation of cell and axon growth cone guidance [58, 60]. Previous work has shown that the mechanisms of utilizing Rho GTPases are quite diverse among different migration systems. For example, single *ced-10/rac1 (lf)* affects distal tip cell (DTC) migration [61], whereas single *mig-2/rhoG (lf)* results in defective migration of Q lineage cells and coelomocytes [59]; many cell migrations are affected in compound mutants of Rho GTPases than their single mutants [61], illustrating high levels of redundancy among Rho GTPase family members. Both active and inactive Rho GTPases are required for their cellular functions, as loss-of-function and CA mutations confer similar effects on cell migration [60].

Most of the work on Rho GTPases in cell migration has focused on Q neuroblast, DTCs, and axon growth cones. While some of the signaling pathways in sex myoblast (SM) migration have been described, no direct link between chemoattractant and actin dynamics has been found. SM migration is an important step in the formation of a functional reproductive system [27]. Somatic tissues in *C. elegans* reproductive system include vulva and uterus, which are located at the gonad in the middle part of a worm. The 16 muscles that connect uterus and vulval opening are

produced by a pair of SMs, the contraction of which induces egg-laying [45]. SMs are born at the posterior of the worm, where they are derived from a single M cell that migrated during the embryonic stage [28] (Figure 3.2). During the second larval stage (L2), SMs migrate anteriorly and stop at the center of the gonad, where they divide and differentiate into the sex muscles [44].

Along SM migration route, several Pn.p cells in the hypodermis at the medial plane are conveniently used as landmarks [44] (Figure 3.2). Those that are relevant to the study of SM migration include P5.p to P9.p cells from anterior to posterior, and P6.p indicates the middle point of the gonad. At the time of SM migration, the average distance between neighboring Pn.p cells is 20 μm [44], and as the animal grows, the distance can increase to over 40 μm when SMs start to divide. SMs are born approximately midway between P8.p and P9.p cells over ventral muscles on the lateral plane; they migrate for about 4 hours anteriorly, and eventually stop at a position above P6.p cells. In *egl-17/fgf* animals, most SMs stop at a position between P7.p and P8.p; whereas in gonad-ablated animals, the average stopping position expands to include P5.p to P8.p (see below) [48].

On the anteroposterior (AP) axis, at least three mechanisms operate in parallel to control SM migration, which include a gonad-dependent attraction (GDA) [44], a gonad-dependent repulsion (GDR) [47], and a gonad-independent mechanism (GIM) [44]. In GDA, EGL-17/Fibroblast Growth Factor (FGF) and EGL-15/FGF Receptor (FGFR) act upstream of a Ras-Raf-MEK-MAPK/ERK pathway to attract SM to the precise gonad center [49, 52, 53]. This pathway provides the main attraction for the anterior movement. Loss-of-function of pathway members results in posteriorly displaced SMs. Since EGL-17/FGF is mainly expressed by a few cells in the gonad and vulva precursor cells (VPCs) that are induced by the gonad [48], this mechanism

relies on the integrity of the gonad, hence the gonad-dependent attraction (GDA). When the gonad is removed in WT animals, SMs can still travel to a position near the gonad center, albeit less precisely. This GIM is composed of a UNC-71/ADAM-UNC-73/GEF-UNC-53/NAV pathway [49]. Surprisingly, when the gonad is removed in GDA mutants, the premature termination of SM migration is relieved, suggesting normally there is repulsion from the gonad that inhibits SM migration, and this GDR may use UNC-6/Netrin and MAB-20/Semaphorin guidance systems [48]. Thus, during SM migration, GIM functions to allow SMs to move to an approximate position near gonad center, and later GDA and GDR finely position SMs to the precise gonad center. On the dorsoventral (DV) axis, SMs are restricted to the ventral side redundantly by FGF and SLIT/Robo signaling [48]. SM migration is robustly controlled, in that single gene loss-of-functions usually do not affect its migration. This highly redundant system illustrates multiple guidance mechanisms in action, thus can deepen our understanding of how different signals are integrated.

In this study, we used gain-of-function approach to systematically investigate the involvement of MIG-2/RhoG, CED-10/Rac1, Rac2/Rac1, and Cdc-42/Cdc42 in controlling SM migration. We found that activating different Rho GTPases has different effects on AP axis and DV axis, with MIG-2 CA and CED-10 affecting DV localization and CDC-42 CA affecting AP migration. Dorsal migration caused by MIG-2 CA is independent of EGL-15/FGFR, SAX-3/SAX3, and SLT-1/SLIT. Thus, this mutation may increase the propensity for dorsal migration rather than being directly involved in guidance. We also found that consistent with their functions in other organisms, Arp2/3 and WASP are involved in actin polymerization in cultured M cells. Our results have started to elucidate the function of Rho GTPases in regulating SM cell

migration, and provide valuable information for future studies on this highly redundant migration system.

RESULTS

MIG-2 accumulates at the leading edge during SM migration

Endogenous MIG-2/RhoG is expressed in SMs [59], suggesting possible roles of MIG-2/RhoG in SM migration. To determine the subcellular localization of MIG-2/RhoG in SM, we constructed an mCherry-mig-2 fluorescent fusion under the control of hlh-8 gene promoter that directs the expression of this transgene specifically in the M lineage cells, including SMs. The CAAX (A for aliphatic amino acids and X for any amino acids) motif of Rho family GTPases at the carboxyl terminus targets small GTPases to the cell membrane where they activate downstream effectors [132]. To preserve this membrane-targeting capacity, we placed mCherry fluorescent tag to the N-terminus of MIG-2/RhoG, leaving the C-terminus intact. When crossed to a strain carrying hlh-8::GFP-CAAX with known GFP localization to the membrane (Figure 3.3(**C**)), mCherry-MIG-2 completely co-localized with the GFP signal, demonstrating the full functionality of its membrane-targeting signal.

In vivo live cell imaging of SM during its migration revealed that MIG-2 accumulates at the cell leading edge towards its direction of movement. SMs migrate anteriorly on the ventral muscles, and we observed that SMs actively extend lamellipodia and lamella with interspersed filopodia at the front of cells as they move over underlying muscle cells (Figure 3.3(**A**)). During this process, MIG-2 at the leading edge undergoes faster turnover, as stronger fluorescence intensity remains at the cell front compared to the back of the cell while the fluorescent protein

undergoes photo-bleaching (Figure 3.3(**B**)). Together, the dynamic behavior of MIG-2 at the leading edge of migrating SM is consistent with its potential role in regulating SM migration.

Mig-2(CA) and ced-10 (lf) act synergistically to control SM dorsoventral localization

To investigate whether mig-2 functions cell-autonomously in SMs to control their migration, we introduced a mig-2 mutation G16V into the hlh-8::mCherry-mig-2 transgene (Figure 3.1). Glycine at position 16 is located in the P-loop region of small GTPases that is important for GTP hydrolysis [61, 133], and corresponding mutation of G12V in K-Ras renders the GTPase constitutively active (CA) [134]. A similar mig-2 G16R CA mutation, when expressed specifically in vulval cells, leads to their migration defects due to activated mig-2 [135]. In contrast, SM migration on the anteroposterior (AP) axis was essentially WT in *mig-2(G16V)* as all SMs arrived at the gonad center (Figure 3.6); however, mCherry-*mig-2(G16V)* caused 7% of SMs to locate to abnormal dorsal or dorsoventral midline positions instead of a ventral position (Figure 3.4(**A**)), suggesting a role for mig-2 in regulating dorsoventral (DV) guidance. In accordance with a role of mig-2 in dorsal mis-localization, activated mCherry-MIG-2 became concentrated on the dorsal surface of dorsally localized SMs, in contrast to its normal localization on the ventral surface when SMs are ventrally localized (Figure 3.4(**B**)). DV guidance defect in mCherry-*mig-2(G16V)* increased to 39% when hlh-8::mCherry-*mig-2(G16V)* transgenic animal was crossed to a gain-of-function (gf) allele *mig-2(gm38)* (Figure 3.4(**A**)). This enhancement could be due to complete elimination of WT mig-2 in the double mutant compared to the hlh-8::mCherry-*mig-2(G16V)* transgenic animal, in which endogenous WT mig-2 was not altered and still functions in the presence of *mig-2(G16V)* transgene. Alternatively, *mig-2(gm38gf)* allele could cause certain non-SM-autonomous changes that affect SM migration, as

mig-2(gm38gf) animals have a plethora of developmental defects [59] whereas hlh-8::mCherry-*mig-2(G16V)* transgenic animals were generally normal.

The weak- to intermediate-DV defects observed in hlh-8::mCherry-*mig-2(G16V)* and *mig-2(gm38gf)* animals suggest the possibility that other genes that are functionally related to mig-2 might also be involved. Ced-10/rac1 is a good candidate as it functions redundantly with mig-2 in many processes, including cell migration, and double loss-of-function (lf) of both genes is embryonically lethal compared to the near-WT appearance of single lf mutants of either gene [61]. Consistent with this, *ced-10(n1993lf)* animals have normal SM migration, and a hlh-8::mCherry-*ced-10(G12V)* CA transgene did not cause any SM migration defects on either body axis. Interestingly, when hlh-8::mCherry-*mig-2(G16V)* was crossed with *ced-10(n1993lf)*, 23% of SMs migrated dorsally (Figure 3.4(**A**)), a three-fold increase over dorsal mis-localization in hlh-8::mCherry-*mig-2(G16V)* alone. This combined effect indicates that mig-2/rhoG and ced-10/rac1 interact synergistically to affect SM DV guidance.

Decoupling of AP and DV control of SM migration in mig-2(gf) mutants

Guidance of SMs on the AP axis and DV axis appear to have overlapping as well as independent pathways. In fact, the first mutants displaying DV localization abnormalities identified were initially known for their involvement in AP guidance. For example, gain-of-function mutation of *let-60/ras* lead to a small percentage of SMs to localize at non-ventral positions, in addition to its ability to partially rescue premature termination of SM on the AP axis in *egl-15/fgfr* mutants [52, 53]. Although the connection between activated LET-60/Ras and SM dorsal localization is unclear, this suggests that removing FGF signaling compromises ventral

restriction as well as AP guidance. Supporting this, loss-of-function of *sax-3/robo*, the SLIT-1 receptor for dorsal repulsion, results in 53% non-ventral SMs in *egl-17/fgf* [48]. Interestingly, dorsally localized SMs migrate to the same extent on the AP axis as do the ventral SMs in *sax-3; egl-17* double mutants [48], indicating that SMs on the dorsal side and ventral side respond equally well to the remaining AP guidance cues. Thus, in the current model of ventral restriction, FGF emanating from the ventral side of the mid body serves dual functions to attract SMs anteriorly as well as ventrally, in parallel to dorsally expressed SLIT that presumably prevents SMs from moving dorsally.

To explore possible interplay between mig-2 and guidance cues in ventral restriction, we used RNAi to knockdown egl-15/fgfr in *mig-2(gf)* mutants displaying non-ventral SMs. There had been ambiguities in the efficiency of RNAi in M lineage cells [105], and we found that RNAi against mCherry gene efficiently knocked down mCherry transgene expression in SMs (not shown). Thus, RNAi by feeding of genes expressed in SM is a powerful alternative to genetic mutations in studying SM migration. Similar to loss-of-function of *egl-15* mutation, RNAi against egl-15 resulted in posteriorly localized SMs compared to normal AP SM localization in control RNAi (Figure 3.5(**A**)). Surprisingly, dorsal localization in *mig-2(gf)* mutants seemed to be independent of FGF signaling, as reducing egl-15/fgfr did not affect the percentage of dorsally located SMs (Figure 3.5(**B**)). Conversely, expression of activated mig-2 did not affect AP migration in egl-15 RNAi, as the AP range of SMs were undistinguishable whether they were located dorsally or ventrally (Figure 3.5(**C**)). Similar results were found for slt-1 and sax-3 RNAi knockdown (Table 3-1; see Discussion). Based on these findings, it is likely that activating mig-2 induces novel activities of SMs that increase their propensity to move

away from the ventral side regardless of the presence of their normal ventral restriction signals; however, this new activity is not sufficient to overcome AP guidance cues to alter SM AP positions.

Cdc-42 affects SM AP localization and M cell morphology

We systematically constructed hlh-8::mCherry-*rho GTPase* transgenes to include both constitutively active and WT versions of ced-10/rac1, mig-2/rhoG, rac-2/rac2, and cdc-42/cdc42. All of the constitutively active versions include a single amino acid change that compromises GTP hydrolysis activity (Figure 3.1). Transgenes were introduced to animals through gene bombardment, and integrated lines were selected and their expression pattern examined. All transgenic animals used in this study have mCherry expression in the M lineage, and a few cells in the head, some of which appear to extend axon-like structures on the ventral side. This expression pattern is consistent with previously reported hlh-8 promoter expression pattern [107].

To quantify SM position along the AP axis, images were taken at L3 stage when SMs have completed their migration and started dividing. SM final position was determined as midway along divided daughter cells, and position zero was defined by the middle point of divided P6.p cells (Figure 3.2). Thus a positive final localization indicates a more anterior placement and a negative one a more posterior placement.

Among all mCherry-*rho GTPase CA* mutants, only mCherry-*cdc-42 CA* conferred a statistically significant change in SM final position. The remaining CA and WT Rho-GTPases tested appeared normal in their SM final position along the AP axis (Figure 3.6). In mCherry-*cdc-42 CA* animals, SMs moved to a slightly more anterior position, 2.7 μm more advanced

compared to GFP WT and mCherry-cdc-42 WT control on average. Given that the average distance between Pn.p cells is 20 μm, this slight difference still makes SM fall within the P6.p compartment, which is not sufficient to cause adverse physiological consequences. Nevertheless, in the context of multiple redundant guidance mechanisms, this result makes Cdc-42 stand out as a specific Rho GTPase that can impact AP migration.

Cdc-42 is a major mediator of *C. elegans* embryonic polarity [136], and we found that mCherry-*cdc-42 CA* affected M cell morphology. M cell is the ancestor of the M lineage, and it gives rise to several postembryonic muscle cells, coelomocytes, as well as the SMs. WT M cells assume a near spherical shape at L1 stage, whereas in mCherry-*cdc-42 CA* animals, 40% of M cells became elongated, extending long, wide protrusion either anteriorly or posteriorly . Since the general morphology of SMs in mCherry-*cdc-42 CA* appeared normal, the significance of the change of M cells has on SM migration is unknown.

Arp2/3 and WASP are involved in M cell actin retrograde flow and spreading

Guidance signals transduced through Rho GTPases eventually activate WASP-family nucleation promoting factors, major activators of branched actin network nucleator Arp2/3 complex [3, 137]. These actin regulators are essential for cell movement, and loss-of-function mutations lead to embryonic lethality [65, 138, 139]. To bypass the embryonic lethality, we isolated and cultured M cells, and used RNAi against these genes to knock down their expressions. This *ex vivo* system allowed us to use high resolution total internal reflection fluorescence (TIRF) microscopy to follow and quantify actin dynamics, which is difficult for intact animals. Actin dynamics were followed by mEGFP tagged calponin homology (CH)

domain of human Utrophin, which selectively binds to polymerized actin (actin filaments) but not to actin monomers, thus reducing background fluorescence [140]. This marker faithfully labels actin filaments in the lamella and lamellipodia (Figure 3.8(**B**)).

In culture, M cell adopted a pancake-like shape on peanut lectin and actively extended and retracted protrusions, which was similar to their activities *in vivo* (Figure 3.8(**A**)). Actin filaments in M cell periphery exhibited prominent retrograde flow, or flow towards cell center (Figure 3.8(**C**)). To measure retrograde flow, we implemented algorithms that allow automated analysis of flow dynamics (Figure 3.9(**A**)) [141]. We found that RNAi against arp-2/arp2 or wsp-1/wasp increased, rather than decreased, actin retrograde flow speed and reduced the cell spreading area (Figure 3.9(**B**)). In resting cells, actin network polymerizes against cell membrane at the cell periphery, and when the coupling of actin network and the substratum is loose, force generated by actin polymerization is balanced by actomyosin contraction towards the cell center [7]. Thus, the increased actin retrograde flow speed we observed may be due to reduced actin polymerization caused by lowered levels of Arp2 or WASP, which is consistent with their roles in promoting actin polymerization. Reduced force from actin polymerization would result in reduced force against the cell membrane, thus explaining reduced cell area/spreading. Our results demonstrate that *C. elegans* WASP and Arp2/3 have conserved function in promoting actin polymerization in M linage cells.

DISCUSSION

Our understanding of the role of Rho family GTPases in the control of SM migration has been very limited, partly due to the complex regulatory mechanisms that operate in parallel to

direct SMs [48], and partly due to the redundancy among Rho family members that has been commonly seen in *C. elegans* [61]. In many cases, in order to disrupt SM migration, components of multiple guidance mechanisms must be compromised. On the other hand, single loss-of-function of mig-2/rhoG has no effect on SM migration [59], and that of ced-10/rac1 likely does not affect SMs from the lack of egg-laying defective phenotype in this mutant [61].

In this study, we used gain-of-function approach to manipulate three Rac subfamily members and one Cdc42 directly in SMs, to reveal cell autonomous effects of these four Rho GTPases on the migration of SMs on different body axes. We found that Cdc-42(CA) displaced SMs slightly anteriorly, whereas other tested Rho GTPases did not affect AP positioning of SMs. On the DV axis, however, we found that MIG-2/RhoG (CA) caused dorsal localization of SMs, and this DV defect was enhanced when combined with *ced-10(lf)* and *mig-2(gf)*. Subcellular localization of MIG-2 to the leading edge of migrating SMs is consistent with its role in directing SM migration, but this function seemed to be independent of FGF signaling and SLIT/Robo signaling. Our results revealed the distinct roles of different Rho family members in regulating separate aspects of SM migration, indicating that AP and DV guidance can be decoupled on the Rho GTPase level, possibly reflecting different guidance cues that are utilized.

Guidance of SM on the AP axis

The molecular identities of components operating in GDA, GIM and GDR suggest that different guidance systems are used: EGL-17/FGF in GDA, UNC-71/ADAM in GIM, and MAB-20/Semaphorin and possibly UNC-6/Netrin in GDR. It is interesting to note that these different guidance systems bear different weights on the outcome of SM migration. For example, single loss-of-function of *egl-17/fgf*, or *egl-15/fgfr*, or its downstream Ras pathway, causes the most

severe phenotype of premature termination of SM migration; in contrast, disruption of GIM components alone has no effect on SM migration. Similar to GIM, compromising genes in GDR alone does not affect SM migration either, and its significance remains unclear. These guidance molecules could affect actin cytoskeleton remodeling to direct SM migration. However, despite the importance of GDA, extensive genetic screens have not found molecules directly link to the actin cytoskeleton in GDA. Based on this observation, it is possible that at least one major function of the FGF signaling in GDA is to allow the expression of molecules that make SMs capable of responding to guidance signals. The major downstream pathway of FGF in SM migration is the Ras-Raf-MEK-MAPK/ERK kinase cascade, and in vulva morphogenesis, a similar Ras pathway downstream of EGF activates the expression of guidance molecules in the Semaphorin pathway, which then act in parallel to a UNC-73/Rac GEF-CED-10/Rac1/MIG-2/RhoG pathway to regulate vulval cell migration [142]. Our results that constitutively active Racs and Cdc42 do not or only mildly affect SM migration on the AP axis indicate that these Rho GTPases are not likely to directly mediate FGF signaling downstream of Ras.

Although we cannot rule out the possibility that the FGF pathway has other undiscovered direct actin remodeling functions, current evidence suggests that at least some instructive cues that control actin dynamics lie in GDR and GIM. Two canonical guidance cues, Netrin and Semaphorin, are implied in GDR. Netrin is expressed mainly on the ventral side, including ventral nerve cord, muscles and vulval cells [143]. Depending on whether cells express UNC-40/DCC or UNC-5 Netrin receptor, Netrin could mediate attraction or repulsion. CED-10/Rac1 acts downstream of Netrin to remodel actin cytoskeleton [144], and MIG-2/RhoG can modulate the subcellular localization of UNC-40/DCC [145]. Although MAB-20/Semaphorin 2A is not as

well studied in *C. elegans*, Semaphorin 1 in the same family is expressed in the tail region, and mediates attraction in the presence of normal levels of CED-10/Rac1 and MIG-2/RhoG, and repulsion through UNC-33/CRMP when their levels are low [146]. In GIM, UNC-73/Rac GEF and UNC-53/NAV that participates in Arp2/3 activation probably act downstream of extracellular matrix protease UNC-71/ADAM to mediate migration of SM to a coarse final position near gonad center [49, 55]. This strongly suggests a possible involvement of Rho GTPases in GDR and GIM. Given the predominance of GDA over the two, it is not surprising that constitutively activating Rho GTPases in these putative pathways did not yield detectable SM migration defects. Taken together, our experiments of constitutively active Rho GTPases on SM migration on the AP axis suggest possible involvement of these Rho GTPases in GDR and GIM, but not directly in GDA.

Guidance of SM on the DV axis

FGF and SLIT/Robo pathways act in parallel to restrict SM migration on the ventral side. Unlike the predominant role of FGF on the AP axis, *egl-17/fgf (lf)* alone does not confer DV localization defects; similar is true for *sax-3/robo (lf)*. Only simultaneous disruption of both signals lead to ~50% dorsal localization, suggesting complete randomness of SM migration on the DV axis [48]. In contrast, in our experiments, activating MIG-2/RhoG alone yields ~40% of dorsal SMs in the most severe case. This is a relatively strong phenotype, given that it often takes double mutations of other genes to give a comparable or even less severe defect. Failure to remain on the ventral side could be due to the weakening of ventral attraction or dorsal repulsion, conversion of ventral restrictions to dorsal ones, or activation of new pathways that overcomes normal ventral restrictions. The absence of genetic interactions between *mig-2(gf)* and egl-

15/fgfr suggests the latter – that activating MIG-2/RhoG could confer a new activity that increases SM's propensity to move towards the dorsal side. This activity seems to be independent of AP guidance, since SMs on the dorsal side and those on the ventral side in *mig-2 (gf)* mutants have similar AP distributions when egl-15 is knocked down. Similar to egl-15 knockdown, RNAi against sax-3/robo or slt-1/slit did not affect DV positioning in mig-2 and/or ced-10 mutants. Since the efficiency of these RNAi treatments was not verified, lack of effects in slt-1 or sax-3 RNAi could be due to insufficient knockdown of their expression. Future inclusion of positive controls that confer known phenotypes in slt-1 or sax-3 knockdown could aid in monitoring RNAi efficiency and determining the interaction of mig-2 with slt-1 and sax-3. Nonetheless, the different responses of DV guidance and AP guidance to activating mig-2 suggest more robust mechanisms on the AP axis than on the DV axis that guard against abnormal migration.

Loss-of-function of Rho GTPases often has similar phenotypes to gain-of-function mutants, indicating requirements of both inactive and active versions of Rho GTPases during normal cell migration [60, 147]. Thus, it is the turnover of Rho GTPases that is important for dynamic actin remodeling underlying rapid cell morphological changes during migration. During normal SM migration, we observed fast turnover of MIG-2 at the leading edge compared to that at the trailing tail. Shifting the pool of activated MIG-2/RhoG through constitutive active mutations likely contribute to the DV defects. CED-10/Rac1 often has redundant roles with MIG-2/RhoG, and we found that decreasing CED-10/Rac1 in *mig-2(gf)* enhances the DV defects, which could be due to a compromised ability to buffer against overly activated MIG-2/RhoG.

In conclusion, through a systematic study of activated Racs and CDC42 Rho GTPases in *C. elegans*, we found that different Rho GTPases affect distinct aspects of SM migration, with Cdc-42/CDC42 in AP migration, and MIG-2/RhoG and CED-10/Rac1 in DV positioning. From a technical perspective, we showed that RNAi can be used effectively to knock down gene expression in the M lineage *in vivo*, and when combined with *C. elegans* cell culture, this can be used to investigate changes on the subcellular level with unprecedented resolution.

Together with previous genetic analysis of SM migration, our results suggest that SM migration has evolved to become a highly robust system, possibly due to its essential role in ensuring propagating large cohorts of offspring. To fully understand the control of SM migration, we need to use different approaches to overcome the redundancy problem. For example, ectopic expression of putative guidance cues can be used to elucidate instructive versus permissive functions, and under these conditions, genetic mutations can be used to screen for disruption of these guidance interactions. RNAi against essential molecules such as Arp2/3 at larval stages would overcome the early lethality problem, and when combined with genetic mutations, they can together disrupt expression of multiple genes, enabling epistatic analysis to order genes into pathways, which would otherwise be difficult to perform due to the high level of redundancy.

MATERIALS AND METHODS

C. elegans strains and culturing

Nematode strains were maintained as described [148]. All experiments were performed at 20°C. The following *C. elegans* strains were used: N2 (wild type), NH3402 [hlh-8::gfp-caax] (kindly provided by M. Stern), NG2475 [*mig-2(gm38)*], and MT5013 [*ced-10(n1993)*].

Transgenic strains were generated by gene bombardment as described [128] and stable lines were selected.

Molecular biology

hlh-8::mCherry-rho gtpase constructs: Customized Gateway® (Invitrogen, Carlsbad, CA) destination vectors was constructed by including hlh-8 promoter ligated to mCherry (pAA65, kindly provided by K. Oegema) sequence and let-858 3'UTR to flank the Gateway® cassette. WT and mutated ced-10, mig-2, and rac-2 coding sequences were obtained by PCR amplification from the following plasmids: pEL209 (ced-10 WT), pEL158 (ced-10 G12V), pEL188 (mig-2 WT), pEL214 (mig-2 G16V), pEL238 (rac-2 WT), and pEL242 (rac-2 G12V) (all kindly provided by E. Lundquist). The resulting PCR fragments were used to generate Gateway® entry clones. These clones, together with cdc-42 entry clones [pDA32 (cdc-42 WT) and pDA34 (cdc-42 Q61L), kindly provided by J. Nance] were recombined with customized hlh-8::mCherry Gateway® destination vector to generate hlh-8::mCherry-rho WT and CA expression clones.

hlh-8::mEGFP-UtrCH construct: mEGFP was generated by introducing A206K mutation in EGFP contained in L3522 plasmid from Fire lab vector kit (Addgene, Cambridge MA) using QuikChange II XL Site-Directed Mutagenesis Kit (Agilent Technologies, Santa Clara, CA). Human Utrophin Calponin Homology (UtrCH) domain was PCR amplified using primers reported in [140] from human cDNA library. hlh-8 promoter was PCR amplified from *C. elegans* genomic DNA. let-858 3'UTR was PCR amplified from L3786 plasmid from Fire lab vector kit (Addgene, Cambridge MA). The above PCR amplified fragments were ligated into modified L3522 (mEGFP) vector to generate hlh-8::mEGFP-UtrCH expression clone.

Analysis of SM migration

Animals were grown to L3 stage and mounted on 5% agrose pad in 2-3 µl of M9 containing 1 mM levamisole, and DIC and epifluorescence images were taken using Olympus IX81 inverted microscope (Olympus, Center Valley, PA). Images were acquired with 60× objective (UPlanSApo, NA = 1.40, Olympus) or 100× objective (Apo N, NA = 1.49, Olympus). For each worm, images of SM planes and Pn.p planes were taken, and fluorescence channel of SM image was merged with DIC channel of Pn.p image to allow measurement of their vertical distance. All image processing was done in ImageJ, available at http://rsbweb.nih.gov/ij.

RNA interference

RNAi feeding plasmids were generated by cloning cDNA of target genes into pL4440 RNAi vector or obtained from Ahringer RNAi library. Plasmids were sequenced to verify sequence correctness. RNAi plasmids were transformed into HT115 *E.coli* and 3 ml culture with ampicillin (100 µg/ml) was grown overnight to 1.5 OD600. 200 µl of overnight culture was mixed with IPTG to a final concentration 0.5 mM, seeded onto NGM plates containing ampicillin (100 µg/ml) and IPTG (1 mM), and induced for 16 hours at room temperature. Synchronized L1 was seeded onto freshly prepared RNAi bacteria and grown to L3 stage at 20°C. RNAi efficiency was verified by RNAi against ama-1, and empty pL4440 plasmid was used as negative control.

For arp-2 and wsp-1 RNAi on cultured cells, dsRNA was synthesized and applied to cell culture as described in [74].

Cell culture and TIRF microscopy

Primary embryonic cell culture was performed as described in [149] using hlh-8::mEGFP-UtrCH animals. Images were taken with Olympus CKX41 tissue culture microscope (Olympus, Center Valley, PA) equipped with a 60×1.49 NA TIRF objective. Time-lapse images were analyzed using software developed by J.K.

ACKNOWLEDGEMENTS

We thank Diya Banerjee for advice and access to resources. We thank Romy Fajardo and Rod La Foy for help with data collection and analysis. We thank Michael J. Stern for the generous gift of *C. elegans* strains. Some strains were provided by the CGC, which is funded by NIH Office of Research Infrastructure Programs (P40 OD010440). We thank Erik A. Lundquist, Jeremy F. Nance and Karen Oegema for kindly providing plasmids. This work is supported by Burroughs Wellcome Fund Interfaces in Science Career Award (Award 1003964) to J.K. S.Z. is a recipient of Virginia Tech Institute for Critical Technology and Applied Science Doctoral Scholars Assistantship.

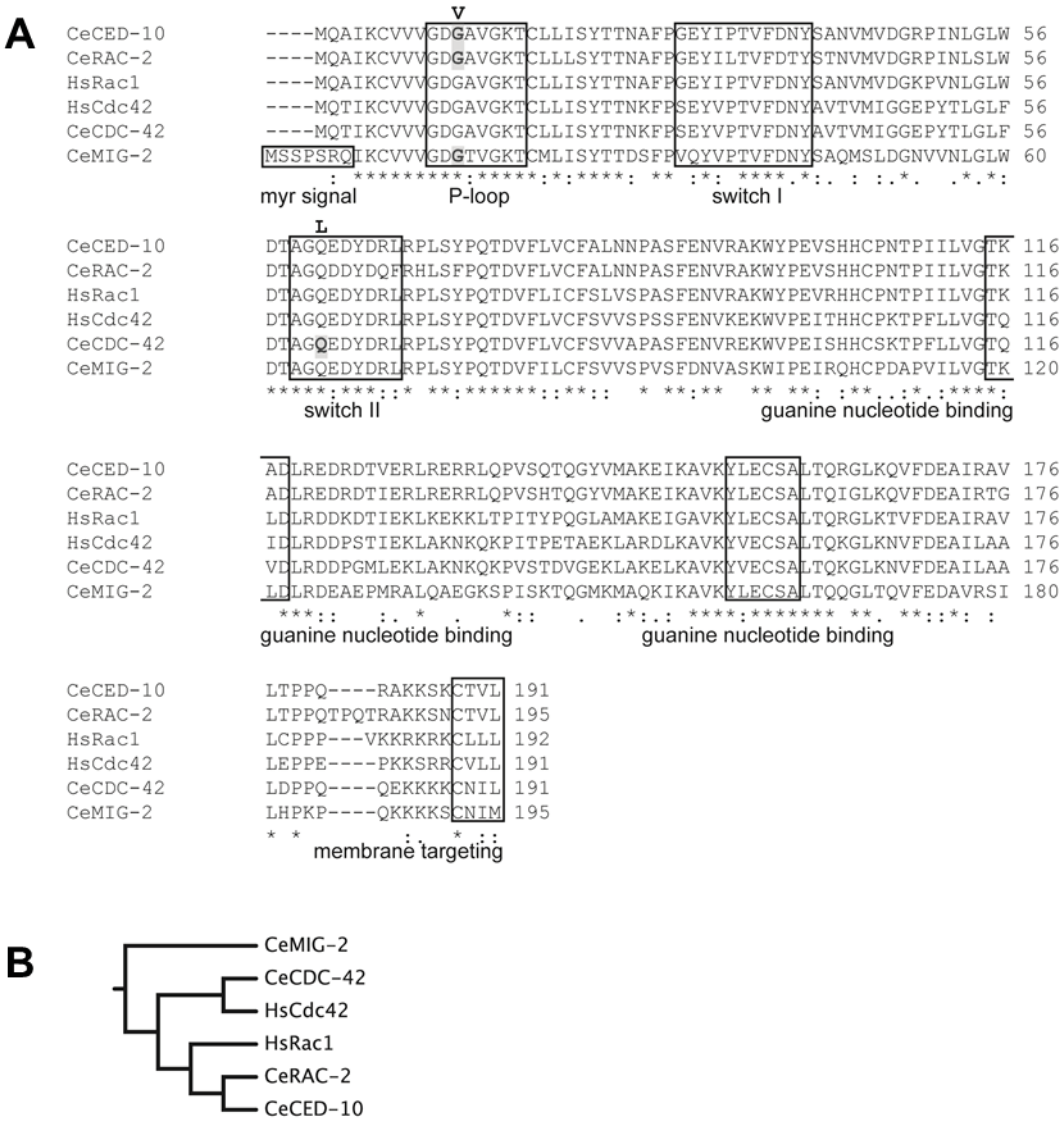

Figure 3.1 *C. elegans* RAC and CDC-42 sequence analysis

(**A**) Sequence alignment of *C. elegans* (Ce) Rho GTPases (CeCED-10, CeRac-2, CeMIG-2 and CeCDC-42) and human (Hs) Rho GTPases (HsRac1 and HsCdc42). Boxed regions indicate conserved residues (except myristoylation signal in CeMIG-2 that is post-translationally modified) that are important for GTPase catalytic activity and subcellular localization [61, 133]. The P-loop binds α- and β-phosphate groups, and switch II is responsible for γ-phosphate

binding. Amino acids substituted in this study are indicated by shaded bold letters, and they are replaced by amino acids above the sequences. G12V (G16V for CeMIG-2) of Racs in the P-loop and Q61L of Cdc-42 in switch II decrease GTP hydrolysis and render Rho GTPases constitutively active. CAAX domain at the C-terminus is post-translationally modified for membrane targeting of Rho GTPases. (**B**) Cladogram showing the relationship among CeCED-10, CeRac-2, CeMIG-2, CeCDC-42, HsRac1 and HsCdc42. There is no CeMIG-2 homolog in humans, and it is a functional equivalent to Racs.

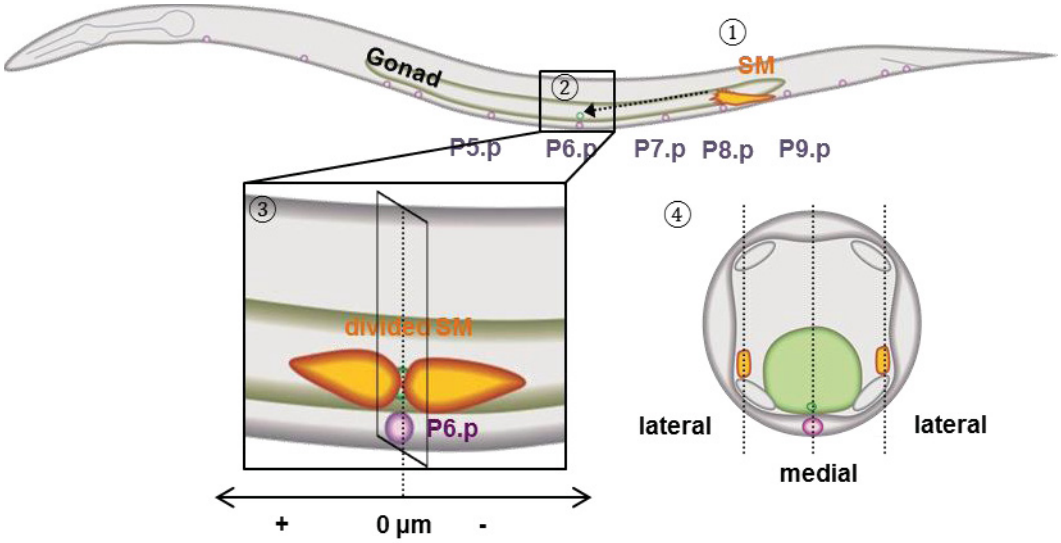

Figure 3.2 Schematic diagram of sex myoblast migration

A *C. elegans* at the stage of SM migration is shown with anterior to the left and ventral side down. Gonad (outlined in green) is in the middle of the animal, below which are Pn.p cells (purple circles). SMs (yellow) shown at ① are born at the posterior between P8.p and P9.p, and migrate to P6.p shown at ②; P5.p to P9.p cells from anterior to posterior indicate approximate range of SM migration in mutant animals. ③ is an enlarged view of ② at a later stage when SMs have completed migration and start to divide. The middle point of divided SMs (two yellow teardrop shapes) is used as SM final position and its vertical distance to P6.p is measured. ④ shows a cross section view from an imaginary plane at ③. SMs migrate on either side of the animal (lateral plane) on the ventral muscle cells (gray ovals), whereas P6.p cell (purple circle) and gonad (green outline) are at the medial plane.

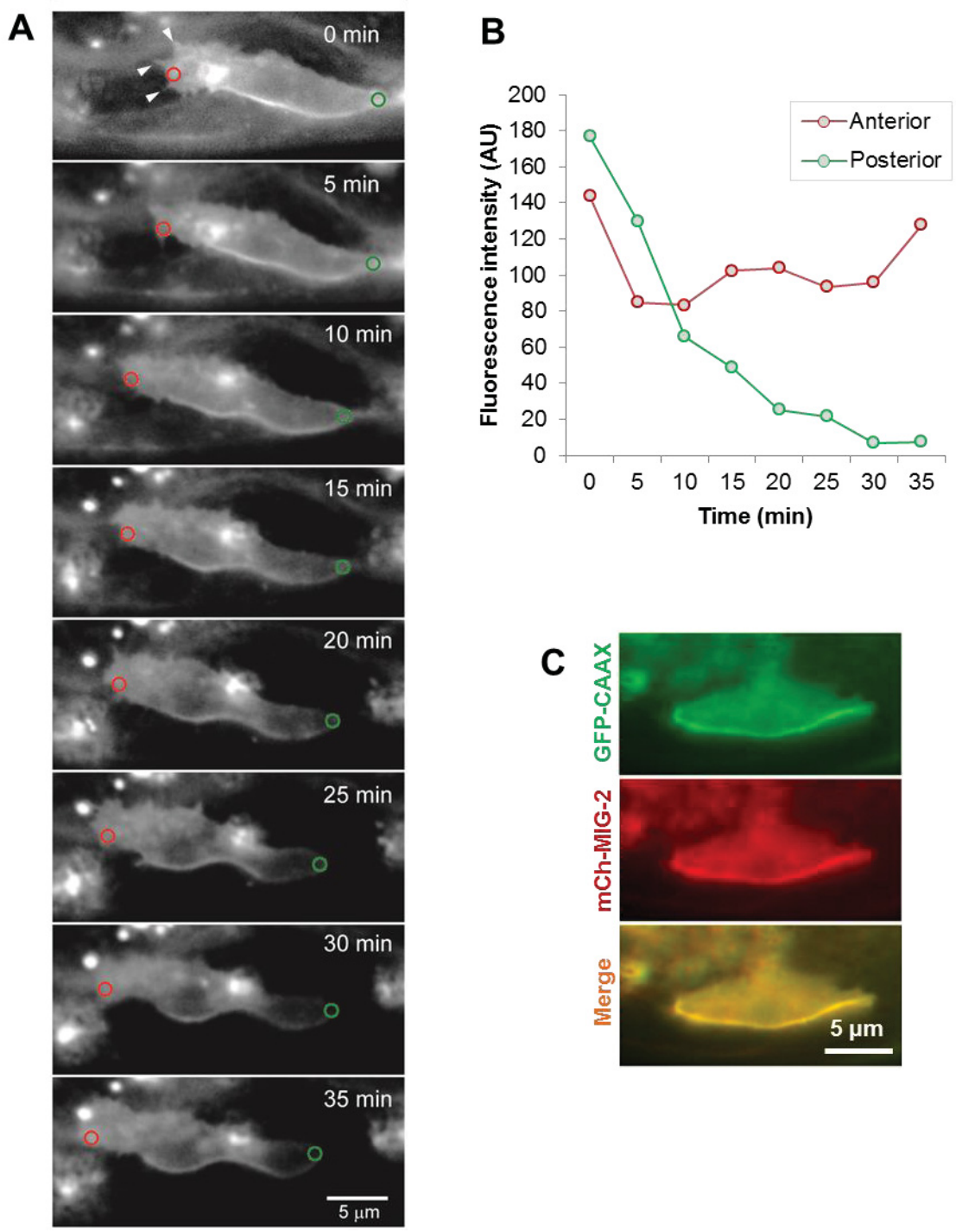

Figure 3.3 MIG-2 concentrates at the leading edge during SM migration

(**A**) Time-lapse series of a migrating SM *in vivo*. Anterior is to the left and ventral down.

SM is labeled with mCherry-MIG-2 (WT). SM is migrating to the left. Arrow heads indicate filopodia extending from the lamellipodia. MIG-2 at the leading edge is more resistant to photobleaching than that at the rear. Red circles at the cell front and green circles at the cell back are used to measure mCherry-MIG-2 fluorescence intensity shown in (B). (**B**) Quantification of fluorescence intensity at the cell front and rear from red and green circles in (A) over time during SM migration. Fluorescence intensity at the cell front remains at a high level, whereas that at the cell rear decreases dramatically over time. (**C**) MIG-2 localizes to the cell membrane in SM. Green is GFP-CAAX that labels cell membrane, and overlaps with red signal by mCherry-MIG-2, as shown in the merge (yellow).

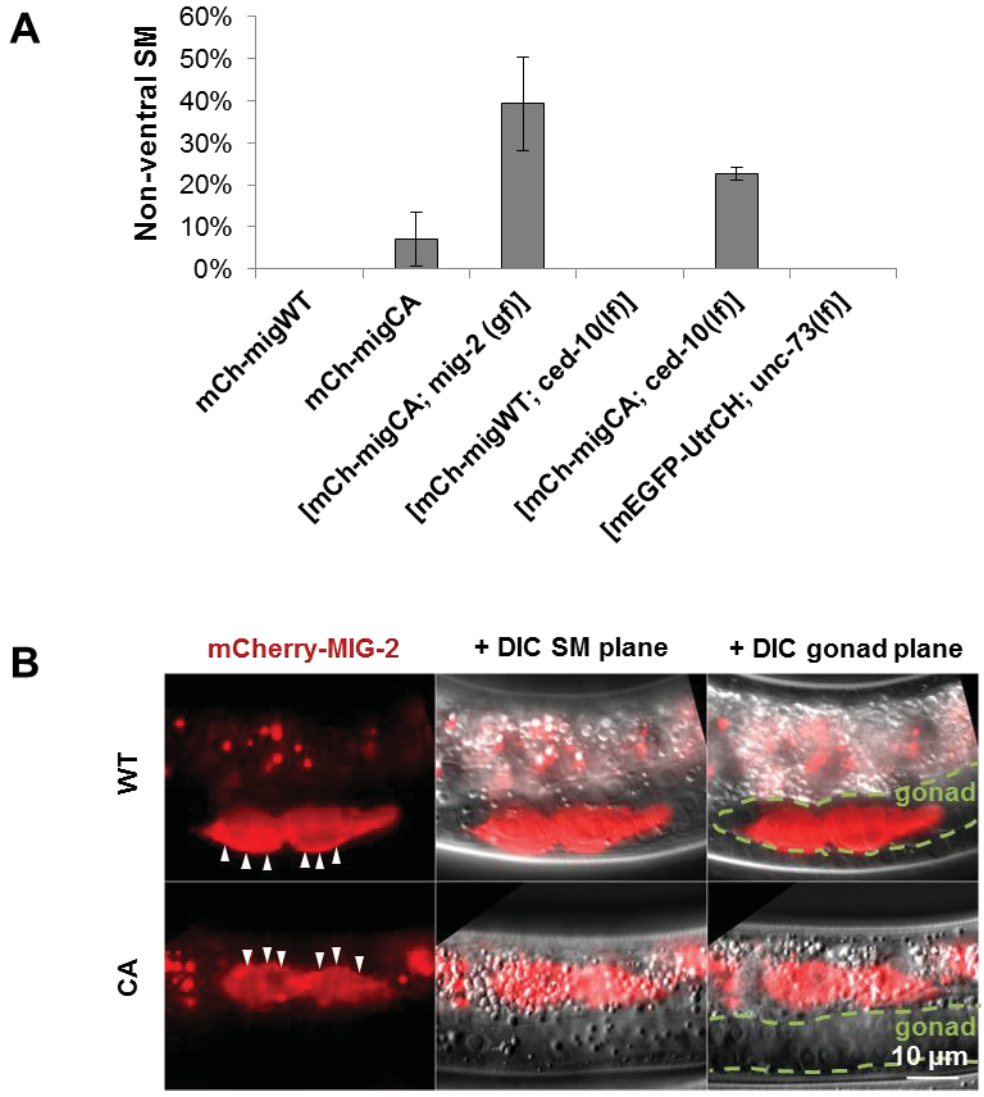

Figure 3.4 mig-2 (CA) and ced-10 synergistically affect SM dorsoventral localization

(**A**) Percentage of non-ventral SM in various mutants. mCh-migWT: mCherry-mig-2 WT transgene expressed in SM; mCh-migCA: mCherry-mig-2 CA expressed in SM; mig-2 (gf): mig-2(gm38) gain-of-function allele; ced-10(lf): ced-10(n1993) loss-of-function allele; unc-73(lf):

unc-73(e936) loss-of-function allele. (**B**) Fluorescence and DIC images of SM daughter cells from the first SM division after their arrival at the gonad. In mCherry-mig-2 WT, MIG-2 concentrates at the ventral membrane, whereas in mCherry-mig-2 CA, MIG-2 accumulates at the dorsal membrane (arrow head). SM and gonad reside on different focal planes, and the far right column combines SM fluorescence image with gonad DIC image to illustrate their relative position (gonad outlined in green). In mCherry-mig-2 WT, SM is in parallel with gonad on the ventral side; in mCherry-mig-2 CA, SM is on the dorsal side away from the gonad.

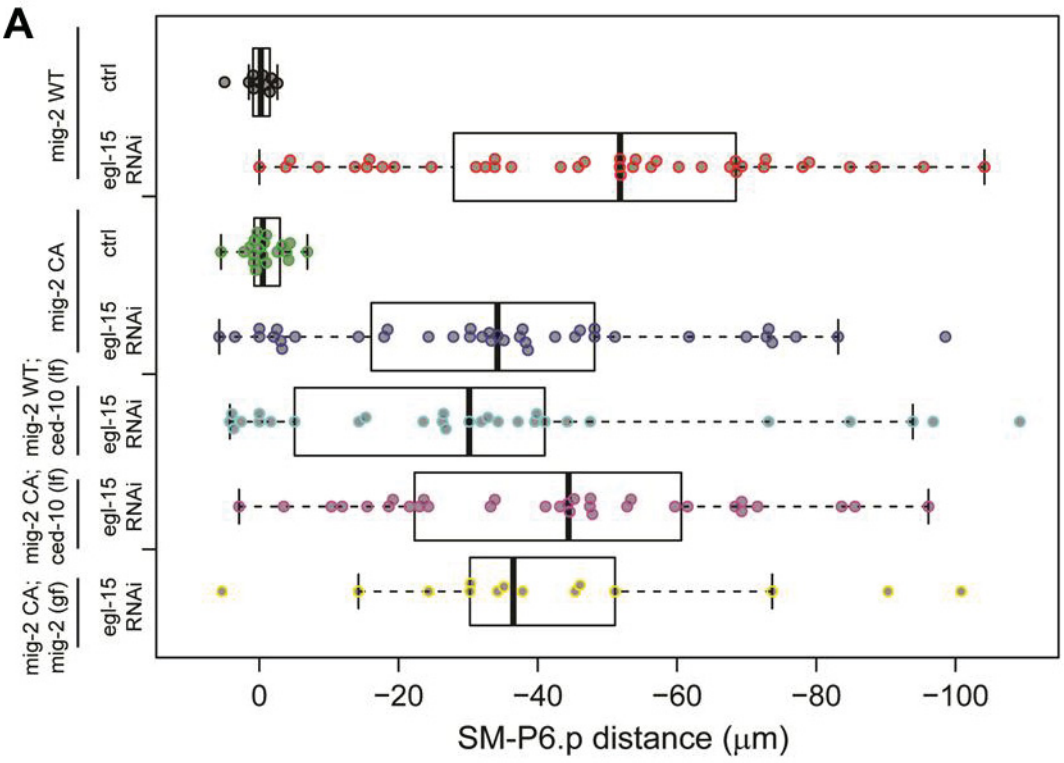
A
mig-2 WT
mig-2 CA
mig-2 WT; ced-10 (lf)
mig-2 CA; ced-10 (lf)
mig-2 CA; mig-2 (gf)
ctrl
egl-15 RNAi
0
−20
−40
−60
−80
−100
SM-P6.p distance (μm)

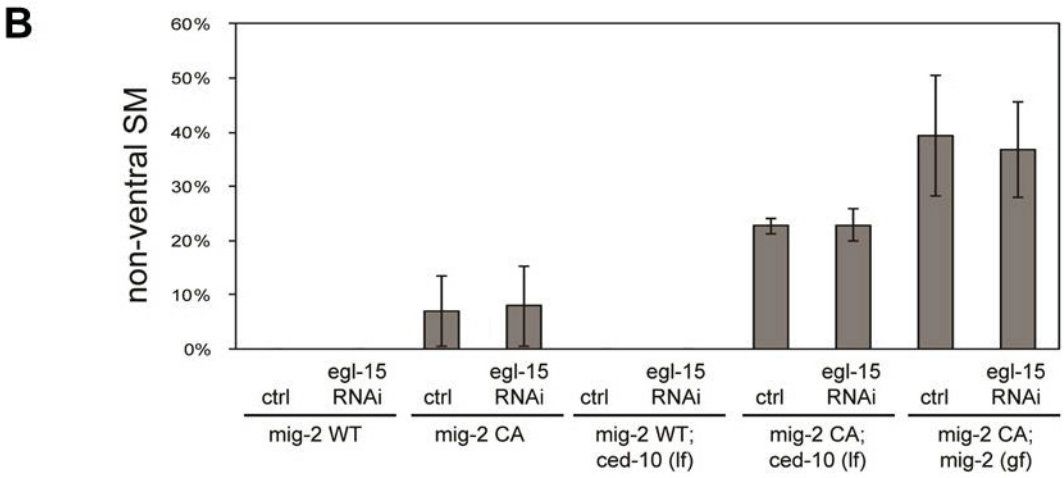
B
non-ventral SM
60%
50%
40%
30%
20%
10%
0%
ctrl
egl-15 RNAi
mig-2 WT
mig-2 CA
mig-2 WT; ced-10 (lf)
mig-2 CA; ced-10 (lf)
mig-2 CA; mig-2 (gf)

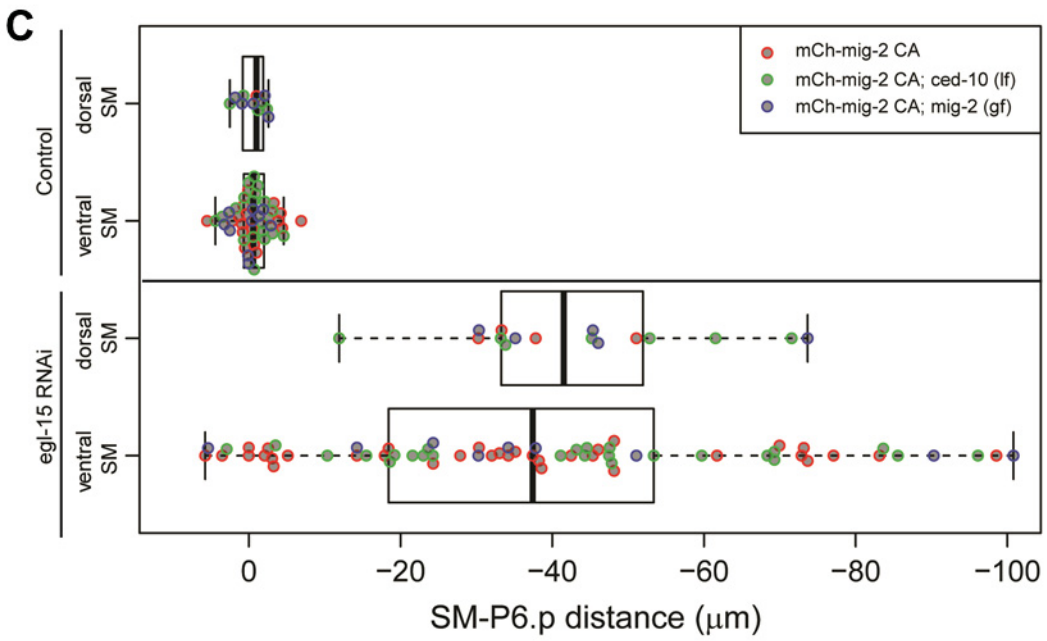

Figure 3.5 mig-2 (CA) affects SM dorsal localization independently of egl-15

(**A, C**) Dot plots of SM positions relative to P6.p on the AP axis in animals treated with RNAi against egl-15 in various mig-2 and ced-10 mutants. Each dot represents a single SM. Box and whisker plot is overlaid to show distribution. Central lines and boxes represent median and upper and lower quartiles of each distribution. Whiskers represent the robust range (quartiles±1.5x the interquartile distance). Dots outside of whiskers are outliers. (**A**) egl-15 RNAi lead to premature termination of migration compared to control in all mutants. No statistically significant difference in AP localization was found among all five groups of mutants treated with egl-15 RNAi. (**B**) Percentage of non-ventral SMs in animals treated with RNAi against egl-15 in various mig-2 and ced-10 genetic backgrounds. No statistically significant difference was found in each pair of control and egl-15 RNAi animals. Similar results were obtained for slt-1 and sax-3 RNAi animals (not shown). (**C**) AP positions of ventrally localized SMs and dorsally localized SMs in control animals and egl-15 RNAi treated animal in various

mig-2 and ced-10 mutants. Data from various mutants are pooled within control group and egl-15 RNAi group to compensate for fewer dorsal SMs. See legend for color representation of the mutants. Box and whisker plots are for overall distribution. No statistically significant differences were found in AP positions between dorsal SM and ventral SM in control animals or egl-15 RNAi treated animals.

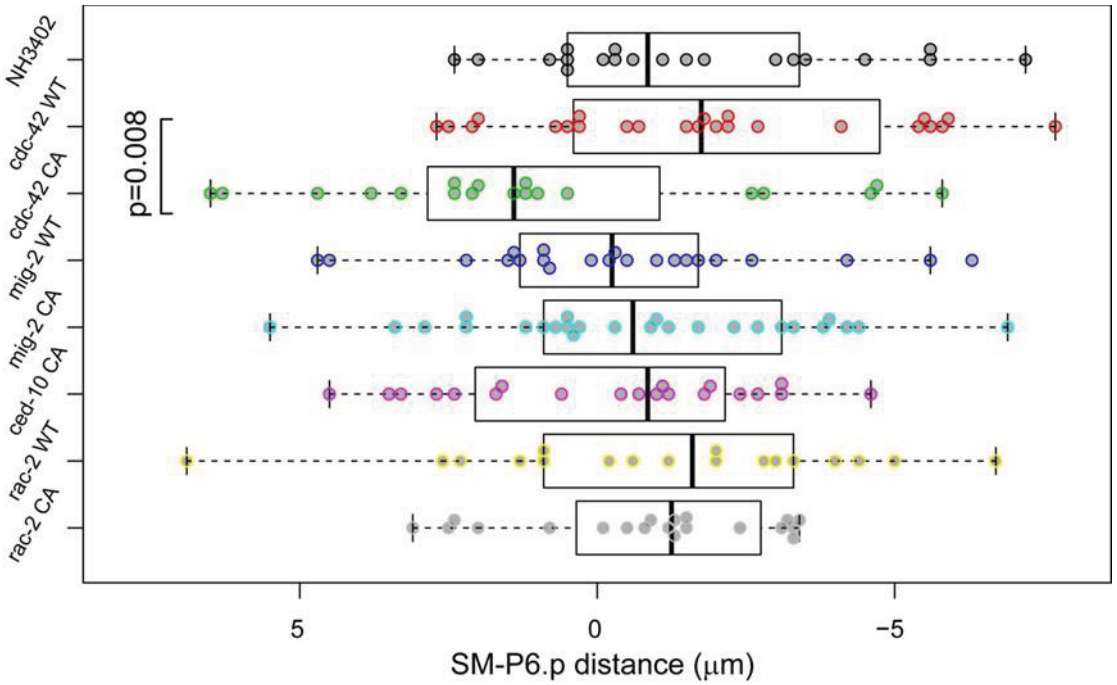

Figure 3.6 cdc-42 (CA) affects SM anteroposterior migration

Dot plots of SM final positions on the AP axis after completion of migration. Results from mCherry-cdc-42, mig-2, rac-2 WT and CA transgenic animals, and those from mCherry-ced-10 CA transgenic animals are shown. NH3402 is a GFP-CAAX marker strain in an otherwise WT genetic background. Statistical difference was found between cdc-42 WT and cdc-42 CA animals, and cdc-42 WT was statistically indistinguishable from NH3402. No statistically significant difference was found among all other strains, including NH3402.

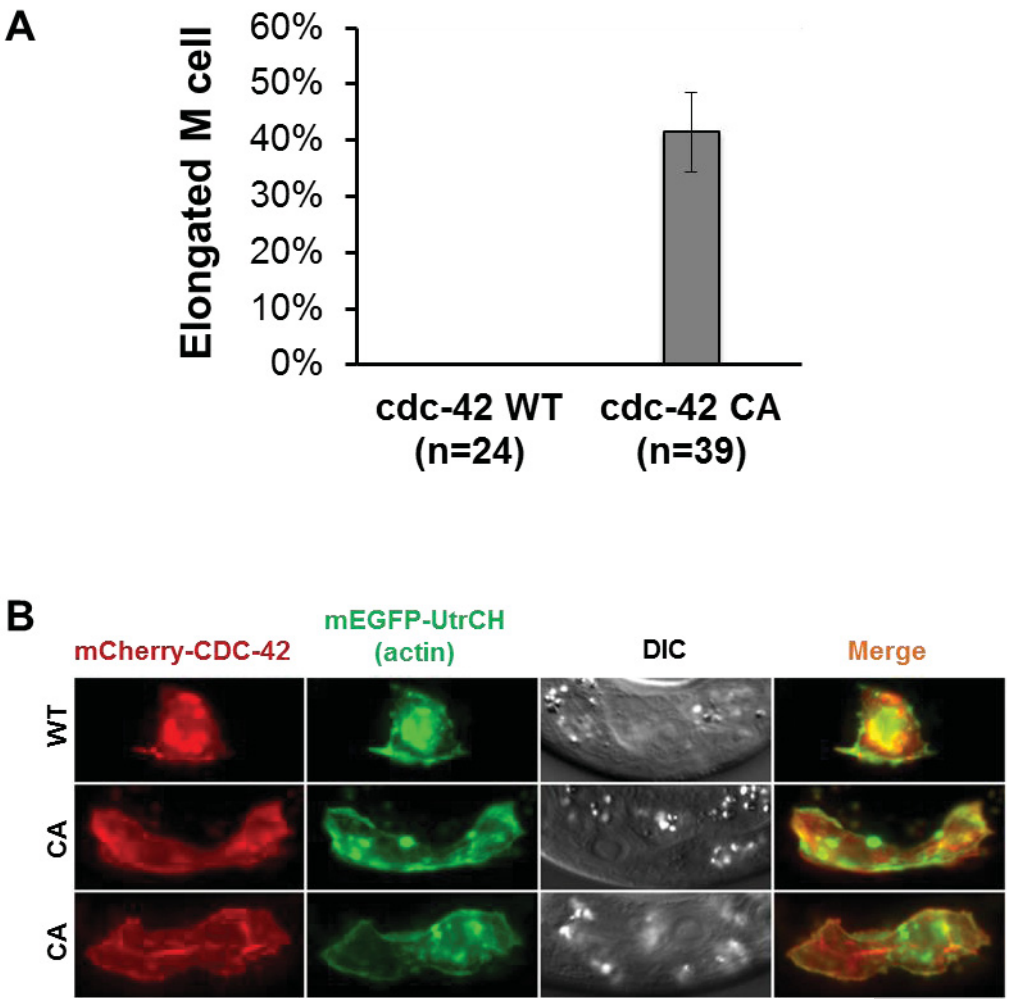

Figure 3.7 cdc-42 affects M cell morphology

(**A**) Percentage of M cells with elongated morphology. (**B**) Fluorescence and DIC images of M cell in L1 larvae in mCherry-cdc-42 WT (top) and CA (middle and bottom) transgenic animals. Red shows CDC-42 and green actin filaments. Middle row shows an elongated M cell extending cytoplasm towards the posterior away from the nucleus, and bottom row an elongated M cell extending cytoplasm anteriorly.

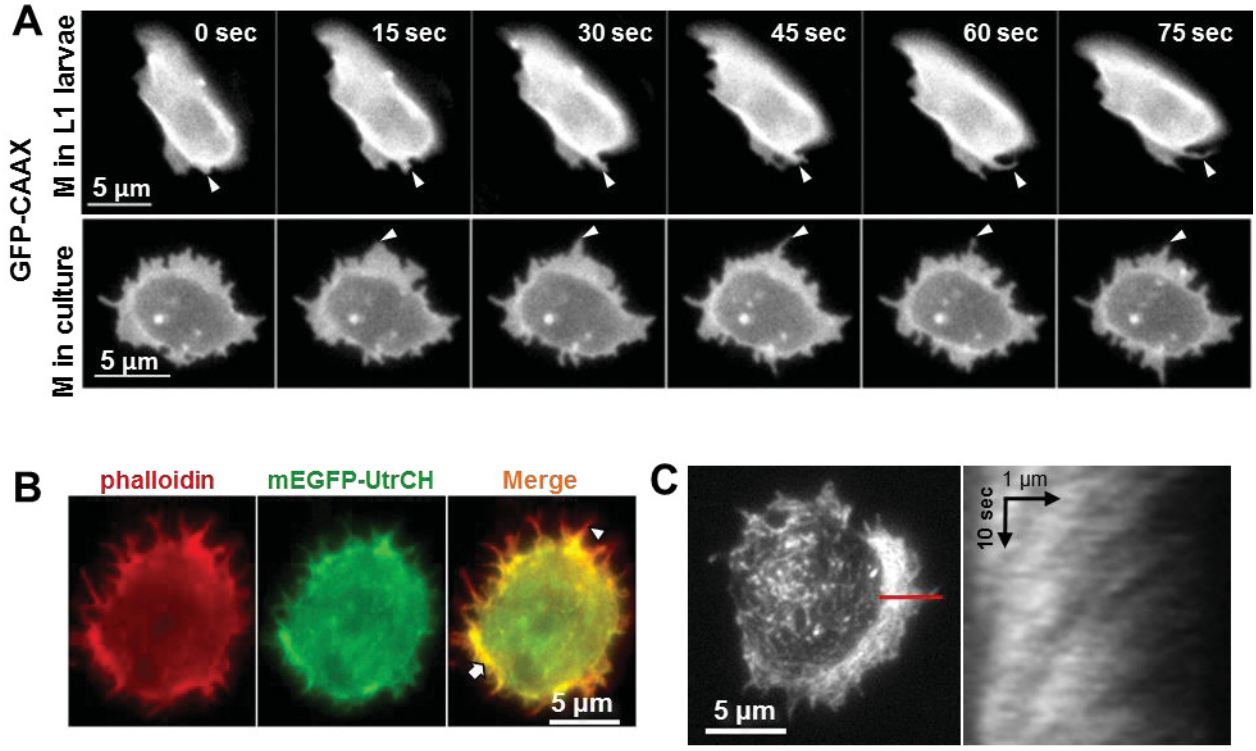

Figure 3.8 Protrusive activity and actin dynamics in cultured M cell

(**A**) Time-lapse series of M cell protrusive activities *in vivo* (top) and in culture (bottom). M cell is labeled with GFP-CAAX on the cell membrane. Arrow heads indicate filopodia. (**B**) mEGFP-Utrophin Calponin Homology domain (UtrCH) faithfully labels actin filaments in lamella/lamellipodia (arrow) stained by TRITC-phalloidin, and less well in filopodia (arrow head). (**C**) A frame from a time-lapse series of actin filament dynamics in cultured M cell expressing mEGFP-UtrCH (left). Kymograph generated from the red line in the lamella/lamellipodia of the cell throughout the time-lapse is show on the right, and displays prominent actin filament retrograde flow towards cell center (to the left on the image).

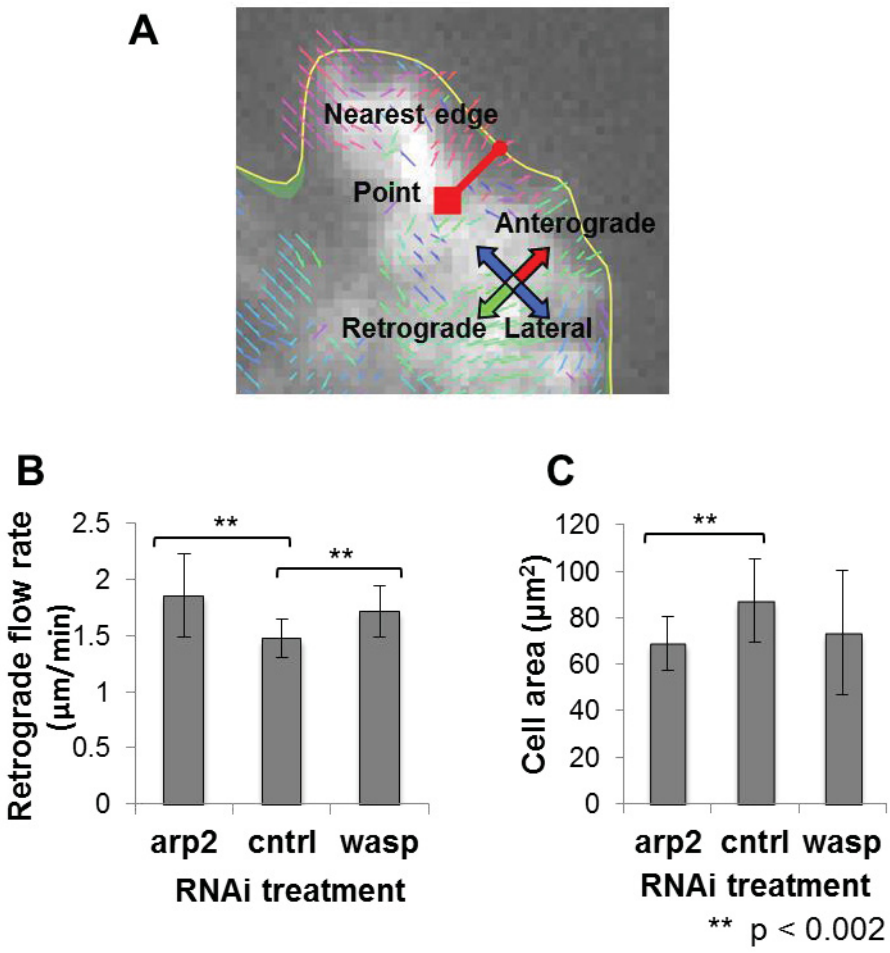

Figure 3.9 arp-2 and wsp-1 RNAi on cultured M cell

(**A**) Example of actin flow-tracking on portions of the lamellipodium of an M cell labeled with mEGFP-UtrCH. Flow direction of point of actin filaments is determined by its relative direction from the nearest cell edge. (**B**) Actin filament retrograde flow rate in control and M cell treated with RNAi against arp-2 or wsp-1. (**C**) Cell area in in control and M cell treated with RNAi against arp-2 or wsp-1.

Table 3-1 Summary of SM migration in control and RNAi-treated mig-2 and/or ced-10 mutants

	mCh-mig-2 WT	*mCh-mig-2 CA*	*mCh-mig-2 WT; ced-10 (lf)*	*mCh-mig-2 CA; ced-10 (lf)*	*mCh-mig-2 CA; mig-2 (gf)*
control*	WT	WT	WT	WT	WT
egl-15	posterior	posterior	posterior	posterior	posterior
egl-20	WT	WT	WT	WT	WT
slt-1	WT	WT	WT	WT	WT
sax-3	WT	WT	WT	WT	WT

* No difference was observed in dorsoventral localization in any of the RNAi treated animals compared to control.

Chapter 4 Conclusions and future directions

CONCLUSIONS

Our understanding of both the conservation of mechanisms that control cell migration and their diversity have benefitted from studying several model organisms. Ideally, a full appreciation of the common features of these mechanisms is only possible by comparing data from all levels of studies. To this end, I approached SM cell migration in *C. elegans* on two levels: (1) by using traditional genetic tools to answer how Rho GTPases are differentially used *in vivo* to control specific aspects of SM migration, and (2) by utilizing and developing new cell culture tools to answer how the actin cytoskeleton is regulated on the cellular level.

In Chapter 2, I described a novel *C. elegans* larval cell isolation procedure. Resistance of the larval cuticle to protease digestion had been the main hurdle to isolating cells. By pre-sensitizing the larval cuticle with DTT and SDS to remove crosslinks and subsequent digestion with pronase E, my method efficiently released larval cells for culture. I modified the method to allow isolation of cells from all four larval stages and overcame bacterial contamination by using semi-defined axenic nematode growth medium. Cells isolated from L1-L4 stages exhibit increased sizes, and muscles from L1 and L4 stages are different in their morphology and number of muscle arms. This observation underscores the importance of studying postembryonic development through different stages. When combined with actin filament markers such as the one used in Chapter 3, larval cell culture can be used to study sub-cellular actin dynamics with high-resolution speckle tracking microscopy – a method that has so far been impossible *in vivo*. I provided detailed protocols on larval cell isolation as well as embryonic cell isolation in the

Appendix. Several C. elegans labs are already benefitting from the study of stage-specific developmental events using larval cell isolation. For example, David Miller (Vanderbilt U.) has combined my larval cell isolation method with cell sorting and RNA-Seq to profile gene expression in L1 stage neurons. These larval neuron expression profiles are much "cleaner" than those previously produced from embryonic cells, in that they report a higher preponderance of neuron-specific genes than do embryonic cell profiles (personal communication).

In Chapter 3, I used constitutively active (CA) transgenes to systematically study Rac and Cdc42 genes that are involved in SM migration. Activation of MIG-2/RhoG leads to dorsally localized SMs and this dorsal mislocalization was enhanced by loss-of-function of ced-10/rac1. The role of mig-2 in regulating SM positioning is consistent with the fast turnover of MIG-2 at the leading edge during SM migration. The dorsal localization caused by mig-2 CA is independent of previously identified dorsoventral (DV) guidance signaling of FGF and SLIT/Robo. Although implied in ventral restriction, mig-2 CA does not affect anteroposterior (AP) migration. Instead, cdc-42 is the sole tested Rho GTPases that affect AP migration. Thus, AP migration and DV localization are differentially affected by constitutively activating Rho GTPases. The lack of response to other CA Rho-GTPases shows the robustness of the redundant mechanisms that regulate SM migration. I also found that actin regulatory proteins WASP and Arp2/3 affect actin retrograde flow and cell spreading in cultured M cells, likely due to their conserved role in promoting actin polymerization. These results start to tie our understanding of upstream guidance signals to the critical hubs formed by Rho GTPases that link these signals to the actin cytoskeleton.

As with migrations of cells such as Q lineage neuroblasts and DTCs, I found that Rac subfamily Rho GTPases MIG-2 and CED-10 control SM migration. CDC-42, which often plays roles in early embryogenesis, is also involved in regulating postembryonic SM migration. WASP and Arp2/3, critical actin polymerization-inducing factors that have established roles in *C. elegans* embryogenesis, directly affect actin filament dynamics in cultured M cells, and possibly in SM migration as well.

FUTURE DIRECTIONS

The above studies provide us with an initial understanding of how Rho GTPases function in SM migration. Additional experiments could help answer several remaining questions.

1. Are MIG-2, CED-10 and CDC-42 necessary for SM migration?

Although CA mutations of MIG-2 and CDC-42 cause SM migration defects, we do not know whether their normal functions are dispensable in SM migration. Since single loss-of-function of mutations often do not yield detectable phenotypes, it is important that double loss-of-function mutations are used. As I demonstrated earlier, RNAi knockdown of gene expression is effective in SMs, and this method can be combined with genetic mutations, especially when double mutations are embryonically lethal. For example, animals with single loss-of-function of one Rac gene could be subjected to RNAi knockdown of another Rac gene during larval stage to allow scoring of SM migration defects. Such pairwise combinations could be used for all Rho GTPases to identify genes that are necessary, and may function redundantly, in SM migration.

2. **How are different Rho GTPases utilized downstream of guidance cues?**

Several SM guidance cues, such as FGF, Netrin, Semaphorin, and SLIT have been identified, but we do not know how they affect migration through Rho GTPases. The mCherry-Rho GTPase (CA) transgenic strains generated in this study can be crossed with loss-of-function of guidance cues to examine possible genetic interactions. Alternatively, sensitized genetic background, such as *sem-5; clr-1* (for compromised GDA) or *unc-53* (for compromised GIM) can be used with loss-of-function of Rho GTPases to identify their involvement in specific guidance mechanisms such as GIM and GDM. Further experiments combined with mutations of specific guidance cues would allow epistasis analysis of Rho GTPases and guidance cues.

3. **What actin regulatory proteins function downstream of Rho GTPases?**

To understand how Rho GTPases affect actin dynamics, actin regulatory proteins acting downstream of Rho GTPases need to be identified. RNAi against WASP, WAVE, Arp2/3 and UNC-34/Enabled in mutants where single guidance mechanisms are compromised (see above for example) would identify their specific involvement in a particular guidance mechanism. Using mutants of Rho GTPases identified in guidance mechanism-specific studies described in 2, RNAi against actin regulatory proteins of potentially same and different mechanisms can identify their epistatic relationships.

4. **How do actin regulatory proteins control actin dynamics downstream of Rho GTPases?**

Larval cell isolation protocol developed in this study can be used to directly observe actin dynamics in mEGFP-Utrophin CH labeled SM cells with high-resolution TIRF microscopy. The

effect of activating Rho GTPase on actin dynamics can be examined by crossing mEGFP-UtrCH strains with mCherry-Rho GTPase (CA) transgene strains. RNAi against actin regulatory proteins identified in Direction 3 above in these transgenic SMs would identify specifically how these proteins participate in regulating actin dynamics induced by activated Rho GTPases. Using fluorescently labeled actin regulatory proteins in isolated SM cells, their spatial and temporal dynamic relationship with mCherry-Rho GTPases and mEGFP-Utrophin CH labeled actin filaments can be investigated using two- and three-color TIRF microscopy to track subcellular localization and their relation to actin protrusion and retrograde flow.

Appendix: Cell isolation and culture

Sihui Zhang and Jeffrey R. Kuhn

Appendix used with permission of WormBook

Zhang S. and Kuhn JR. Cell isolation and culture (February 21, 2013), WormBook, ed. The C. elegans Research Community, WormBook, doi/10.1895/wormbook.1.157.1, http://www.wormbook.org.

Abstract

Cell isolation and culture are essential tools for the study of cell function. Isolated cells grown under controlled conditions can be manipulated and imaged at a level of resolution that is not possible in whole animals or even tissue explants. Recent advances have allowed for large-scale isolation and culture of primary *C. elegans* cells from both embryos and all four larval stages. Isolated cells can be used for single-cell profiling, electrophysiology, and high-resolution microscopy to assay cell autonomous development and behavior. This chapter describes protocols for the isolation and culture of *C. elegans* embryonic and larval stage cells. Our protocols describe isolation of embryonic and L1 stage cells from nematodes grown on high-density NA22 bacterial plates and isolation of L2 through L4 stage cells from nematodes grown in axenic liquid culture. Both embryonic and larval cells can be isolated from nematode populations within 3 hours and can be cultured for several days. A primer on sterile cell culture techniques is given in the appendices.

1 Background

The methodology of culturing isolated cells has been available for over a century. The first reported primary cultures were explants of frog neuronal fibers [150] and dissociated sponges [151] that grew and differentiated over the course of several days. By the 1950s, the introduction of protease digestion, defined media, and antibiotics made vertebrate cell culture a more widely accessible technique.

Aside from amoeba-like nematode sperm [152], *C. elegans* cells have proved to be far more difficult to isolate and culture than vertebrate or insect cells. The main difficulty has been that

the chitinous shell of embryos and the tough outer cuticle of larval and adult worms are resistant to cell and tissue explantation. Early methods involving mechanical segregation of embryonic cells by cutting and extruding eggs [153], or laser cutting followed by extrusion [154], or shearing eggs by passage through a Hamilton syringe [155] provided enough viable blastomeres to follow individual embryos and to test culture media. However, yields were low and few cells survived the process. Chemically dissolving the egg shell with a mixture of chitinase and chymotrypsin [156] followed by gently pulling the embryos through a glass needle to disrupt the vitelline layer [72] greatly increased the viability of embryonic cells. Subsequent work found that more vigorous pipetting after egg shell digestion [157-160] could extract large populations of embryonic cells for culture.

In contrast to embryos, the tough cuticle of larval and adults nematodes formed an almost impenetrable barrier to post-embryonic cell culture. Although releasing eggs from gravid adults with hypochlorite and a strong base is a mainstay technique of embryo isolation [161], adult and larval cells are dissolved in the process. Researchers can gain access to adult cells for electrophysiology by immobilizing and filleting individual nematodes [162], but the technique is challenging and individual cells cannot be separated and cultured. The introduction of gentle chemical disruption of the larval cuticle and subsequent release of cells through repetitive pipetting [163] has now allowed primary culture of *C. elegans* cells from all four larval stages.

The protocols collected here provide comprehensive techniques and media recipes for large-scale isolation and culture of primary embryonic and larval cells from *C. elegans*. We suggest equipment and supplies for cell culture in Appendix A and Appendix B. We include common cell culture techniques in Appendix C for those unfamiliar with working in a sterile culture hood.

2 Growing worms on NA22 bacterial plates

Both embryonic and larval cell isolations require 30 to 50 µl of compacted eggs or larvae per preparation. NA22 bacteria grow in thick layers on peptone-augmented agar plates and provide a richer food source than do OP50 bacteria, which is standardly used for nematode maintenance. A large number of worms can obtained by growing synchronized worms at high densities on 100 mm diameter NEP plates seeded with NA22 bacteria (NEP-NA22). Gravid adults from these plates are bleached in an alkaline solution (egg preparation) to obtain sterile eggs that can be used directly for embryonic cell isolation. Alternatively, eggs may be hatched overnight to produce synchronized L1 larvae for cell isolation or for synchronized axenic culture to obtain L2 through L4 stage cells (Figure A- 1).

Preparing NEP-NA22 plates

2.1.1 Materials

- Sterile petri dishes, 100 mm diameter
- NaCl
- Peptone
- Agar
- Cholesterol, 5 mg/ml (w/v) in ethanol. Do not autoclave.
- **1 M magnesium sulfate** ($MgSO_4$) in ddH_2O, autoclaved.
- **1 M potassium phosphate pH 6.0.** Mix 35.6 g K_2HPO_4 with 108.3 g KH_2PO_4 in 0.8 L ddH_2O, and adjust pH to 6.0. Bring to 1 L in ddH_2O and autoclave.

- **Nystatin Suspension** (Sigma N1638). Fungicide, 10,000 units/mL in DPBS.
- **LB Broth – Miller formulation.** NA22 bacteria grow well in moderate or high salt formulations of Lysogeny broth (10g/L NaCl). 2X YT media may also be used to grow NA22 bacteria.
- **NA22 bacteria.** NA22 bacteria may be obtained from the Caenorhabditis Genetics Center (CGC).

2.1.2 Pouring NEP Plates

1. Dissolve the following components in ddH_2O and bring to 1 L with ddH_2O

Component	Qty/1 L
NaCl	1.2 g
peptone	20 g
agar	25 g

2. Add a large stir bar and autoclave on a liquid cycle for 30 to 40 minutes.
3. Cool to approximately 60°C while stirring.
4. Using aseptic techniques, add the following stock solutions

Stock solution	Qty/1 L
5 mg/ml cholesterol (in ethanol)	1 ml
1 M $MgSO_4$ (autoclaved)	1 ml
1 M potassium phosphate pH 6.0 (autoclaved)	25 ml
100x Nystatin (stock 10,000 U/ml, final 100 U/ml)	10 ml

5. Pour 18 ml of medium each into 100 mm diameter petri dishes.

2.1.3 Seeding plates with NA22 bacteria

1. Aseptically inoculate 30 to 50 ml of LB broth with a colony of NA22 bacteria and grow overnight at 37ºC.

2. To each NEP plate, add 1 ml of NA22 culture and spread over the entire NEP plate surface.
3. Let seeded plates stand upright at room temperature for 3 to 4 days or until dry.
4. Invert seeded plates and store at 4ºC.

Propagating and synchronizing worms on NEP-NA22 plates

2.1.4 Materials

- NaCl
- Potassium phosphate monobasic (KH_2PO_4)
- Sodium phosphate dibasic (Na_2HPO_4)
- **M9 media** (recipe below)
- **1 M magnesium sulfate** ($MgSO_4$) in ddH_2O, autoclaved.

2.1.5 M9 media

1. Dissolve the following components in ddH_2O and bring to 1 L with ddH_2O

Component	**Qty/1 L**
Potassium phosphate monobasic (KH_2PO_4)	3 g
NaCl	5 g
Sodium phosphate dibasic (Na_2HPO_4)	6 g

2. Autoclave the solution for 30 minutes on a liquid cycle.
3. Allow solution to cool to room temperature and then add

Stock solution	**Volume**
1 M Magnesium sulfate ($MgSO_4$)	1 ml

4. $MgSO_4$ will precipitate out of solution at temperatures above 55°C. Do not add $MgSO_4$ before autoclaving M9 or before the autoclaved liquid has cooled.
5. Store at room temperature

2.1.6 Growing synchronized worms on NEP-NA22 plates

1. Seed NEP-NA22 plates by chunking worms from NGM-OP50 plates or any other source.
2. Grow worms for several generations until plates are full of gravid adults.
3. Wash worms from plate by pipetting 10 ml of ddH_2O directly onto the plate surface. Repeat and collect suspended worms in a 15 ml conical tube. Worms may be collected from several plates by washing the next plate with the same suspension of worms.
4. Settle the worms for approximately 2 minutes at room temperature in a 15 ml conical tube.
5. Remove excess ddH_2O, leaving 7 ml of worm suspension.
6. Follow protocol 0 (Preparing eggs or hatched larvae) to produce synchronized L1 in M9 media.
7. The next day, count the hatched worms and plate 20,000 of synchronized L1 per plate onto NEP-NA22 plates.
8. Grow at 20 to 25°C until the worms reach gravid adult stage.

Growing synchronized worms at 20,000 per plate ensures that worms reach adult stage just before the plate starts to starve. One plate of such culture typically yields 100,000 to 200,000 eggs, which can be used to seed 5 to 10 NEP-NA22 plates. If an insufficient number of worms are obtained in the first round, repeat steps 3 through 8 above.

Preparing eggs or hatched larvae

2.1.7 Materials

- 5 M sodium hydroxide (NaOH) in ddH_2O.
- **Fresh sodium hypochlorite** (household bleach). Purchase a fresh bottle of bleach every two weeks.

2.1.8 Procedure

1. Start with gravid adults suspended in 7 ml of ddH_2O.
2. To lyse worms and obtain eggs, add 1 ml of 5 M NaOH and 2 ml of fresh sodium hypochlorite (bleach) to the worm suspension. Vortex the suspension continuously at the highest speed of a laboratory vortex mixer for the entire 5 minute incubation. Do not exceed 5 minutes of lysis.

Do not contaminate the outside rim of the conical tube or the cap with bacteria in the worm suspension. These bacteria do not contact the bleach/NaOH solution and may contaminate subsequent cultured cells.

3. Pellet the lysed worms at 1,300 g for 1 minute in a clinical centrifuge and discard the supernatant.

Some egg preparation protocols subsequently separate eggs from lysed adult carcasses by floating the eggs on a layer of sucrose. We have found that the sucrose flotation step can be skipped with no effect in cell isolation outcome as long as adults are vortexed continuously during the alkaline hypochlorite treatment. Continuous vortexing sufficiently breaks down adult carcasses with little harm to the eggs.

4. Wash the pellet 3 times by resuspending in 10 ml sterile ddH_2O and centrifuging at 1,300 g for 1 minute each. Insure that the pellet is thoroughly distributed before centrifugation.

Eggs from this step can be used directly for embryonic (0) or L1 (0) cell isolation if the washing steps are done under sterile conditions in a cell culture hood.

5. To synchronize worms by hatching, resuspend eggs with 10 ml of M9 in a 15 ml conical tube and rotate at room temperature overnight.

3 Axenically Growing Worms in CeHR Liquid Culture

C. elegans larvae grown on bacteria cannot be used directly for larval cell isolation. Because the limited antibiotics used in cell culture media are bacteriostatic rather than bactericidal, contamination is always a risk. To overcome this problem CeHR medium, a bacteria-free worm culture medium developed by Eric Clegg's group [164], is used for growing larvae for cell isolation. The CeHR basal medium, consisting of, growth factors, nucleic acids and minerals, can be prepared separately and stored for an extended time period as frozen aliquots. Complete CeHR medium is prepared by adding skim milk to thawed CeHR basal medium. Switching from a bacterial diet to axenic medium is simply accomplished by inoculating CeHR medium with L1 larvae from a sterile egg preparation of worms grown on bacteria (Figure A- 2). *C. elegans* develop in CeHR axenic medium at a pace similar to growth on NA22 or OP50 bacterial plates. The recipe and assembly steps for CeHR medium shown below are based on a protocol from Nass and Hamza [165]. Although the recipe is laborious, CeHR medium for approximately 50 flasks of nematodes can be prepared in one day and stored in frozen aliquots.

Preparing CeHR medium component solutions

3.1.1 Materials

- 1 M KOH
- 0.1 M NaOH
- Concentrated HCl
- Ethanol
- **High temperature ultra-pasteurized (UHT) skim milk.** UHT sterilized milk has a long shelf life. It is typically sold in aseptic cartons in most grocery stores throughout the world. In the U.S.A., Horizon brand boxed milk is available in most grocery stores.
- **Additional components (listed below).** Additional materials along with suggested sources and catalog numbers are listed in the tables below. "Storage" refers to the temperature at which the dry chemical is stored according to the manufacturer's recommendations. RT refers to room temperature.

CeHR components are mixed under non-sterile conditions unless otherwise indicated. The final medium is assembled and filtered under sterile conditions.

3.1.2 Vitamin and growth factor stock mix

1. To 60 ml ddH_2O add the following components.

Component	g	Storage	Source	Cat. #
N-Acetylglucosamine	0.150	4°C	Calbiochem	1079
DL-Alanine	0.150	RT	Calbiochem	1250
Nicotinamide	0.075	RT	Sigma	N-3376
D-Pantethine	0.0375	4°C	Sigma	P-2125
Pantothenate (Ca)	0.075	4°C	Sigma	P-6292
Pteroylglutamic Acid (Folic Acid)	0.075	RT	ACROS	21663-0100
Pyridoxamine.2HCl	0.0375	-20°C	Sigma	P-9158
Pyridoxine.HCl	0.075	RT	Sigma	P-6280
Riboflavin 5-PO4(Na)	0.075	-20°C	Sigma	R-7774
Thiamine.HCl	0.075	RT	Sigma	T-1270

2. To 5 ml of 1 M KOH add the following components.

Component	g	Storage	Source	Cat. #
p-Aminobenzoic Acid	0.075	4°C	Sigma	A-9878
Biotin	0.0375	4°C	Sigma	B-4639
Cyanocobalamine (B-12)	0.0375	4°C	Sigma	V-2876
Folinate (Ca)	0.0375	RT	Sigma	F-7878
Nicotinic acid	0.075	RT	Sigma	N-0761
Pyridoxal 5'-phosphate	0.0375	-20°C	Sigma	P-3657

3. To 1 ml of ethanol add the following component.

Component	g	Storage	Source	Cat. #
(±) α-L-lipoic acid, oxidized form	0.0375	4°C	Sigma	T-1395

4. Mix solutions from steps 1 through 3, and bring to 100 ml with ddH_2O.

5. Freeze as 10 ml aliquots in 15 ml conical tubes and store at -20°C.

3.1.3 Nucleic acid mix stock

1. To 60 ml ddH_2O add the following components in order.

Component	g	Storage	Source	Cat. #
Adenosine 5'-PO_4 (Na)	1.74	-20°C	Sigma	A-1752
Cytidine 5'-PO_4 (Na)	1.84	4°C	Sigma	C-1006
Guanosine 2'- & 3'-PO_4 (Na)	1.82	-20°C	Sigma	G-8002
Uridine 5'-PO_4 (Na)	1.84	-20°C	Sigma	U-6375
Thymine (*add last*)	0.63	RT	Sigma	T-0376

2. Bring to 100 ml with ddH_2O.

3. Freeze in 10 ml aliquots in 15 ml conical tubes and store at -20°C.

3.1.4 Mineral mix

1. To 150 ml ddH_2O add the following components.

Component	g	Storage	Source	Cat. #
$MgCl_2.6H_20$	0.82	RT	Sigma	M-2393
Sodium Citrate	0.58	RT	Sigma	S-4641
Potassium Citrate. H_2O	0.98	RT	Sigma	P-1722
$CuCl_2.2H_2O$	0.014	RT	Fisher	C455-500
$MnCl_2.4H_2O$	0.04	RT	Fisher	M87-100
$ZnCl_2$	0.02	RT	Sigma	Z-0152
$Fe(NH_4)_2(SO_4)_2.6H_2O$	0.12	RT	Fisher	F-1018
$CaCl_2.2H_2O$	0.04	RT	Fisher	C70-500

2. Bring to 200 ml with ddH_2O and store at 4°C.

3.1.5 Hemin chloride solution

1. Add 19.5 mg of Hemin chloride to 10 ml of 0.1 M NaOH.

Component	g	Storage	Source	Cat. #
Hemin chloride	0.0195	RT	Frontier Scientific	H651-9

2. Adjust pH to 8.0 with concentrated HCl.

3. Bring to 15 ml with 0.1 M NaOH. The final concentration will be 2 mM (1.3 mg/ml).

4. Use immediately or store at -20ºC in dark or foil covered containers for up to 2 weeks.

3.1.6 Cholesterol

1. Add 50 mg of cholesterol to 10 ml of ethanol for a final concentration of 5 mg/ml.

Component	g	Storage	Source	Cat. #
Cholesterol	0.05	RT	J.T. Baker	F676-05

3.1.7 MEM Amino Acid Mixes

1. Purchase the following amino acid mixtures and store at 4ºC.

Component	Storage	Source	Cat. #
MEM Essential Amino Acid Mix (50x)	4°C	GIBCO	11130-051
MEM Non-essential Amino Acid Mix (100x)	4°C	GIBCO	11140-050

Only open the bottles in the culture hood.

3.1.8 Potassium phosphate monobasic

1. Bring 6.13 g of KH_2PO_4 to 100 ml in ddH_2O for a final concentration of 0.45 M. Store at 4ºC.

3.1.9 High temperature ultra-pasteurized (UHT) skim milk

1. Disinfect the unopened box by spraying the outside with 70% ethanol. Wipe with kimwipes.
2. Move the box to the culture hood and open it.
3. Divide the milk into 10 ml aliquots in 15 ml conical tubes.
4. Store at -20ºC and thaw as needed.

3.1.10 Other components

1. Make each of the following components separately in the indicated final volume of ddH_2O.

Component	g	Final Volume	Stock	Source	Cat. #
Choline di-acid citrate	0.885	15 ml	4°C	Sigma	C-2004
i-Inositol	0.648	15 ml	RT	Sigma	I-5125
d-Glucose	13.15	50 ml	RT	Sigma	G-7520
HEPES (Na salt)	3.9	15ml	RT	Sigma	H-3784
Lactalbumin hydrolysate	4.25	25 ml	4°C	Sigma	L-9010

3.1.11 Assembling CeHR basal medium

Perform all procedure in the culture hood under sterile conditions.

1. Place a 500 ml or larger, 0.22 µm bottle-top vacuum filter in the culture hood.
2. Disconnect the vacuum or leave the vacuum off.
3. Add following solutions to the reservoir in order.

Solution	Volume
Choline	5 ml
Vitamin mix	5 ml
i-Inositol	5 ml
Hemin chloride	5 ml
ddH_2O	125 ml

Hemin chloride will precipitate after filtration. The subsequent nucleic acid mix will re-solubilize this precipitate.

4. Connect or turn on the vacuum and wait for solutions to pass through the filter.
5. Disconnect or turn off the vacuum and add

Solution	Volume
Nucleic acid mix	10 ml

6. Swirl the vacuum unit to solubilize any unfiltered hemin chloride precipitate.
7. Connect or turn on the vacuum and wait for solutions to pass through the filter.

   Disconnect or turn off the vacuum.

8. Add the following components to the reservoir in order.

Solution	Volume
Mineral mix	50 ml
Lactalbumin	10 ml
MEM Essential Amino Acid Mix (50x)	10 ml
MEM Non-essential Amino Acid Mix (100x)	5 ml
0.45M KH_2PO_4	10 ml
d-Glucose	25 ml
HEPES (Na salt)	5 ml
ddH_2O	125 ml
Cholesterol	0.5 ml

9. Connect or turn on the vacuum and wait for solutions to pass through the filter. Disconnect or turn off the vacuum.
10. Remove the filter unit, cap the bottle with a sterile top, and gently swirl the solution until mixed.
11. The above procedure yields approximately 395 ml CeHR basal medium. Aliquot 8 ml each to several 15 ml conical tubes. Store aliquots at -20°C.

Establishing and maintaining CeHR worm culture

3.1.12 Materials and equipment

- **CeHR Media** (protocol 0)**.**
- T25 tissue culture flasks (25 cm^2 surface), uncoated, with vented caps.
- Incubated orbital shaker.

3.1.13 Procedure

1. Follow protocol 0 (Propagating and synchronizing worms on NEP-NA22 plates).

2. Follow protocol 0 (Preparing eggs or hatched larvae) to produce synchronized L1 in sterile M9 media.

Eggs are initially sterilized during the alkaline hypochlorite digestion. All subsequent steps must be performed in a cell culture hood with sterile media.

3. Allow worms to hatch to L1 stage in sterile M9 media overnight on a laboratory rotator.
4. Optional: Prepare a new 15 ml conical tube by adding 0.5 ml of sterile ddH_2O. Mark the level of the water, remove the water, and transfer 10 ml of newly hatched larvae to this tube.
5. Sterilely remove 5 µl of worm suspension. Count the number of worms under a dissecting microscope and divide by 0.005 to estimate the density of synchronized larvae per ml in the original suspension.
6. Pellet larvae at 1,300 g for 1 minute in a clinical centrifuge.
7. Remove most of the supernatant to leave 0.5 ml of total volume and resuspend the pellet. Multiply the density calculated from step 5 by 20 to estimate the density of concentrated larvae.
8. Thaw one aliquot of CeHR basal medium per flask. Add 2 ml of freshly thawed skim milk to every 8 ml of CeHR basal medium. Mix and transfer 10 ml of complete CeHR medium into a T25 tissue culture flask.
9. Seed worms at 40,000 to 80,000 larvae per flask of CeHR medium.
10. Grow worms at 70 RPM in an incubated orbital shaker at 22°C until gravid adults begin to lay eggs.

Sterile CeHR medium (with milk) is cloudy but will clear as worms consume the nutrients. Check the flask frequently after seeding. If the media becomes cloudier over time, it is likely contaminated. Check a small aliquot for contamination and discard the flask according to your institution's safety policies.

11. Once gravid adults form, sterilely collect the CeHR suspension in a 15 ml centrifuge tube.

If the incubated shaker is also used to culture bacteria, thoroughly disinfect the outside of the flask with 70% ethanol before transferring to the cell culture hood.

12. Centrifuge worms at 1,300 g for 1 minute, remove the supernatant, and resuspend with 7 ml of sterile ddH_2O.
13. Follow protocol 0 (Preparing eggs or hatched larvae) to produce synchronized L1 in sterile M9 media.

Worms harvested from CeHR medium can be frozen using standard procedures.

14. Repeat steps 3 through 8 and inoculate new CeHR culture flasks by seeding worms 40,000 to 80,000 larvae per flask of CeHR medium.
15. Grow larvae on a shaker to the desired stage for larval cell preparation. Alternatively, allow worms to grow to gravid adult stage and prepare and hatch eggs in M9 media. Seed new flasks of CeHR media with synchronized larvae to maintain a sterile, synchronized population of nematodes for subsequent experiments.

The first generation of larvae will grow slower in CeHR (7 to 10 days) and unsynchronized as worms adapt to the new environment. The second generation grows faster and synchronized, reaching gravid adult stage in approximately 3 to 4 days

[165] (Figure A- 3). Do not use the first generation of larvae previously grown on NEP plates for cell isolation. Use the second generation of worms adapted to CeHR for larval cell isolation.

4 Common Nematode Cell Culture Materials and Techniques

A number of media formulations have been used to support the survival of isolated *C. elegans* cells. Like insect culture media [166], nematode cell culture media are maintained at higher osmolarities than those used for vertebrate cell culture. Although intact nematodes can survive osmotic stresses [167, 168], cultured *C. elegans* cells lack the secretory cells (renal system) of the whole animal and thus may be sensitive to osmotic stress. An osmotic pressure of 340 mOsm, approximately twice what is used for vertebrate cell culture [166], is ideal for supporting the survival and differentiation of *C. elegans* embryonic cells [159].

The first reported *C. elegans* cell culture medium was developed by Edgar (Edgar's Growth Media, EGM) for growing embryonic blastomeres [156, 169]. EGM is a complex and rich medium containing amino acids, salts, and nucleic acid precursors, with fats and cholesterol provided by addition of egg yolk. EGM osmolarity is supplemented by addition of polyvinylpyrrolidone (PVP) and inulin. In an effort to simplify EGM, Bloom and Horvitz [157] tested several formulas based on commercially available insect media. They found that L-15 supplemented with nucleic acid precursors, fetal bovine serum to provide growth factors, fats, and cholesterol, and PVP and inulin to increase osmolarity, provided an optimal mix for supporting neuronal outgrowth. Christensen *et al* [159] further simplified the L-15-based embryonic growth media by dispensing with nucleic acid precursors and replacing PVP and

inulin with sucrose to increase osmolarity. The cell culture medium that we describe below is the Christensen L-15-based medium, with osmolarity adjusted to the recommended 340 mOsm.

Preparing L-15/FBS cell culture medium

4.1.1 Materials

- **L-15 insect media** (Invitrogen 21083-027).
- **Fetal Bovine Serum** (FBS, Invitrogen 16000-077).
- **Penicillin-Streptomycin solution** (Sigma P4458). 5,000 units penicillin and 5 mg streptomycin/ml
- **Sucrose, 60% w/v in ddH_2O**. Autoclave and use aseptically.
- Osmometer calibration standards.

4.1.2 Procedures

1. Equilibrate the osmometer to room temperature overnight.
2. Thaw FBS overnight at 4ºC.
3. Assemble the following components sterilely in the cell culture hood.

Component and final concentration	Stock	Qty/500 ml
L-15 insect media	1x	450 ml
10% FBS	100%	50 ml
50 U/ml penicillin + 50 μg/ml streptomycin (Sigma P4458)	100x	5 ml

Minimize freezing and thawing of FBS. If using a new bottle of FBS, use the culture hood to sterilely pour any remaining FBS into 50 ml tubes (protocol 0 in Appendix C) and freeze the aliquots. Thereafter, thaw one aliquot at a time.

4. Remove the L15/FBS medium from the culture hood.
5. Calibrate the osmometer according to the manufacturer's instructions.
6. Using bench-top aseptic methods (flame, autoclaved pipette tips), adjust the osmolarity of the L15/FBS to 340±5 mOsm with 60% sucrose. Approximately 8.5 ml of sucrose will be required.
7. In a tissue culture hood, re-sterilize the medium with a 0.22 μm vacuum filter unit (protocol 0 in Appendix C).
8. Store at 4°C.

Preparing egg buffer

4.1.3 Materials

- 1 M HEPES in ddH_2O, pH 7.3. Store at 4ºC.
- **2 M NaCl in ddH_2O.** Store at room temperature.
- **2 M KCl in ddH_2O.** Store at room temperature.
- **1 M $CaCl_2$ in ddH_2O**. Store at room temperature.
- **1 M $MgCl_2$ in ddH_2O.** Store at room temperature.
- Osmometer calibration standards.

4.1.4 Procedures

1. Assemble the following components at room temperature and bring to 500 ml with ddH2O

Components and final concentration	Stock	Qty/500 ml
25 mM HEPES pH 7.3	1 M	12.5 ml
118 mM NaCl	2 M	29.5 ml
48 mM KCl	2 M	12 ml
2 mM $CaCl_2$	1 M	1 ml
2 mM $MgCl_2$	1 M	1 ml

2. Calibrate the osmometer according to the manufacturer's instructions.
3. Adjust osmolarity to 340±5 mOsm by diluting with sterile ddH_2O.
4. In a tissue culture hood, sterilize the buffer with a 0.22 μm vacuum filter unit (protocol 0 in Appendix C).
5. Store at 4°C.

Acid washing coverslips

4.1.5 Materials and equipment

- **Coverslips.** Choose a size and thickness appropriate for the microscope.
- Sterile petri dishes, 35 mm diameter.
- **1 M HCl.** Concentrated HCl is 12.2 M. Slowly add 82 ml of concentrated HCL (drop-wise) to 0.8 L of ddH_2O while stirring. Bring to 1 L with additional ddH_2O. Store at room temperature in a glass bottle.
- 70% v/v ethanol in ddH2O. Make fresh each time.
- Absolute ethanol.
- Heated water bath
- Water bath sonicator

- Large Pyrex or metal container for autoclaving coverslips.
- Aluminum foil.

4.1.6 Procedure

1. Fill a glass beaker or wide-mouth glass jar with 1 M HCl, separate coverslips, and drop them one at a time into the beaker.

Clean one box (1 oz) of coverslips at a time at most.

2. Heat the beaker at 50 to 60ºC for 4 to 16 hrs.
3. Gently pour off the HCl and discard according to your institution's safety policies.
4. Rinse the coverslips once by swirling with ddH_2O, allow the coverslips to settle and pour off water.
5. Fill the container with ddH_2O and sonicate in a water bath for 30 minutes. Repeat sonication once with fresh ddH_2O and discard the ddH_2O.
6. Fill the container with freshly made 70% ethanol and sonicate for 30 minutes. Discard the ethanol.
7. Fill the container with absolute ethanol and sonicate for 30 minutes. Discard the ethanol

"Drying", or removing the coverslips of residual water with absolute ethanol must be done stepwise. Do not switch coverslips directly from ddH_2O to absolute ethanol.

8. Fill the container with absolute ethanol, cover tightly, and store for up to 1 year. Do not store coverslips and ethanol in plastic containers.
9. To sterilize coverslips for use, remove coverslips one at a time from the ethanol with forceps and layer them at the bottom of a large pyrex beaker, glass petri dish, rectangular

metal dish, or empty pipet tip box. Multiple layers may be separated with sheets of aluminum foil.

10. Cover the container with aluminum foil, add a strip of autoclave tape, and autoclave on a dry/gravity cycle

Many coverslip sterilization protocols recommend flame-drying coverslips. Open flames are no longer recommended for use inside of a cell culture hood.

11. Open the autoclaved packet of coverslips in the cell culture hood and decontaminate forceps with 70% ethanol. Using the forceps, place coverslips in sterile 35 mm petri dishes. Store the dishes in the culture hood.

Coating coverslips with peanut lectin

4.1.7 Materials and equipment

- **Peanut lectin** (*Arachis hypogaea* agglutinin, Sigma L0881, 5 mg)
- **Acid washed coverslips in 35 mm petri dishes.** Individual coverslips are ideal for subsequent fixation and antibody staining after several days in culture.
- OR
- **Glass-bottom culture dishes** (Mat Tek corporation, P35G-1.0-14-C). These 35 mm diameter petri dishes have a coverslip affixed across a hole in the bottom of the dish. They can be used for high-resolution imaging of live nematode cells with an inverted microscope. Cells in glass-bottom chambers may be imaged and placed back in the incubator for later study. Chambers with different coverslip thicknesses are available to match the microscopy

objective you will use. Glued coverslips can be removed from the dish using a glass bottom dish fluid (Mat Tek DCF OS 30) following the manufacture's procedure. Alternatively, glass bottom culture dishes may be constructed from acid washed coverslips using the method of Kline [170]. Sterilize dishes with 70% ethanol and allow them to dry at the back of the cell culture hood.

Mat Tek Glass bottom dishes used directly from a sterile sleeve do not require acid washing. Coat them directly with peanut lectin

- Parafilm

4.1.8 Coating coverslips with peanut lectin

Perform the following procedure in a tissue culture hood and use sterile techniques.

1. Dissolve peanut lectin with cold sterile ddH_2O in the original vial at 4°C overnight. If the vial is small, sterilely pour the lyophilized powder into a 50 ml conical tube before adding ddH_2O.
2. Transfer the solution from a vial to a sterile 50 ml conical tube and rinse the vial with additional cold sterile ddH_2O. Keep track of the amount of water added in each step. Bring to a final concentration of 0.5 mg/ml with additional sterile ddH_2O.
3. To coat Mat Tek glass bottom dishes, add 100 µl of 0.5 mg/ml peanut lectin to the coverslip and incubate at room temperature for 20 to 60 minutes. This peanut lectin solution can be collected and reused once to coat more coverslips.
4. Wash the dishes 5 times with 2 ml sterile ddH_2O. Aspirate the liquid with a glass pipet connected to a vacuum trap after each wash.

5. To dry, place the dishes at the back of cell culture hood (most sterile environment) and tilt the lids so that they only partially cover the dish. Wait at least 1 hour or until dry.
6. If dishes are not used immediately, use parafilm to wrap the dish and lid, and store at 4°C.

Peanut lectin-coated dishes can be stored for extended period, whereas peanut lectin solution is less stable. Coat a large batch of dishes with fresh peanut lectin solution and store at coated dishes at 4ºC.

Counting cells in a Hemocytometer (Figure A- 4)

1. Clean and dry the hemocytometer and coverglass with 70% ethanol and kimwipes.
2. Dampen the mounts with a wet kimwipe or by exhaling on the hemocytometer.
3. Place the hemocytometer coverglass across the mounts, center, and gently press down.

Hemocytometer coverglass is thicker than standard #0 or #1 coverglass and does not warp under liquid surface tension.

4. Insure that the cell suspension is well-mixed and pipette a 10 µl drop of cell suspension into one inlet of the hemocytometer. Wait 1 minute for cells to settle on the grid.
5. Place the hemocytometer on a phase contrast microscope and find the grid. Each corner square has an area of 1 mm^2 and a depth of 0.1 mm for a total volume of $1x10^{-4}$ ml.
6. Count the total cells in all 4 corner-squares of the grid. The corner-squares are divided into 16 smaller squares for convenience. Intact cells will appear phase dark with a bright, white phase ring surrounding the cell.

With practice, cells may be distinguished from debris by phase contrast. Continuously shift the focal plane up and down while counting to look for phase rings around cells. A

differential interference contrast (DIC) or Hoffman modulation contrast (HMC) microscope with a 40x or 63x objective may also be used to count small cells.

7. After counting the cells in all 4 corner-squares, divide by 4 to get the average number of cells per 1 mm^2 cell area. Multiply this number by $1x10^4$ to obtain the average number of cells per ml.

For cells that lay on an edge, only count cells that cross the top or left edge of a corner square.

8. Disassemble the hemocytometer. Clean and dry the hemocytometer and coverglass with 70% ethanol and kimwipes. Wrap both in lens tissue or kimwipes and store them in a safe location.

5 Embryonic Cells

To isolate embryonic cells, gravid adults from two to three synchronized NEP-NA22 plates are dissolved to release mixed-stage embryos. Egg shells are digested with chitinase and embryos are further dissociated through pipetting. Cells are released primarily from pre-comma stage embryos. Undissociated late stage embryos and large cell clumps are separated from dissociated cells by passing the suspension through a 5 µm mesh filter. Isolated embryonic cells adhere to peanut lectin and differentiate into cells of L1 stage characteristics. The embryonic cell isolation protocol described below was developed by the Strange laboratory [159, 160]. We have modified it slightly with an alternate to sucrose flotation of eggs that produces similar yields as the original protocol. We have included an extended cell filtration method that produces higher yields in our hands. See Table A- 1 below for typical yields from embryonic cell isolation.

Embryonic Cell Isolation and Culture

5.1.1 Materials and equipment

- **Chitinase** (Sigma C6137).
- Sterile egg buffer.
- Laboratory rotator.
- 3 ml syringes.
- 18-gauge syringe needles.
- Sterile syringe filters, 5 μm pore size (Pall Corp. 4650).

5.1.2 Chitinase solution

9. Dissolve chitinase to 1 U/ml in cold sterile egg buffer.
10. Store 500 μl aliquots at -80°C.

5.1.3 Procedures (Figure A- 5)

1. Follow steps procedures 0 (Propagating and synchronizing worms on NEP-NA22 plates) and 0 (Preparing eggs or hatched larvae) to prepare sterile eggs from 2 to 3 NEP-NA22 plates that were seeded with 20,000 hatchlings per plate.

Perform the following procedure in the cell culture hood and use autoclaved or filter sterilized water and media.

2. Resuspend eggs in 5 ml egg buffer. Pellet eggs at 1,300 g for 1 minute in a clinical centrifuge and remove the supernatant. Pellet again at 1,300 g for 1 minute to remove as much liquid as possible. Leave approximately 100 μl of pelleted eggs.

3. Optional: transfer any excess eggs to another 15 ml conical tube and add 10 ml of M9. Allow to hatch overnight to seed the next round of worm culture.

The embryonic cell isolation protocol described in [159, 160] separates eggs from adult carcasses by floating eggs on a layer of sucrose. This sucrose flotation step can be skipped with little difference in cell isolation outcomes if adult worms are continuously vortexed during alkaline hypochlorite digestion.

4. Thaw a tube of 500 µl 1 U/ml chitinase. Add 100 µl of chitinase stock to the 100 µl egg pellet and transfer to a 1.5 ml microcentrifuge tube. Rinse the original conical tube 4 times with 100 µl chitinase each time and transfer the chitinase and any suspended eggs to the same 1.5 ml tube. Rotate the reaction at room temperature for 1 hour on a laboratory rotator.

Do not vortex to mix embryos or cell suspensions in the following steps.

5. Stop the reaction by adding 800 µl of L-15/FBS and invert the tube several times to mix.
6. Pellet digested embryos at 900 g for 3 minutes at 4°C. Remove the supernatant.
7. Resuspend the pellet with 800 µl of L-15/FBS. Dissociate cells by pipetting the suspension up and down with a 1000 µl pipette tip against the tube side. Repeat a total of 70 times.
8. Monitor the progress of the digestion every 20 to 30 strokes. Touch the pipet tip to the larval suspension to pick up 1 to 2 µl of reaction, spot this sample on a glass slide, and examine under a tissue culture microscope.

9. When most embryos are dissociated into single cells, pellet at 900 g for 3 minutes at 4°C. Undissociated embryos should be those at or beyond the comma stage (Figure A- 6).
10. Remove the supernatant and gently resuspend the pellet with 0.5 ml of L-15/FBS. Label this tube "Cells" and keep the cell suspension on ice until ready to filter.
11. A total of 10 ml of L-15/FBS will be used to filter the suspension of dissociated embryos. Sterilely pour or pipet 12 to 15 ml of L-15/FBS into a 50 ml conical tube to use for the following wash steps.
12. Prepare ten 1.5 ml microcentrifuge tubes and label them "Fraction 1" through "Fraction 10".
13. **Fraction 1:** Attach an 18-gauge needle to a 3 ml syringe. Draw 1 ml of L-15/FBS into the syringe. Then, slowly draw 0.5 ml of cell suspension into the same syringe. Be careful not to mix the two solutions.

Be careful to only immerse the tip of the needle into the L-15/FBS stock solution.

14. Detach the needle and attach a sterile 5 μm pore-size filter to the syringe. Use the same filter for all subsequent wash steps. Gently eject the liquid through the filter into the tube marked "Fraction 1". Approximately 0.5 ml of liquid will remain in the filter.
15. **Fraction 2:** Pipette 1 ml of L-15/FBS into the original tube marked "Cells", swirl the tube to wash. Reattach the same 18- gauge needle to the syringe and draw the suspension into the syringe. Discard the needle and reattach the 5 μm filter. Gently eject the liquid into the tube marked "Fraction 2".

Excessive syringe pressure will damage the cells, while low pressure reduces cell yields in the first two fractions. Collecting additional fractions 3 through 10 and assaying cell yields can compensate for variations in syringe pressure between users and different brands of syringe and filter. We recommend that each user optimize the number of collected fractions for syringe, pressure, and filter. Fewer fractions may be collected once repeatability is established.

16. **Fractions 3-5:** Attach a new 18- gauge needle to the syringe and draw 3 ml of L-15/FBS into the syringe. Remove the needle and reattach the 5 μm filter. Gently eject the 1 ml at a time into the tubes marked "Fraction 3" through "Fraction 5".
17. **Fractions 6-8:** Reattach the 18- gauge needle to the syringe and draw 3 ml of L-15/FBS into the syringe. Remove the needle and reattach the 5 μm filter. Gently eject the 1 ml at a time into the tubes marked "Fraction 6" through "Fraction 8".
18. **Fractions 9-10:** Reattach the 18- gauge needle to the syringe and draw 2 ml of L-15/FBS into the syringe. Remove the needle and reattach the 5 μm filter. Gently eject the 1 ml at a time into the tubes marked "Fraction 9" and "Fraction 10".
19. To assay cell purity, sample 5 μl of cell suspension from each fraction, place onto a microscope slide and observe under a cell culture microscope. Keep the fractions with most cells and little debris (Figure A- 7).

The expected outcomes of the filtration are: fraction 1-3: milky with very small pieces of particles (discard); fraction 4: a few cells mixed with some debris (discard); fractions 5-10: several cells mixed with little debris (keep).

20. Pellet tubes with the most pure cells in a microcentrifuge at 900 g for 3 minutes at 4 °C. Remove all but the last 10 to 20 µl supernatant.
21. Gently resuspend cell pellet with the residual medium left in the tube. Combine cell suspensions into one tube and resuspend to approximately 500 µl with L-15/FBS.
22. Use a hemocytometer to count cell density in 10 µl of cell suspension and calculate total number of cells in the suspension (Protocol 0).
23. Resuspend cells with L-15/FBS to a final density of $5x10^6$ to $20x10^6$ cells /ml.
24. Plate 30-50 µl of cell suspension onto the center of peanut lectin-coated glass bottom dishes. Place dishes in a plastic container with a gas exchange hole and humidified with kimwipes wetted with ddH_2O. Allow cells to adhere overnight in a 20 to 23°C incubator.
25. The next day, pre-warm L-15/FBS to room temperature.
26. Wash off unbound cells and larval debris once with 1 ml of L-15/FBS. Aspirate or pipette to remove the media.
27. Add 0.5 to 1 ml of fresh L-15/FBS to the dish and return to the incubator.

6 Larval Cells

Freshly synchronized L1 larvae from one to three NEP-NA22 plates are used for L1 cell isolation. Synchronized CeHR worm culture is used for later stage larval cell isolation. For all stage larval cell isolation, a brief chemical treatment (SDS-DTT) is used to pre-sensitize worm cuticle. The cuticle is then enzymatically digested with pronase E and cells are released with mechanical disruption (pipetting). SDS-DTT and pronase E treatment times have been optimized by stage to reduce cell damage and promote cell survival. See section 5 (Embryonic Cells) for typical yields from larval cell isolation.

Prepare larval cell isolation reagents

6.1.1 Materials

- **1 M HEPES, pH 8.0.** Make a 1M solution in ddH_2O and bring to pH 8.0.
- **10% Sodium dodecyl sulfate (SDS).** Make a 10% (w/v) solution in ddH_2O and store at 4ºC.
- **1 M Dithiothreitol (DTT)**. Make 1 M stocks in room temperature ddH_2O, aliquot, and store at −20ºC. As a reducing agent, DTT is the most sensitive chemical in the larval dissociation protocol and a likely cause of poor larval dissociation. Purchase small bottles of DTT (5 to 10 g) and store at −20ºC in a box with desiccant. Wrap the bottle top with parafilm after each use. DTT may precipitate in cold water. When thawing either DTT stock or SDS-DTT stocks, warm the aliquot in your hand and vortex the aliquot until clear.
- **60% Sucrose**. Make a 60% (w/v) solution in ddH_2O and autoclave.
- Egg buffer.
- L-15/FBS media.
- 15 mg/ml Pronase E (Sigma P8811) in egg buffer.

6.1.2 SDS-DTT solution

1. Assemble the following components:

Component and final concentration	Stock	10.25 ml
20 mM HEPES pH 8.0	1 M	0.2 ml
0.25% SDS	10%	0.25 ml
200 mM DTT	1 M	2 ml
3% sucrose	60%	0.5 ml

ddH_2O	--	7.3 ml

2. In a tissue culture hood, sterilize SDS-DTT solution using a 0.2 µm syringe filter. Store 200 µl aliquots at -20°C.

6.1.3 Pronase E solution

1. Dissolve Pronase E to 15 mg/ml in cold sterile egg buffer with vortexing.
2. Store 100 µl aliquots at -20°C.

Isolating and Culturing L1 cells

1. Seed 2 to 3 NEP-NA22 plates with 20,000 synchronized L1 per plate (see protocol 0, Propagating and synchronizing worms on NEP-NA22 plates) (Figure A- 8).
2. Allow worms to reach gravid adult stage.
3. Use the same 10 ml of ddH_2O to wash gravid adults from each plate and dispense the combined worm suspension into one 15 ml conical tube.
4. Centrifuge at 1,300 g for 1 minute in a clinical centrifuge. Remove water from the top of the supernatant to leave 7 ml of total volume.

Perform the following procedure in the cell culture hood and use filter sterilized or autoclaved water and media.

5. Use protocol 0 (Preparing eggs or hatched larvae) to obtain eggs in M9 buffer. Allow the eggs to hatch overnight on a laboratory rotator.

Wipe pipettors with 70% ethanol after possible contact with bacteria during egg isolation.

6. The next day, pre-warm L-15/FBS and egg buffer to room temperature.

For the following steps, do not vortex to mix larvae or cell suspensions.

7. Pellet synchronized L1 by centrifugation at 1,300 g for 1 minute in a clinical centrifuge. Remove M9.
8. Resuspend the larval pellet with 10 ml of sterile ddH_2O and gentle pipetting. Pellet worms again by centrifugation (1,300 g for 1 minute). Sterilely pour off the supernatant, leaving roughly 1 ml total of pellet and supernatant.
9. Prepare a 1.5 ml microcentrifuge tube by filling it with 40 µl of sterile ddH_2O and marking the water level on the outside of the tube.
10. Transfer pelleted larvae to the prepared microcentrifuge tube. Pellet larvae at 16,000 g for 2 minutes in a microcentrifuge and carefully remove the residual ddH_2O with a 200 µl pipette tip to leave a compact pellet.
11. Use 20 to 40 µl of compacted L1 for isolation. If pellet is larger than 40 µl, resuspend the pellet in a small amount of ddH2O and remove some of the suspended larvae. Re-pellet the suspension and check the level of packed larvae before beginning (Figure A- 9).
12. Add 200 µl freshly thawed SDS-DTT solution to the larval pellet and gently flick the bottom of the tube with the fingertip until mixed. Incubate for exactly 2 minutes at room temperature.

DTT precipitates at low temperature. Warm the SDS-DTT aliquot in the hand to thaw and vortex until it is clear of precipitates before using.

13. Immediately after the SDS-DTT treatment, add 800 µl egg buffer to the reaction. Flick gently to mix.

14. Pellet larvae at 16,000 g for 1 minute. Remove the supernatant and wash 5 more times with 1 ml egg buffer per wash. Resuspend pellets by flicking the tube for each wash.

Note: It is critical to perform steps 12 – 14 quickly, as L1 survival drops dramatically if incubated in SDS-DTT for more than 2 minutes.

15. Add 100 µl freshly thawed 15 mg/ml pronase E to washed larval pellet, flick to mix, and incubate at room temperature for 7 to 9 minutes.
16. Pipette the larvae suspension with a 200 µl tip during the digestion. Adjust the pipetting volume to the approximate volume of the suspended pellet. Slowly pull suspended larvae into the pipette tip. Then, press down to force the pipette tip against the bottom of the microcentrifuge tube and slowly eject the contents. Take approximately 6 to 8 seconds for the downward stroke. Repeat the cycle of up/down strokes a total of 60 to 90 times during the incubation.
17. Monitor the progress of the digestion every 2 to 3 minutes (every 20-30 strokes). Touch the pipet tip to the larval suspension to pick up 1 to 2 µl of reaction, spot this sample on a glass slide, and examine under a tissue culture microscope.
18. Stop the reaction by diluting with 900 µl of L-15/FBS.
19. Centrifuge the digested larvae at 9,600 g for 5 minutes at 4°C. Remove supernatant and wash 2 more times with 1 ml L-15/FBS per wash. Pipette the suspension to mix each time (Figure A- 10).
20. To remove most of the undigested larvae and debris, resuspend the pellet with 1 ml L-15/FBS and settle the suspension on ice for 30 minutes.
21. Gently transfer the top 800 µl cell suspension devoid of large larval debris to a new tube.

22. Use a hemocytometer to count cell density in 10 µl of cell suspension and calculate total number of cells in the suspension (Protocol 0).

Count only large and medium sized cells. Small cells are difficult to distinguish from debris.

23. Centrifuge the cell suspension at 9,600 g for 5 minutes at 4°C.

The embryonic cell isolation protocol pellets cells at a lower relative centrifugal force of 900 g. The higher speeds used here slightly increase the yield of small cells without introducing cellular damage.

24. Resuspend cells with L-15/FBS to a final density of $5x10^6$ to $6x10^6$ cells /ml according to the cell number calculated in step 22.
25. Plate 30 to 50 µl of cell suspension onto the center of peanut lectin-coated glass bottom dishes. Place dishes in a plastic container with a gas exchange hole and humidified with kimwipes wetted with ddH_2O. Allow the cells to adhere overnight in a 20 to 23°C incubator.
26. The next day, pre-warm L-15/FBS to room temperature.
27. Wash off unbound cells and larval debris once with 1 ml of L-15/FBS. Aspirate or pipette to remove the media.

Some cells require more than 24 hours to adhere (David Miller, personal communication). Experiment with adhesion times before washing debris and unattached cells from the coverslip.

28. Add 0.5 to 1 ml of fresh L-15/FBS to the dish and return to the incubator.

Isolating and Culturing L2 – L4 cells

Perform the following procedure in the cell culture hood and use filter sterilized or autoclaved water and media. Do not vortex to mix larvae or cell suspensions.

1. Grow larvae to the desired stage in CeHR medium. Harvest 1 to 2 flasks of worms for the cell preparation (Figure A- 11).
2. For each flask, split the 10 ml of CeHR larvae culture into two 15 ml conical tubes. Add 5 ml of sterile ddH_2O to each 5 ml of larvae culture and mix by inverting the tubes several times. Place tubes in a clinical centrifuge and set the speed to 1,300 g. Start the centrifuge, wait 5 seconds, and stop the centrifugation.

Although the centrifuge will not reach its maximum speed, a brief, five-second centrifugation separates larvae from large particulate matter in the CeHR medium.

3. Remove the supernatant with a pipet and add 10 ml of sterile ddH_2O to each tube and invert the tube several times to resuspend the larvae. Pellet the larvae again for 5 seconds in a clinical centrifuge.
4. Repeat step 3 two more times for a total of three ddH_2O washes.
5. Remove most of the supernatant, leaving approximately 1 ml of total pellet and supernatant.
6. Prepare a 1.5 ml microcentrifuge tube by filling it with 80 µl of sterile ddH_2O and marking the water level on the outside of the tube.

7. Transfer pelleted larvae to the prepared microcentrifuge tube. Pellet larvae at 16,000 g for 2 minutes in a microcentrifuge and carefully remove the residual ddH_2O with a 200 µl pipette tip to leave a compact pellet.
8. Use 30 to 80 µl of compacted L2–L4 for isolation. If pellet is larger than 80 µl, resuspend the pellet in a small amount of ddH_2O and remove some of the suspended larvae. Re-pellet the suspension and check the level of packed larvae before beginning (Figure A-12).
9. Add 200 µl freshly thawed SDS-DTT solution to the larval pellet and gently flick the bottom of the tube with the fingertip until mixed. Incubate for exactly 4 minutes at room temperature.

DTT precipitates at low temperature. Vortex the thawed SDS-DTT until it is clear of precipitates before using.

10. Immediately after the SDS-DTT treatment, add 800 µl egg buffer to the reaction. Flick gently to mix.
11. Pellet larvae at 16,000 g for 1 minute. Remove the supernatant and wash 5 more times with 1 ml egg buffer per wash. Resuspend pellets by flicking the tube for each wash.

Note: It is critical to perform steps 9 – 11 quickly, as larval survival drops dramatically if incubated in SDS-DTT for more than 4 minutes.

12. Add 100 µl freshly thawed 15 mg/ml pronase E to washed larval pellet, flick to mix, and incubate at room temperature for 20 to 25 minutes.

13. Pipette the larvae suspension with a 200 µl tip during the digestion. Adjust the pipetting volume to the approximate volume of the suspended pellet. Slowly pull suspended larvae into the pipette tip. Then, press down to force the pipette tip against the bottom of the microcentrifuge tube and slowly eject the contents. Take approximately 6 to 8 seconds for the downward stroke. Repeat the cycle of up/down strokes a total of 140 to 160 times during the incubation.
14. Monitor the progress of the digestion every 3 to 5 minutes (every 30-50 strokes). Touch the pipet tip to the larval suspension to pick up 1 to 2 µl of reaction, spot this sample on a glass slide, and examine under a tissue culture microscope.
15. Stop the reaction by diluting with 900 µl of L-15/FBS.
16. Centrifuge the digested larvae at 9,600 g for 5 minutes at 4°C. Remove supernatant and wash 2 more times with 1 ml L-15/FBS per wash. Flick the tube gently to mix each time (Figure A- 13).
17. To remove most of the undigested larvae and debris, resuspend the pellet with 1 ml L-15/FBS and settle the suspension on ice for 30 minutes.
18. Gently transfer the top 800 µl cell suspension devoid of large larval debris to a new tube.
19. Use a hemocytometer to count cell density in 10 µl of cell suspension and calculate total number of cells in the suspension (Protocol 0).

Count only large and medium sized cells. Small cells are difficult to distinguish from debris.

20. Centrifuge the cell suspension at 9,600 g for 5 minutes at 4°C.

21. Resuspend cells with L-15/FBS to a final density of $5x10^6$ to $6x10^6$ cells /ml according to the cell number calculated in step 19.
22. Plate 30 to 50 µl of cell suspension onto the center of peanut lectin-coated glass bottom dishes. Place dishes in a plastic container with a gas exchange hole and humidified with kimwipes wetted with ddH_2O. Allow the cells to adhere overnight in a 20 to 23°C incubator.
23. The next day, pre-warm L-15/FBS to room temperature.
24. Wash off unbound cells and larval debris once with 1 ml of L-15/FBS. Aspirate or pipette to remove the media.

Some cells require more than 24 hours to adhere (David Miller, personal communication). Experiment with adhesion times before washing debris and unattached cells from the coverslip.

25. Add 0.5 to 1 ml of fresh L-15/FBS to the dish and return to the incubator.

7 Applications of Cell Isolation and Culture

Isolated cells provide stage-specific developmental "snapshots" of cell-autonomous behaviors. Cells isolated from different stages vary in their morphologies (Figure A- 14). Both cell size and the fraction of multinucleate cells increase in isolates from L2 to L4 stages [163]. This increase mirrors cell growth and formation of syncytia in the maturing larvae. L2 to L4 cells also show a richer variety of morphologies than do embryonic [159] and L1 stage cells [163], where either muscle (L1) or muscle and neurons (embryonic) predominate in culture.

Cellular cross-talk can influence cellular differentiation in mixed cell cultures [171-173]. To compensate, mixed cell populations can be reduced to single cell types through fluorescence-activated cell sorting (FACS, or flow cytometry). Both high and low abundant embryonic cells from GFP marker strains can be isolated, sorted, and cultured for several days [159, 160]. Larval cells can be sorted and enriched using similar methods (D. Miller, personal communication). Thus, mono-cell culture provides a finely controlled environment to study cell-autonomous differentiation and behavior.

When combined with FACS, cell isolation can also be used to profile individual embryonic or larval cells in a near-*in vivo* state. Cell isolation can be performed in approximately two hours and modern flow cytometry instruments can sort through thousands of cells per second. Thus, cells can be isolated and ready for experiments within three hours of separation from their *in vivo* niches. For example, the transcriptome [174-176] or proteome [177, 178] of specific cell types can be profiled with microarrays or mass spectrometry of FACS sorted cells. By isolating embryonic through L4 stage cells, cell linages can be followed over the course of development. More traditional techniques such as co-immunoprecipitation and Western blots can be used to follow cell-specific protein-protein interactions. In each case, the extension of cell isolation from embryos to larvae has the potential to substantially further the study of physiological, cellular, and molecular phenomena at the single cell level.

Co-culture of two different cell populations is increasingly being used to study specific cell-cell interactions [179, 180]. We envision that sorting and co-culture of two different cell populations will provide a unique opportunity to study specific non-cell-autonomous interactions in nematodes. For example, cells providing morphogens or trophic factors could be co-cultured

with appropriate cells types to test models of stage-specific vulval development [181, 182], neuronal guidance cues [183, 184], or stem cell niches [185, 186]. Stage-specific signal generation or response could be studied by varying the isolation time of one of the two cell populations.

Isolated cells spread on two-dimensional substrates also can be used to observe sub-cellular dynamics with greater precision than available *in vivo*. For example, total internal reflection fluorescence (TIRF) microscopy can follow fluorescent "speckles" in cells containing one to a few fluorophores [187]. TIRF microscopy limits excitation to thin "evanescent wave" at the coverslip-buffer interface and substantially reduces both background fluorescence and photobleaching. This 100 – 200 nm thick, exponentially decaying excitation layer [188] only weakly penetrates the 100 – 150 nm thick cuticle of L1 worms and cannot penetrate the 260 – 350 nm thick cuticle of L4 worms [189] or the 300 – 400 nm thick eggshell [190]. Consequently, *in vivo* TIRF microscopy in *C. elegans* has been limited to one-cell and two-cell embryos [191]. In contrast, TIRF microscopy performs optimally on isolated cells on planar substrates. TIRF microscopy of isolated cells can be used to track the cytoskeleton (Figure A- 15) [192, 193], adhesion complexes [194, 195], or endocytosis/exocytosis [196-198] with great detail.

Large-scale embryonic cell culture was originally applied to electrophysiology [159]. Although recording of voltages and ion currents through thin glass pipettes can be done in individual filleted animals [162, 199], the filleting technique is extremely demanding. In contrast, isolated neurons can be produced in abundance and followed for two weeks in culture. Isolated cells are easy to access with patch pipettes for single channel to whole cell recording [reviewed

in 200]. The protocols outlined here will extend isolated-cell electrophysiology to postembryonic lineages.

Neuronal genesis *in vivo* is complete by stage L2 [201], but neurons undergo dramatic post-mitotic changes over the course of development [202, 203]. Cells lose most processes during the isolation step, but neurons from all stages regenerate dendrites and long axons on peanut lectin coated glass over the course of several days [163]. Thus, neuronal isolation from later larval stages could be used to partially recapitulate the dramatic axonal growth and guidance *in vitro* that occurs during larval development *in vivo*. Co-culture of neurons with target cells or gradients of trophic factors could be used to study the specificity of axonal targeting *ex vivo*.

Acknowledgements

We thank Diya Banerjee for helpful discussions and technical advice. This work was supported by a Burroughs-Wellcome Career Award at the Scientific Interface to JRK and a Virginia Tech Institute for Critical Technology and Applied Science Doctoral Fellowship to SZ.

Appendix A. Equipment for Nematode Cell Culture

- **Class II laminar flow hood.** A class II microbiological safety cabinet passes all outside air through a HEPA filtered inlet and thus provides a sterile working area free from dust and microbial contamination. Class II cabinets also contain a UV light source to maintain sterility inside the cabinet when the cabinet is not in use. In a typical class II cabinet, outside air is pulled in through a grating just below the sash. Outside air is kept separate from the working area and channeled toward a HEPA filter at the top of the cabinet. Filtered air is then blown downward into the working environment. A grating at the back of the work surface

recirculates some of this air through the HEPA filter, while the rest escapes to the outside under the sash. Slight positive pressure inside of the working area creates an invisible curtain, sandwiched between the inlet grating and the bottom of the sash, that separates the outside environment from the filtered air inside the working environment. The working surface just beyond the inlet grating can be maintained as sterile. Class II cabinets are available with or without an adjustable sash. Either is sufficient for nematode cell culture. Ideally, the cabinet should be placed in a dedicated tissue culture room. If a dedicated room is not available, place the cabinet in a low-traffic area of the laboratory (Figure A- 16).

A class I fume hood used for working with volatile or toxic chemicals is not sufficient for cell culture. These cabinets only filter exhaust air and are designed to protect the user from contamination, not the working area inside of the cabinet.

- **Laboratory incubator for 20º (optional).** Nematode cells should be kept in a sterile environment at a constant temperature and away from any plates containing bacteria. A CO_2 supply is not necessary to maintain media pH. Many standard 37º tissue culture incubators can be converted to a 20º incubator by closing the CO_2 valve and attaching a chilled circulating bath filled with tap or distilled water (not deionized) to the incubator's water jacket. If an incubator is not available, dishes with cultured cells can be kept at room temperature and away from bacteria plates in sterile, plastic containers. (Suggested model: Nuaire NU-4750 incubator and Julabo F12 water bath)
- **Laboratory refrigerator/freezer combination.** A separate refrigerator/freezer unit for tissue culture media and ingredients is recommended to minimize contamination.

- **Two-stage vacuum trap for aspiration.** Construct an aspirator for the culture hood using two Buchner or Erlenmeyer flasks, two 1-hole or 2-hole rubber stoppers, glass Pasteur pipets or glass tubes, and Tygon tubing as shown above. Use a 1000 ml or larger flask for the first stage trap. Connect the second stage to a vacuum supply or pump through a vacuum filter to protect the pump from residual water vapor.

- **Stainless steel pipet sterilization boxes.** Obtain at least two sterilization boxes and keep one autoclaved box of pipettes in the culture hood at all times. (Suggested model: Fisher Scientific 03-475-5 rectangular box for 9 in Pasteur pipets)

- **Set of pipettes for flow hood.** Keep a separate set of autoclavable 2 - 20 µl, 20 - 200 µl, and 100 - 1000 µl pipettes to be used only for cell culture. Autoclave the pipettes according to the manufacturer's instructions. Autoclave again every one to two months or in case of contamination.

- **Tissue culture microscope.** An inverted, phase contrast microscope with 10x, 20x, and 40x phase-contrast objectives and a long working distance condenser should be used for observing the extent of cell extraction, for counting cells, and for cell maintenance.

- **Stereo dissecting microscope.** A standard stereo microscope used for nematode maintenance and counting.

- **High-resolution epi-fluorescence/DIC inverted microscope.** An inverted microscope with objective lens below the specimen may be used for observing the behavior of cultured cells. We recommend epi-fluorescence illumination for locating GFP expressing cells and differential interference contrast (DIC) optics for observing cellular behavior. Alternatively,

an upright microscope with a water-immersion lens may be used for imaging cultured cells plated on glass-bottom petri dishes.

- **Osmometer.** Either a vapor pressure osmometer or freezing point depression osmometer can be used to estimate and adjust cell culture media osmolarity before filtration. Adjustment is done infrequently, and a shared osmometer or one located in a different building is sufficient. (Suggested model: Wescor Vapro 5520 or 5600)
- **Clinical centrifuge.** Either a fixed-angle or swinging bucket centrifuge for 15 ml conical tubes with a maximum speed of 1,300 g can be used for pelleting nematodes and floating eggs on sucrose. (Suggested model: Fisher Scientific 228 Benchtop Centrifuge)
- **Refrigerated centrifuge.** Use a refrigerated centrifuge with maximum speed of ~16,000 g for 1.5 ml tubes. If a refrigerated microcentrifuge is not available, keep one non-refrigerated microcentrifuge in a cold room or laboratory refrigerator and one non-refrigerated microcentrifuge at room temperature on a nearby bench-top.
- **Portable serological pipet-aid for flow hood.** An electric pipet-aid with aspiration and dispensing buttons and a sterile inlet filter. This pipet-aid should be used only for cell culture. Keep a supply of spare filters to replace wetted or contaminated filters.
- **Hemocytometer.** Obtain a standard, four-quadrant glass hemocytometer slide for counting cells. Note that hemocytometers use non-standard, 0.5 mm thick coverslips. These thick coverslips do not bend under liquid surface tension and insure a consistent volume for cell counting. Hemocytometer coverslips can be rinsed and reused indefinitely, but keep at least one extra coverslip at hand in case of breakage.

- **Glass bottles.** Cell culture glassware should be kept separate from other laboratory glassware to limit contamination from residual detergents, salts, lipids, and proteins. Obtain a new set of 500 and 1000 ml Pyrex or borosilicate glass bottles with GL45 caps and label them as "Cell Culture Only" with a paint pen. Wash all new glassware in a detergent compatible with tissue culture such as Decon 90 or 7X to remove factory and storage contaminants. Fill the bottle with deionized water and autoclave on a liquid cycle with the tops loose. Wash and rinse bottles once more. Fill with deionized water, and autoclave again. Thereafter, do not use detergents in tissue culture glassware or limit their use.
- **Reusable filter holders (Nalgene DS0320-5045).** Nutrient-rich culture media must be sterile filtered for storage and use. Reusable, autoclavable bottle-top filter holders are less expensive over time than disposable filter bottles. Obtain two to four 500 ml filter holders that screw onto standard GL45 threaded bottles. Alternatively, disposable bottle top filter sterilizers may be used to save time.
- **Laboratory rotator.** A slow tube rotator or vertical carousel may be used to hatch nematode eggs.
- **Incubated orbital shaker.** A variable speed incubated shaker is used to grow nematodes in CeHR axenic media at 22ºC. A non-sterile shaker/incubator may be used if nematodes are grown in T25 flasks with vented 0.2 μm filter caps for gas exchange. Alternatively, an open-air shaker may be used if larval stage is regularly monitored during growth in CeHR media.
- **Vortex mixer.** General-purpose laboratory variable-speed mixer for 1.5, 15, and 50 ml conical tubes.

Appendix B. Disposable Supplies for Cell Culture

- **Serological pipets (10 ml, 5 ml).** Sterile, graduated, plastic pipets for tissue culture come individually wrapped and have a cotton plug at one end to prevent wetting of the pipet-aid filter. Keep several in a bin or rack very close to the culture hood to minimize arm and body motion that might waft unfiltered air into the hood. Always store pipets in the same orientation to prevent accidentally opening them from the wrong end.
- **Sterile pipette tips.** Autoclave racks of pipette tips and keep at least one box of each size in the culture hood at all times. Do not remove from the hood after opening.
- Glass Pasteur pipets.
- **Sterile syringes (10 ml, 3 ml).** Use individually wrapped syringes.
- **Sterile syringe filters, 0.22 µm pore size, either PVDF or PES.** Use individually wrapped filters for sterilizing small quantities of liquids.
- **Sterile syringe filters, 5 µm pore size.** Large pore filters are used for embryonic cell isolation. They are not required for larval stage cell isolation (Suggested model: Pall Corp. 4650).
- **Sterile membrane filters, 0.22 µm pore size, 47 mm diameter.** Membrane filter diameter should match the diameter of the reusable bottle-top filter housing. (Suggested Model: Millipore GSWG047S6). Membrane filters are not required if disposable bottle-top filters are used.

- **Disposable vacuum filters, 0.2 – 0.22 μm pore size,(500 ml).** Disposable filters with integrated plastic receiving flasks are available from a number of manufacturers. They are a convenient substitute for reusable bottle-top filters.
- **Sterile conical tubes (15 ml, 50 ml).** Purchase either in bulk or in disposable Styrofoam racks. Open the plastic sleeve only at one end and only in the hood. The plastic sleeve may be discarded if the rack is left permanently in the hood. If the rack needs to be removed from the hood to make room, roll the open end of the plastic sleeve closed and affix with tape before removing from the sterile environment.
- **Spray bottle with 70% ethanol.** Do not use pure ethanol (190-200 proof), as it is not as effective at killing mold and bacteria as 70% ethanol.
- **Kimwipes.** Either large or small kimwipes (Kimberly-Clark) or equivalent low lint wipe should be kept near but not within the cell culture hood. An acrylic kimwipe box holder affixed to the culture hood above the sash is a convenient location.
- **Powder free gloves.** Powdered residue from the manufacturing process will contaminate culture media and cells. Keep powder-free, residue-free latex, vinyl, or nitrile gloves near the culture hood, but not within it.
- 1.5 ml microcentrifuge tubes with snap caps.
- **T25 tissue culture flasks, uncoated, with vented caps.** These 25 cm^2 surface area canted neck flasks are used for growing larvae in axenic growth media. The vented cap contains a 0.2 μm filter for sterile gas exchange. They are not required for embryonic or L1 stage cell culture.

- **Osmometer calibration standards and sample discs.** Calibration standards come in sealed glass ampoules that should be used immediately and discarded. For a vapor pressure osmometer, consult the manufacturer for the appropriate disposable sample disc filters. (Suggested models: Wescor Opti-Mole 100, 290, and 1000 mmol/kg standards and Wescor sample discs).
- **Sodium Hypochlorite (household bleach).** Only use bleach to sterilize glass or plastic. Halides such as bleach corrode metal. Do not use bleach to sterilize stainless steel or any other metal surfaces.

Appendix C. Sterile Techniques for Nematode Cell Culture

Because *C. elegans* do not harbor any known human, mouse, or primate infectious agents, nematode cell culture requires only Bio-Safety Level 1 (BSL-1). Nevertheless, maintaining cells in culture requires attention to sterility beyond that required by the aseptic techniques as practiced by most laboratories that maintain nematodes. Cell culture media containing fetal bovine serum (FBS) are rich in nutrients and highly prone to bacterial and fungal contamination, even in the presence of limited antibiotics. Numerous resources on sterile technique for cell culture are available and include books [204], technical handbooks from major media suppliers (GIBCO), and online videos (YouTube). The equipment, supplies, and rules listed below are the minimum needed to extend common *C. elegans* sterile techniques to nematode cell culture.

Before starting cell culture

Open flames are no longer recommended for use inside of a class II laminar flow hood (Centers for Disease Control and Prevention, CDC). An open flame presents a fire

hazard when used with 70% ethanol. Furthermore, heat disrupts the airflow pattern within the cabinet and can damage the HEPA filter.

1. Tie back long hair and remove any rings, watches, or bracelets. Wash both hands and wrists thoroughly with antibacterial soap.
2. Don a laboratory coat and powder free latex or vinyl gloves after washing and drying.
3. Spray gloves with 70% ethanol and dry with kimwipes.
4. Change gloves after leaving or reentering the culture area.

Do not touch your face, hair, pockets, clothes, or phone while working in the hood. Turn off your cell phone to avoid distractions. If you accidentally touch any potentially contaminated surface, decontaminate gloves with ethanol or change gloves depending on the extent of the potential contamination.

5. Before working in the culture hood, turn off the UV lamp, turn on the blower, and raise the sash to the working mark if the sash is adjustable.
6. Organize the work surface so that the area immediately in front is clear. Thoroughly spray the work surface inside the hood with 70% ethanol and wipe with kimwipes.

Disinfect often. When leaving the culture hood for more than 30 minutes or when changing operators, disinfect the work surface with 70% ethanol.

7. Disinfect items such as pipet-aids, bottles, and tubes with 70% ethanol and wipe with kimwipes before placing them in the culture hood.
8. Move permanent residents of the hood such as sterile pipette boxes and racks for conical tubes to either side of the work surface when not in use.

HEPA filters remove most particulate matter from air, but a small fraction of a percent of dust, bacteria, spores, etc. pass through. This percentage increases with filter age, so have the culture hood checked and certified yearly. Though the chances of contaminating your cultures and media in the hood are much slimmer than on a bench, they are not zero. When training, it may be helpful to visualize a constant rain of contaminating particles inside of the hood.

After finishing cell culture

1. Organize the work surface of the culture hood. Move any permanent residents of the hood such as racks and pipette tip boxes to either side of the work surface.
2. Disinfect the culture hood work surface with 70% ethanol.
3. Disinfect the vacuum trap by aspirating a small amount of household bleach directly into the Tygon tubing. Follow with distilled water. Spray and wipe the tubing end with 70% ethanol. Discard liquid in the trap according to your institution's safety policies.
4. Lower the sash to its closed position (if adjustable), turn off the blower, and turn on the UV lamp.
5. Organize and disinfect any other open bench tops in the cell culture area with 70% ethanol.
6. If any at-hand stocks such as serological pipets or gloves are low, refill the drawer or container. Properly dispose of sharps containers and trash when full.

Be mindful of coworkers. Unlike your personal laboratory bench, cell culture areas are usually shared resources. Sloppiness can ruin your colleagues' experiments. When you

are done, insure that the cell culture area is tidy, organized, and clean. Remember that cleanup is an essential part of any experiment!

Opening and closing containers in the culture hood

1. Disinfect any bottles and containers before placing in the culture hood. Spray the outsides and bottoms with 70% ethanol and wipe down with kimwipes.
2. Reorganize containers to minimize motion during each step in a protocol. For example, if you are right handed, place pipette tip boxes to the right of any media bottles you are working with. Work slowly and deliberately.

Only open sterile containers in the culture hood. If a container must be left open for an extended period (i.e. UV sterilization), place it at the back of the culture hood to minimize contamination from room air.

3. Before picking up a pipette or pipet-aid, use two hands to loosen the screw tops of any containers you will be using.
4. For conical tubes, unscrew the cap with thumb and index finger while holding the tube in your hand. Lift the cap from the tube in thumb and index finger while holding the tube in the same hand. With practice, you will be able to remove the top without dropping the tube or touching the tube rim. Alternatively, the tube may be kept in a rack while removing and replacing the top.
5. For larger bottles, unscrew the top, then grasp the top between index and middle fingers and lift it off. This leaves the thumb and index fingers free to grab the sides of the bottle. The bottle may then be lifted or tilted without setting the top down.

An inverted top collects particulate contaminants. Keep tops upright (facing down) at all times. If a top must be temporarily put down, place it face down on a disinfected area of the hood's work surface.

6. Close the bottle tightly before removing from the culture hood,

Preparing glass bottles for cell culture

1. Before using bottles for media, rinse glassware and bottle tops 5 times in distilled water followed by 5 times in deionized water (ddH_2O). Let stand while cleaning additional glassware then pour out any residual water.

Rinse used media bottles in distilled water soon after emptying them of media to prevent the buildup of dry contaminants.

2. Thread the top onto the bottle so that it is attached but loose enough for steam to escape. Cover the cap and bottle top with aluminum foil. Insure that the foil overlaps at least the top 1/4 of the bottle, is free of tears and holes, and is loose enough for steam to escape beneath the foil.
3. Place a short strip of autoclave tape across the top of the foil and autoclave on a dry/gravity cycle.
4. After cooling, gently tighten the bottle top through the foil and store with foil cover in a closed cabinet or on a shelf in a low-traffic area.

Once sterilized, bottles should only be opened and closed in the culture hood.

Preparing and using 1.5 ml centrifuge tubes for cell culture

1. Fill a small glass or autoclave-compatible plastic beaker with microcentrifuge tubes and cover with a double layer of aluminum foil insuring adequate overlap of the beaker rim.
2. Affix a strip of autoclave tape and autoclave on dry/gravity. Store with foil cover in a closed cabinet or on a shelf in a low-traffic area.
3. Before use, decontaminate the bottom and sides of the beaker with 70% ethanol and place in the culture hood.
4. To withdraw a tube, gently remove the foil without flattening it and place the tented foil top face down on a disinfected area of the work surface.
5. Gently shake the container until one tube can be reached without touching any others.
6. Recover the container with foil and keep it in the culture hood until empty.

Only open the container under the culture hood. If contaminated, or if the foil-cover tears, retrieve a fresh beaker of tubes. Clean, unused tubes may be autoclaved again to sterilize.

Preparing reusable bottle-top filters

Convenient, disposable bottle-top filters are available from a number of manufacturers. Reusable bottle-top filters provide a more cost effective solution for laboratories on a more restricted budget.

1. Wash and rinse filter holders 5 times in distilled water and 5 times in deionized water as with glass bottles.

2. Remove the GL45 cap from a glass bottle and screw the bottom of the filter to the bottle (Figure A- 17).
3. Use blunt forceps or gloved hands to place a 47 mm diameter, 0.22 µm filter into the holder. Discard any blue filter spacer.
4. Assemble the filter holder loosely to allow steam to penetrate.
5. Wrap a piece of aluminum foil vertically around the filter holder and at least the top 1/4 of the bottle. Pinch and roll the two ends of the foil together. Cover the top of the filter with another piece of foil. Hand-crimp the foil to the bottle at the bottom. Tape the foil to the bottle with short strips of autoclave tape.

To prevent foil tearing, align the folded seam with the filter's vacuum connector.

6. Place a GL45 bottle cap you removed earlier face down on a double-layered piece of foil. Wrap the foil around the cap completely and affix with autoclave tape.
7. Autoclave the filter and cap on a dry/gravity cycle and store with the foil covers in a closed cabinet or on a shelf in a low-traffic area.

Filtering media with disposable or reusable bottle-top filters

1. Before use, unwrap the filter holder in the flow hood under sterile conditions and tighten all fittings by hand.
2. Attach the vacuum line and filter a small quantity of media into the filter to test for leaks. If no leaks were found, pour the remaining media to be filtered into the reservoir under vacuum.

3. After filtering media, remove the filter, unwrap the bottle cap under the culture hood, and close the bottle.

If the filter becomes clogged, remove the vacuum line and gently unscrew the filter from the sterile bottle. Pour the remaining liquid from the filter reservoir back into the source bottle. Temporarily cap the already filtered liquid. Use a fresh bottle-top filter to process the remainder of the liquid and sterilely pour the two filtered contents together.

Using syringe filters

1. Place a wrapped syringe filter and appropriately sized syringe in the culture hood.
2. Syringe filters are wrapped with molded polystyrene covering the outlet side and a flat paper/foil cover on the inlet side. Remove the paper/foil cover but do not remove the filter from the polystyrene wrapping.
3. Unwrap the syringe and pull the plunger completely out. The plunger may be temporarily placed back within the syringe wrapping or upside-down on the disinfected work surface.
4. Twist the syringe tip onto the filter top until snug.
5. While holding the syringe, lift the filter out of its plastic wrapping. Do not touch the filter disc.
6. Pour the liquid to be filtered into the upright syringe.
7. Gently replace the plunger onto the top of the syringe while holding the assembly over the destination container.
8. Gently press the plunger until a seal is made, then increase pressure to filter the remaining liquid.

9. Cap the container and discard the filter and syringe according to according to your institution's safety policies.

 *Syringe filters always retain some residual unfiltered liquid. To avoid contamination, do not attempt to force this remaining liquid through the filter.*

Pipetting in the culture hood

1. Only open serological pipets under the culture hood. Insure that there are no tears or cuts in the pipet wrapping. If the pipet aid is stored outside of the hood, disinfect with 70% ethanol and wipe before placing it in the culture hood.
2. With one hand, grasp the top of the wrapping. In the other hand, grasp the pipet upright with thumb pressing vertically against the clear plastic side.
3. While placing pressure on the pipet with the thumb, use the other hand to pull the top of the wrapping toward the thumb. This punctures the top of the pipet through the paper side of the wrapping. Fold the wrapping down without touching the pipet.
4. Insert the pipet into the pipet-aid and twist to seat. Turn the pipet until the markings are easily readable and remove from the wrapping.
5. Dip only the tip of the pipet into the source liquid without touching the rim of the container.
6. Aspirate the desired amount. Watch the liquid level in the pipet to prevent overfilling and wetting the cotton plug and pipet-aid.

 *Gloves, pipettes, bottles, etc. pick up particulate matter while outside of the hood and shed it inside of the hood. Do not pass hands, bottles, etc. over the mouth of any open*

container. When pipetting, tilt both the container and the pipette at an angle so that neither the pipet-aid nor the hands are directly above the container mouth.

7. Dispense the contents above any existing liquid without touching the rim of the destination container or any existing contents inside of the destination container.

For accurate micropipetting, dispense the liquid with the pipette tip touching the inside rim of the destination container. Discard the tip.

8. To minimize back-contamination, dip the pipet back into the source container *only* if you are sure that it did not touch any other liquid or surface during the transfer.
9. When changing liquids or if the pipet becomes contaminated, discard the pipet and use a fresh pipet. Use the same care with pipette tips.

Watch the pipet at all times before and during liquid transfer to insure that it does not touch the outside of any container or any surface.

10. Discard of used pipets according to your institution's safety policies.

Pouring liquids

1. Hold the source bottle far enough above the destination bottle so that the rims of the two never touch.
2. Gently pour the source liquid into the destination container with one smooth motion.

Wipe up any spills immediately. Blot the spill dry. Decontaminate the spill area with 70% ethanol and wipe dry with kimwipes.

Aspirating liquids with Pasteur pipets

1. Fill stainless steel boxes or cylinders with Pasteur pipets, narrow end down.
3. Tape the lid to the side of the box with a short strip of autoclave tape and autoclave on dry/gravity.
4. Keep at least one autoclaved box in the culture hood. Cut or remove the autoclave tape before use.
5. When ready to aspirate, turn on the vacuum supply. If the vacuum valve or switch is outside of the culture hood, decontaminate gloves with ethanol or change them.
6. Grasp the Pasteur pipet box horizontally with both hands and remove the top.
7. Shake the pipet box horizontally until one pipet is extended more than any others.
8. Grasp the end of this pipet between two free fingertips and withdraw it.

Alternately, with the hand facing away from the box, grasp the end of the pipet between the backs of two fingers, and withdraw the pipet. This orientation prevents the pipet tip from touching any contaminating surface while the box is reassembled.

9. Carefully place the lid back on the box and put the box down.
10. While touching only the top end of the pipet, insert it into the Tygon tubing on the vacuum trap.
11. Aspirate the liquid from the top down, touching only the inside of the container with the pipet tip.
12. Change pipets between samples to avoid cross contamination of experiments.
13. Discard of used glass pipets according to your institution's safety policies.

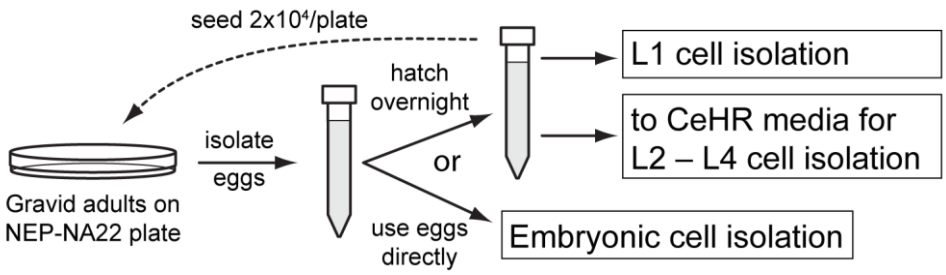

Figure A- 1 Using NEP-NA22 plates

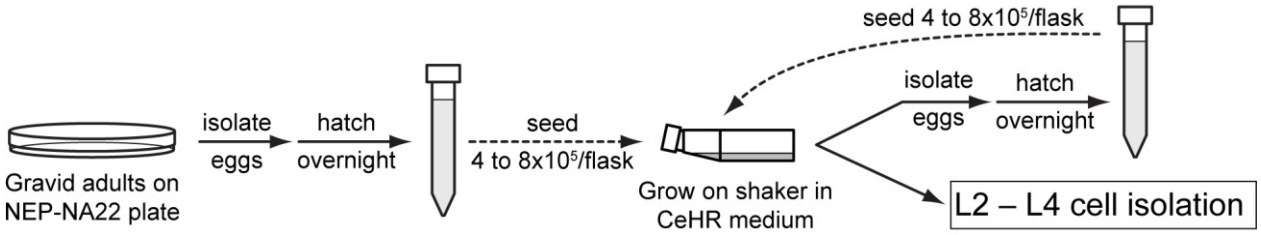

Figure A- 2 Maintaining and using CeHR flasks

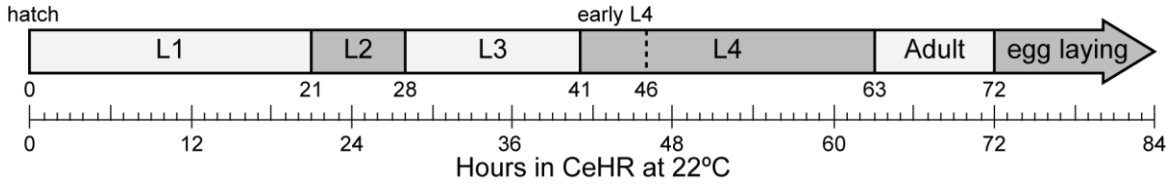

Figure A- 3 Approximate growth rate of nematodes at 22ºC after adaptation to CeHR [1]

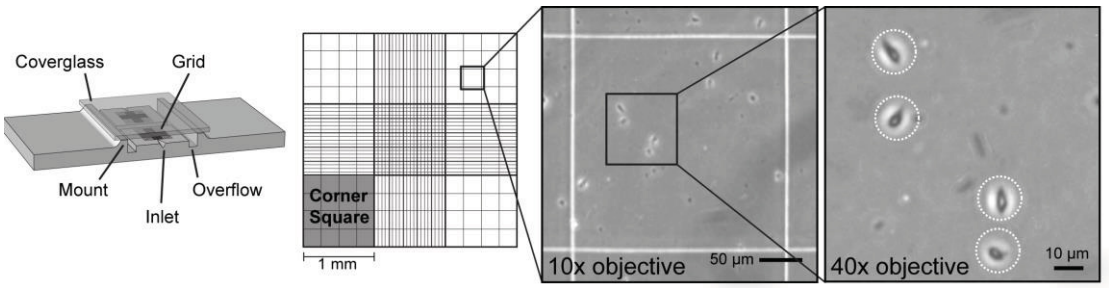

Figure A- 4 Hemocytometer used for counting cells

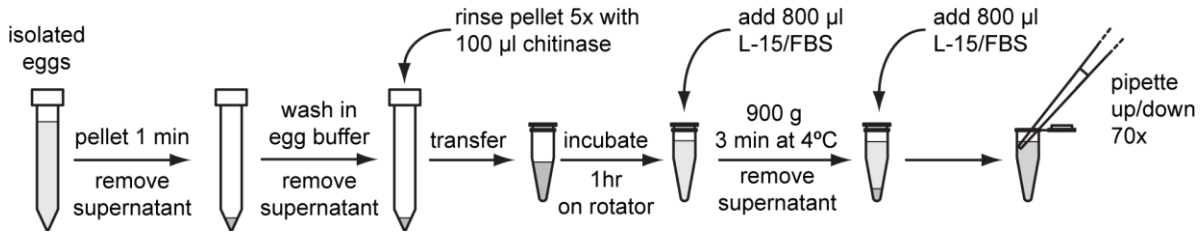

Figure A- 5 Chitinase digestion and dissociation of embryos

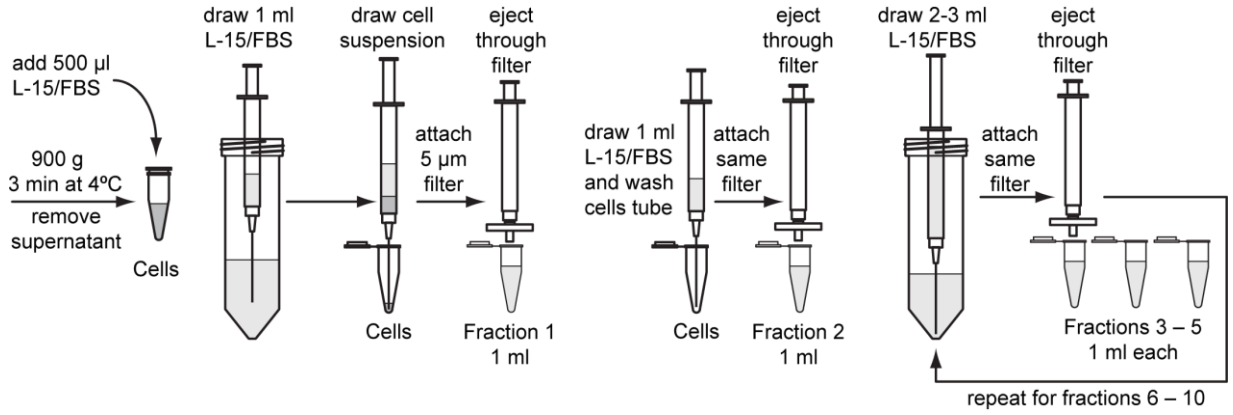

Figure A- 6 Filter separation of embryonic cells from debris

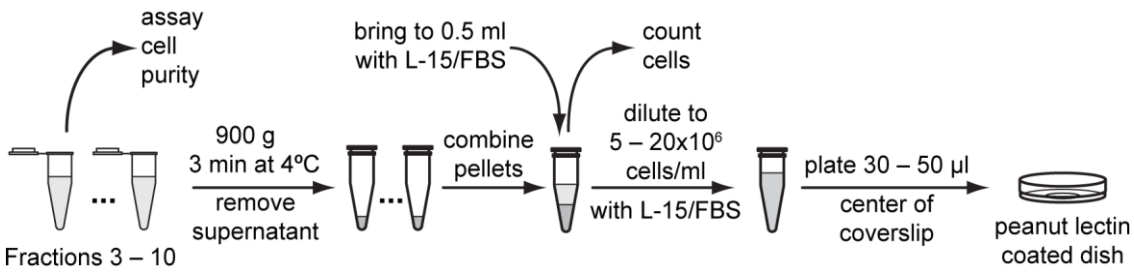

Figure A- 7 Plating cells from the purest fractions

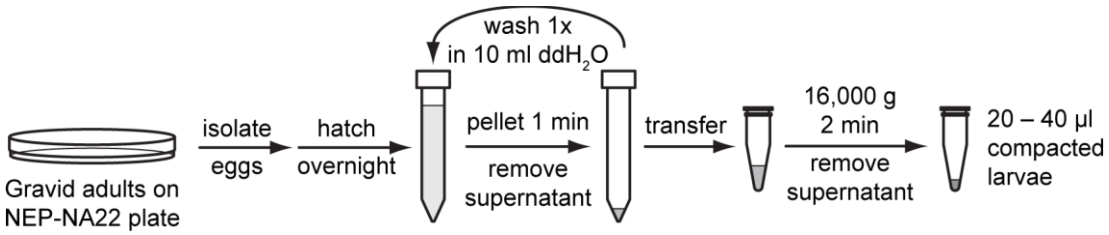

Figure A- 8 Harvesting L1 for cell culture

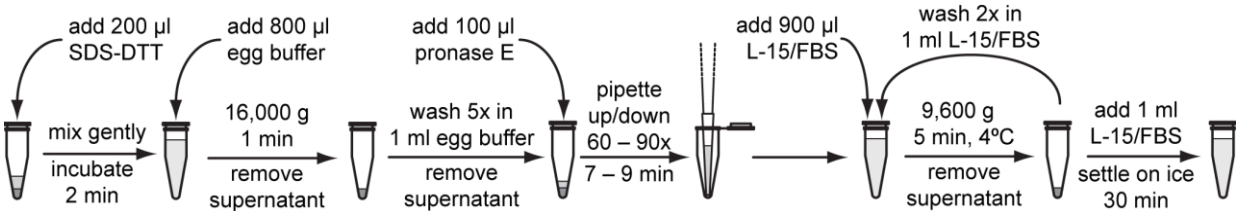

Figure A- 9 Digesting L1

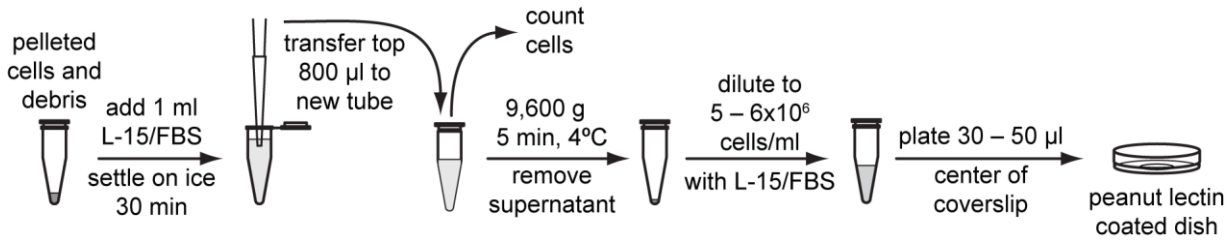

Figure A- 10 Cleaning and plating L1 cells

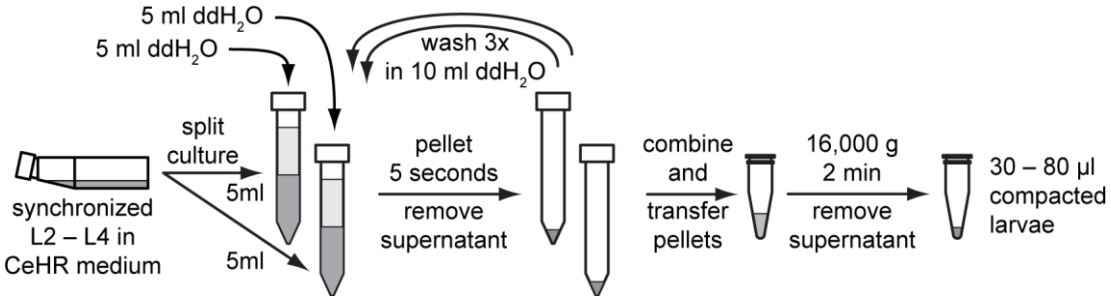

Figure A- 11 Harvesting L2 – L4 for cell culture

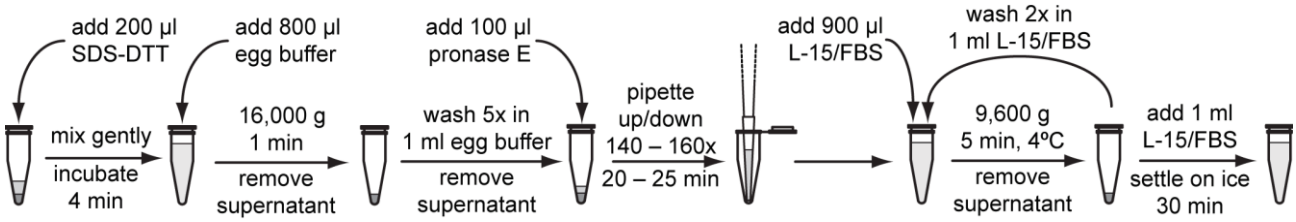

Figure A- 12 Digesting L2 – L4

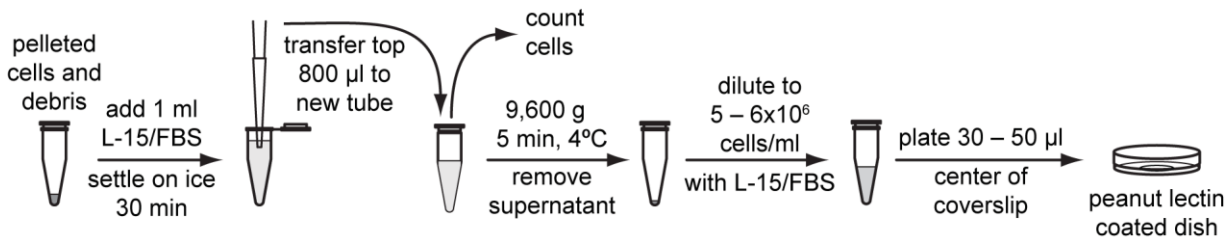

Figure A- 13 Cleaning and plating L2 – L4 cells

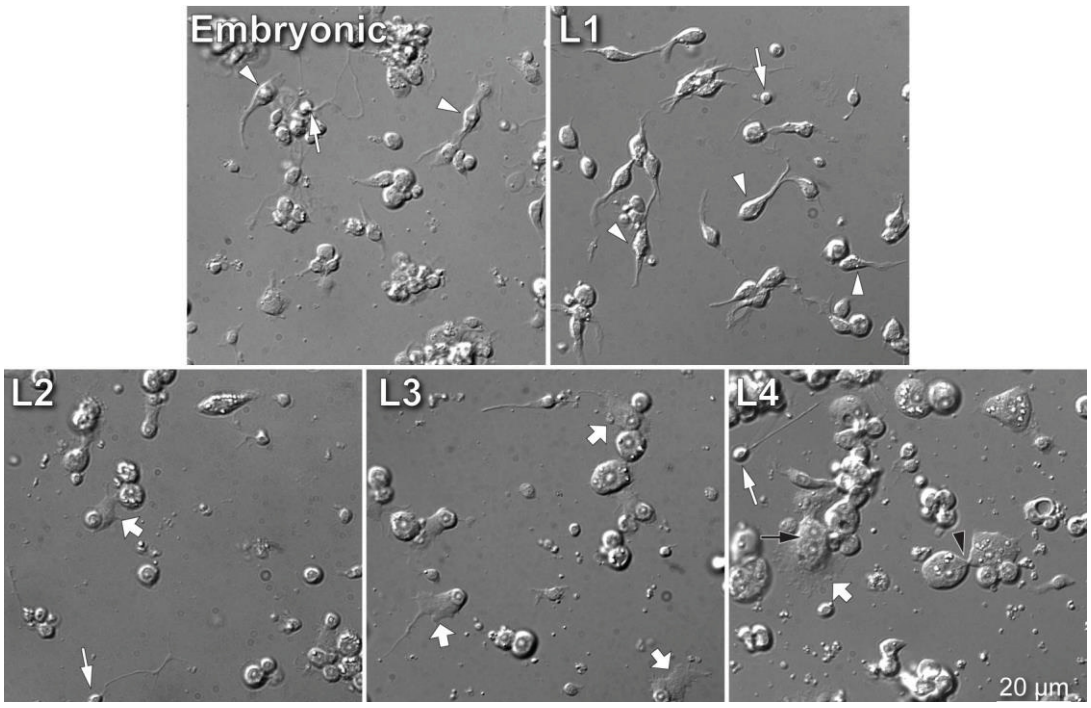

Figure A- 14 DIC micrographs of one-day culture of cells from embryos and L1 through L4 stage larvae

Several cellular morphologies can be seen including muscle cells (white arrowhead), neurons (white arrow), and cells with large protrusions (large white arrows). L4 stage cell morphologies include multiple nuclei (black arrow) and cleavage furrows (black arrowhead).

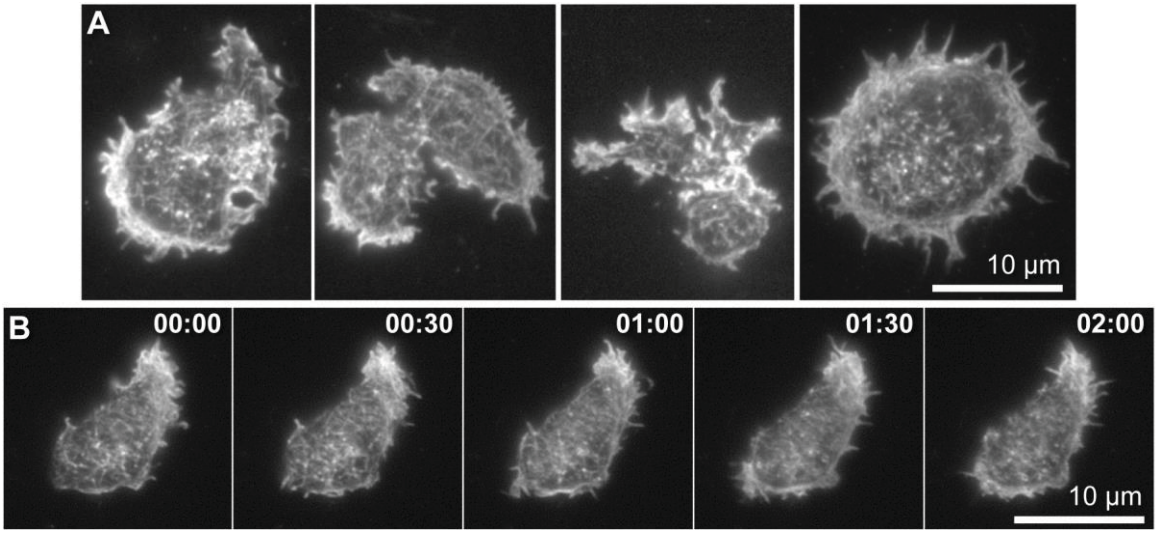

Figure A- 15 Actin filaments in isolated embryonic M-lineage cells

(A) Actin filaments were labeled with the actin binding domain of Utrophin [205] linked to mEGFP. Live cells from this hlh-8::mEGFP-UtrCH marker strain were imaged with total internal reflection fluorescence (TIRF) microscopy. (B) Time-lapse TIRF micrograph of actin filaments in an isolated M-lineage cell. Times shown in min:sec.

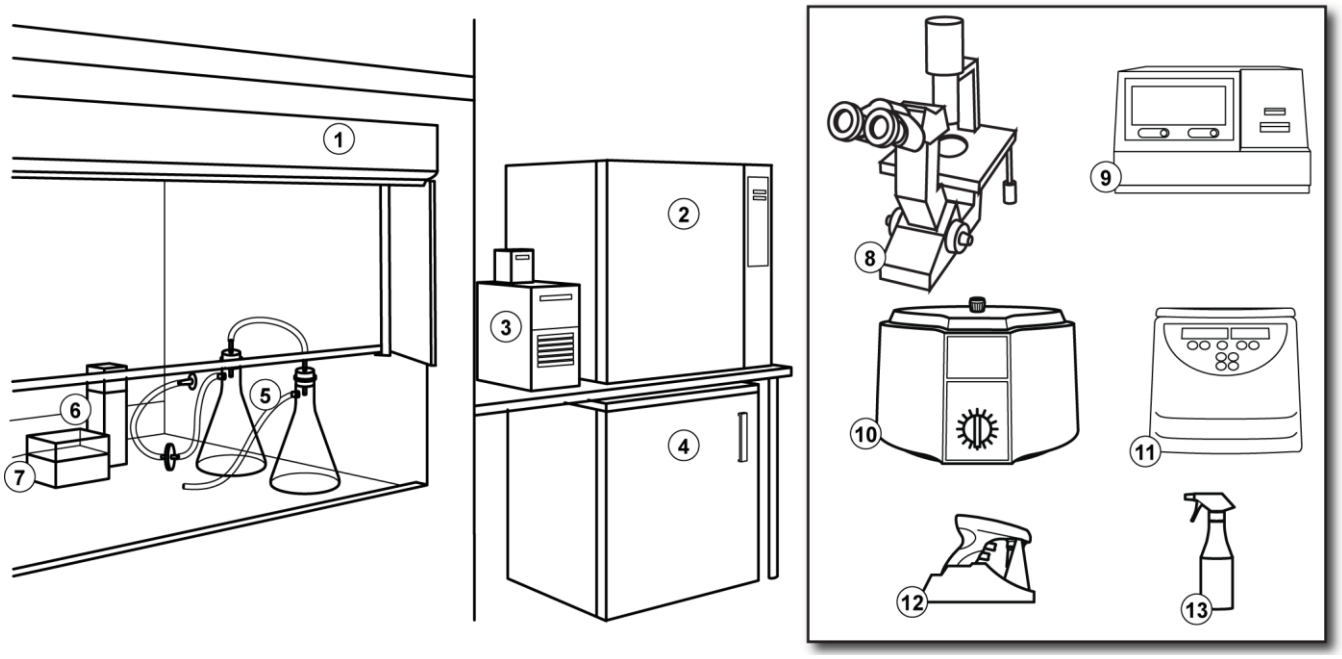

Figure A- 16 Major cell culture equipment and supplies

(1) class II flow hood; (2) incubator with (3) chilled water supply; (4) refrigerator/freezer; (5) vacuum trap; (6) box for sterile glass pipets; (7) pipette tips; (8) microscope; (9) osmometer; (10) clinical centrifuge; (11) refrigerated microcentrifuge; (12) pipet-aid; (13) spray bottle with 70% ethanol.

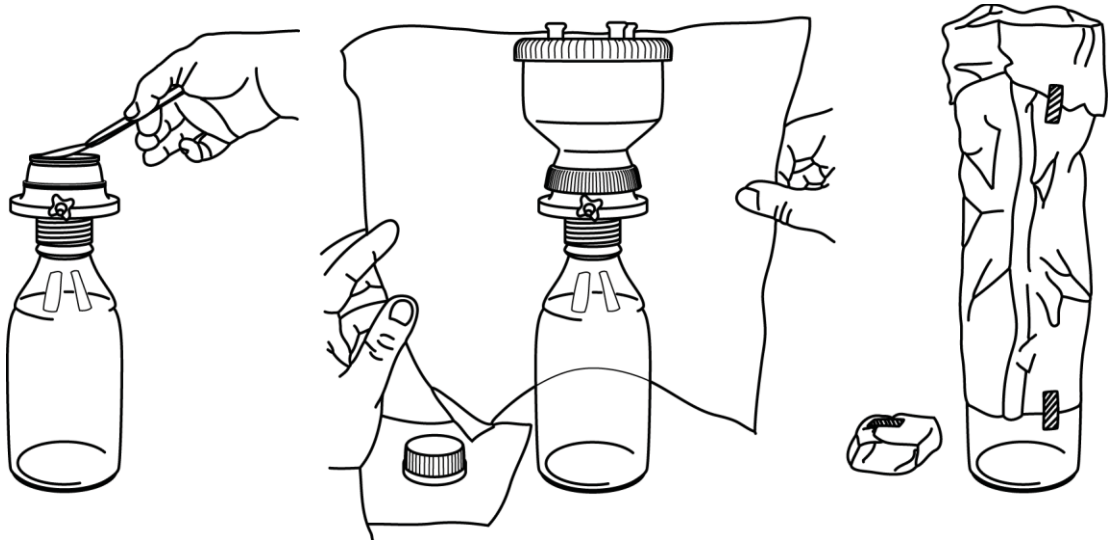

Figure A- 17 Assemble reusable bottle-top filters

Add a 0.22 membrane filter to the bottle-top filter housing and loosely assemble the filter housing. Wrap both the filter and a bottle cap in foil and affix with autoclave tape.

Table A- 1 Typical yields for embryonic and larval cell isolation

Cell Source	Cells per µl packed eggs or larvae	Cells per egg or larva
Embryo	$6.1 \pm 2.9 \times 10^4$	3.8 ± 1.8
Stage L1	$2.7 \pm 1.9 \times 10^4$	2.5 ± 1.7
Stage L2 – L4	$7.8 \pm 1.7 \times 10^4$	—

References

1. Szilagyi, M., *Global Alterations in Gene Expression During Organophosphate Pesticide Intoxication and Recovery: Interim Report. Report No. USAMRICD-TR-06-02*, 2006, U.S. Army Medical Research Institute of Chemical Defense.
2. Abercrombie, M., J.E. Heaysman, and S.M. Pegrum, *The locomotion of fibroblasts in culture. I. Movements of the leading edge.* Exp Cell Res, 1970. **59**(3): p. 393-8.
3. Pollard, T.D. and G.G. Borisy, *Cellular motility driven by assembly and disassembly of actin filaments.* Cell, 2003. **112**(4): p. 453-65.
4. Lowery, L.A. and D. Van Vactor, *The trip of the tip: understanding the growth cone machinery.* Nat Rev Mol Cell Biol, 2009. **10**(5): p. 332-43.
5. Hall, A., *Rho family GTPases.* Biochem Soc Trans, 2012. **40**(6): p. 1378-82.
6. Hall, A., *Rho GTPases and the control of cell behaviour.* Biochem Soc Trans, 2005. **33**(Pt 5): p. 891-5.
7. Parsons, J.T., A.R. Horwitz, and M.A. Schwartz, *Cell adhesion: integrating cytoskeletal dynamics and cellular tension.* Nat Rev Mol Cell Biol, 2010. **11**(9): p. 633-43.
8. Small, J.V., et al., *The lamellipodium: where motility begins.* Trends Cell Biol, 2002. **12**(3): p. 112-20.
9. Abercrombie, M., *Croonian Lecture, 1978 - Crawling Movement of Metazoan Cells.* Proceedings of the Royal Society B-Biological Sciences, 1980. **207**(1167): p. 129-+.
10. Le Clainche, C. and M.F. Carlier, *Regulation of actin assembly associated with protrusion and adhesion in cell migration.* Physiol Rev, 2008. **88**(2): p. 489-513.
11. Bugyi, B. and M.F. Carlier, *Control of actin filament treadmilling in cell motility.* Annu Rev Biophys, 2010. **39**: p. 449-70.
12. Mullins, R.D., J.A. Heuser, and T.D. Pollard, *The interaction of Arp2/3 complex with actin: nucleation, high affinity pointed end capping, and formation of branching networks of filaments.* Proc Natl Acad Sci U S A, 1998. **95**(11): p. 6181-6.
13. Svitkina, T.M. and G.G. Borisy, *Arp2/3 complex and actin depolymerizing factor/cofilin in dendritic organization and treadmilling of actin filament array in lamellipodia.* J Cell Biol, 1999. **145**(5): p. 1009-26.
14. Ridley, A.J., *Life at the leading edge.* Cell, 2011. **145**(7): p. 1012-22.
15. Kolodkin, A.L. and M. Tessier-Lavigne, *Mechanisms and molecules of neuronal wiring: a primer.* Cold Spring Harb Perspect Biol, 2011. **3**(6).
16. Heasman, S.J. and A.J. Ridley, *Mammalian Rho GTPases: new insights into their functions from in vivo studies.* Nat Rev Mol Cell Biol, 2008. **9**(9): p. 690-701.
17. Nobes, C.D. and A. Hall, *Rho, rac, and cdc42 GTPases regulate the assembly of multimolecular focal complexes associated with actin stress fibers, lamellipodia, and filopodia.* Cell, 1995. **81**(1): p. 53-62.
18. Ridley, A.J. and A. Hall, *The small GTP-binding protein rho regulates the assembly of focal adhesions and actin stress fibers in response to growth factors.* Cell, 1992. **70**(3): p. 389-99.
19. Ridley, A.J., et al., *The small GTP-binding protein rac regulates growth factor-induced membrane ruffling.* Cell, 1992. **70**(3): p. 401-10.

20. Rotty, J.D., C. Wu, and J.E. Bear, *New insights into the regulation and cellular functions of the ARP2/3 complex.* Nat Rev Mol Cell Biol, 2013. **14**(1): p. 7-12.
21. Sit, S.T. and E. Manser, *Rho GTPases and their role in organizing the actin cytoskeleton.* J Cell Sci, 2011. **124**(Pt 5): p. 679-83.
22. Rossman, K.L., C.J. Der, and J. Sondek, *GEF means go: turning on RHO GTPases with guanine nucleotide-exchange factors.* Nat Rev Mol Cell Biol, 2005. **6**(2): p. 167-80.
23. Shakir, M.A. and E.A. Lundquist, *Analysis of Cell Migration in Caenorhabditis elegans.* Methods Mol Biol, 2005. **294**: p. 159-73.
24. Wong, M.C., M. Martynovsky, and J.E. Schwarzbauer, *Analysis of cell migration using Caenorhabditis elegans as a model system.* Methods Mol Biol, 2011. **769**: p. 233-47.
25. Lee, M. and E.J. Cram, *Quantitative analysis of distal tip cell migration in C. elegans.* Methods Mol Biol, 2009. **571**: p. 125-36.
26. Antebi, A., et al., *Cell and Growth Cone Migrations*, in *C. elegans II*, D.L. Riddle, et al., Editors. 1997: Cold Spring Harbor (NY).
27. Horvitz, H.R. and P.W. Sternberg, *Nematode postembryonic cell lineages.* J Nematol, 1982. **14**(2): p. 240-8.
28. Sulston, J.E., et al., *The embryonic cell lineage of the nematode Caenorhabditis elegans.* Dev Biol, 1983. **100**(1): p. 64-119.
29. Chai, Y., et al., *Live imaging of cellular dynamics during Caenorhabditis elegans postembryonic development.* Nat Protoc, 2012. **7**(12): p. 2090-102.
30. Hedgecock, E.M., et al., *Genetics of cell and axon migrations in Caenorhabditis elegans.* Development, 1987. **100**(3): p. 365-82.
31. Whangbo, J. and C. Kenyon, *A Wnt signaling system that specifies two patterns of cell migration in C. elegans.* Mol Cell, 1999. **4**(5): p. 851-8.
32. Harterink, M., et al., *Neuroblast migration along the anteroposterior axis of C. elegans is controlled by opposing gradients of Wnts and a secreted Frizzled-related protein.* Development, 2011. **138**(14): p. 2915-24.
33. Zinovyeva, A.Y., et al., *Complex network of Wnt signaling regulates neuronal migrations during Caenorhabditis elegans development.* Genetics, 2008. **179**(3): p. 1357-71.
34. Sundararajan, L. and E.A. Lundquist, *Transmembrane proteins UNC-40/DCC, PTP-3/LAR, and MIG-21 control anterior-posterior neuroblast migration with left-right functional asymmetry in Caenorhabditis elegans.* Genetics, 2012. **192**(4): p. 1373-88.
35. Honigberg, L. and C. Kenyon, *Establishment of left/right asymmetry in neuroblast migration by UNC-40/DCC, UNC-73/Trio and DPY-19 proteins in C. elegans.* Development, 2000. **127**(21): p. 4655-68.
36. Dyer, J.O., R.S. Demarco, and E.A. Lundquist, *Distinct roles of Rac GTPases and the UNC-73/Trio and PIX-1 Rac GTP exchange factors in neuroblast protrusion and migration in C. elegans.* Small GTPases, 2010. **1**(1): p. 44-61.
37. Ou, G. and R.D. Vale, *Molecular signatures of cell migration in C. elegans Q neuroblasts.* J Cell Biol, 2009. **185**(1): p. 77-85.
38. Shakir, M.A., J.S. Gill, and E.A. Lundquist, *Interactions of UNC-34 Enabled with Rac GTPases and the NIK kinase MIG-15 in Caenorhabditis elegans axon pathfinding and neuronal migration.* Genetics, 2006. **172**(2): p. 893-913.

39. Wong, M.C. and J.E. Schwarzbauer, *Gonad morphogenesis and distal tip cell migration in the hermaphrodite.* Wiley Interdiscip Rev Dev Biol, 2012. **1**(4): p. 519-531.
40. Lehmann, R., *Cell migration in invertebrates: clues from border and distal tip cells.* Curr Opin Genet Dev, 2001. **11**(4): p. 457-63.
41. Lucanic, M. and H.J. Cheng, *A RAC/CDC-42-independent GIT/PIX/PAK signaling pathway mediates cell migration in C. elegans.* PLoS Genet, 2008. **4**(11): p. e1000269.
42. Tannoury, H., et al., *CACN-1/Cactin interacts genetically with MIG-2 GTPase signaling to control distal tip cell migration in C. elegans.* Dev Biol, 2010. **341**(1): p. 176-85.
43. Cram, E.J., H. Shang, and J.E. Schwarzbauer, *A systematic RNA interference screen reveals a cell migration gene network in C. elegans.* J Cell Sci, 2006. **119**(Pt 23): p. 4811-8.
44. Thomas, J.H., M.J. Stern, and H.R. Horvitz, *Cell interactions coordinate the development of the C. elegans egg-laying system.* Cell, 1990. **62**(6): p. 1041-52.
45. Schafer, W.F., *Genetics of egg-laying in worms.* Annu Rev Genet, 2006. **40**: p. 487-509.
46. Trent, C., N. Tsuing, and H.R. Horvitz, *Egg-laying defective mutants of the nematode Caenorhabditis elegans.* Genetics, 1983. **104**(4): p. 619-47.
47. Stern, M.J. and H.R. Horvitz, *A normally attractive cell interaction is repulsive in two C. elegans mesodermal cell migration mutants.* Development, 1991. **113**(3): p. 797-803.
48. Branda, C.S. and M.J. Stern, *Mechanisms controlling sex myoblast migration in Caenorhabditis elegans hermaphrodites.* Dev Biol, 2000. **226**(1): p. 137-51.
49. Chen, E.B., C.S. Branda, and M.J. Stern, *Genetic enhancers of sem-5 define components of the gonad-independent guidance mechanism controlling sex myoblast migration in Caenorhabditis elegans hermaphrodites.* Dev Biol, 1997. **182**(1): p. 88-100.
50. Burdine, R.D., C.S. Branda, and M.J. Stern, *EGL-17(FGF) expression coordinates the attraction of the migrating sex myoblasts with vulval induction in C. elegans.* Development, 1998. **125**(6): p. 1083-93.
51. Lo, T.W., et al., *Caenorhabditis elegans fibroblast growth factor receptor signaling can occur independently of the multi-substrate adaptor FRS2.* Genetics, 2010. **185**(2): p. 537-47.
52. Sundaram, M., J. Yochem, and M. Han, *A Ras-mediated signal transduction pathway is involved in the control of sex myoblast migration in Caenorhabditis elegans.* Development, 1996. **122**(9): p. 2823-33.
53. DeVore, D.L., H.R. Horvitz, and M.J. Stern, *An FGF receptor signaling pathway is required for the normal cell migrations of the sex myoblasts in C. elegans hermaphrodites.* Cell, 1995. **83**(4): p. 611-20.
54. Ishii, N., et al., *UNC-6, a laminin-related protein, guides cell and pioneer axon migrations in C. elegans.* Neuron, 1992. **9**(5): p. 873-81.
55. Huang, X., et al., *UNC-71, a disintegrin and metalloprotease (ADAM) protein, regulates motor axon guidance and sex myoblast migration in C. elegans.* Development, 2003. **130**(14): p. 3147-61.
56. Schmidt, K.L., et al., *The cell migration molecule UNC-53/NAV2 is linked to the ARP2/3 complex by ABI-1.* Development, 2009. **136**(4): p. 563-74.
57. Hao, J.C., et al., *C. elegans slit acts in midline, dorsal-ventral, and anterior-posterior guidance via the SAX-3/Robo receptor.* Neuron, 2001. **32**(1): p. 25-38.

58. Alan, J.K. and E.A. Lundquist, *Analysis of Rho GTPase function in axon pathfinding using Caenorhabditis elegans.* Methods Mol Biol, 2012. **827**: p. 339-58.
59. Zipkin, I.D., R.M. Kindt, and C.J. Kenyon, *Role of a new Rho family member in cell migration and axon guidance in C. elegans.* Cell, 1997. **90**(5): p. 883-94.
60. Lundquist, E.A., *Rac proteins and the control of axon development.* Curr Opin Neurobiol, 2003. **13**(3): p. 384-90.
61. Lundquist, E.A., et al., *Three C. elegans Rac proteins and several alternative Rac regulators control axon guidance, cell migration and apoptotic cell phagocytosis.* Development, 2001. **128**(22): p. 4475-88.
62. Wu, Y.C., et al., *Distinct rac activation pathways control Caenorhabditis elegans cell migration and axon outgrowth.* Dev Biol, 2002. **250**(1): p. 145-55.
63. Demarco, R.S. and E.A. Lundquist, *"RACK"-ing up the effectors: Receptor for activated C kinase acts downstream of Rac GTPase signaling in growth cone outgrowth.* Small GTPases, 2011. **2**(1): p. 47-50.
64. Demarco, R.S. and E.A. Lundquist, *RACK-1 acts with Rac GTPase signaling and UNC-115/abLIM in Caenorhabditis elegans axon pathfinding and cell migration.* PLoS Genet, 2010. **6**(11): p. e1001215.
65. Shakir, M.A., et al., *The Arp2/3 activators WAVE and WASP have distinct genetic interactions with Rac GTPases in Caenorhabditis elegans axon guidance.* Genetics, 2008. **179**(4): p. 1957-71.
66. Quinn, C.C., D.S. Pfeil, and W.G. Wadsworth, *CED-10/Rac1 mediates axon guidance by regulating the asymmetric distribution of MIG-10/lamellipodin.* Curr Biol, 2008. **18**(11): p. 808-13.
67. deBakker, C.D., et al., *Phagocytosis of apoptotic cells is regulated by a UNC-73/TRIO-MIG-2/RhoG signaling module and armadillo repeats of CED-12/ELMO.* Curr Biol, 2004. **14**(24): p. 2208-16.
68. Baum, P.D. and G. Garriga, *Neuronal migrations and axon fasciculation are disrupted in ina-1 integrin mutants.* Neuron, 1997. **19**(1): p. 51-62.
69. Lints, R. and D.H. Hall, *Reproductive system, egglaying apparatus.* WormAtlas, 2009.
70. Cowan, A.E. and J.R. McIntosh, *Mapping the distribution of differentiation potential for intestine, muscle, and hypodermis during early development in Caenorhabditis elegans.* Cell, 1985. **41**(3): p. 923-32.
71. Edgar, L.G. and J.D. McGhee, *DNA synthesis and the control of embryonic gene expression in C. elegans.* Cell, 1988. **53**(4): p. 589-99.
72. Goldstein, B., *Induction of gut in Caenorhabditis elegans embryos.* Nature, 1992. **357**(6375): p. 255-7.
73. Bloom, L., *Genetic and molecular analysis of genes required for axon outgrowth in caenorhabditis elegans.* PhD dissertation to Massachusetts Institute of Technology, 1993.
74. Christensen, M., et al., *A primary culture system for functional analysis of C. elegans neurons and muscle cells.* Neuron, 2002. **33**(4): p. 503-14.
75. Strange, K., M. Christensen, and R. Morrison, *Primary culture of Caenorhabditis elegans developing embryo cells for electrophysiological, cell biological and molecular studies.* Nat Protoc, 2007. **2**(4): p. 1003-12.

76. Zhang, Y., et al., *Identification of genes expressed in C. elegans touch receptor neurons.* Nature, 2002. **418**(6895): p. 331-5.
77. Francis, M.M. and A.V. Maricq, *Electrophysiological analysis of neuronal and muscle function in C. elegans.* Methods Mol Biol, 2006. **351**: p. 175-92.
78. Von Stetina, S.E., et al., *Cell-specific microarray profiling experiments reveal a comprehensive picture of gene expression in the C. elegans nervous system.* Genome Biol, 2007. **8**(7): p. R135.
79. Fox, R.M., et al., *A gene expression fingerprint of C. elegans embryonic motor neurons.* BMC Genomics, 2005. **6**: p. 42.
80. Fox, R.M., et al., *The embryonic muscle transcriptome of Caenorhabditis elegans.* Genome Biol, 2007. **8**(9): p. R188.
81. Meissner, B., et al., *An integrated strategy to study muscle development and myofilament structure in Caenorhabditis elegans.* PLoS Genet, 2009. **5**(6): p. e1000537.
82. Caldwell, K.A., et al., *Investigating bacterial sources of toxicity as an environmental contributor to dopaminergic neurodegeneration.* PLoS One, 2009. **4**(10): p. e7227.
83. Sobkowiak, R. and A. Lesicki, *Genotoxicity of nicotine in cell culture of Caenorhabditis elegans evaluated by the comet assay.* Drug Chem Toxicol, 2009. **32**(3): p. 252-7.
84. Shih, J.D., et al., *The SID-1 double-stranded RNA transporter is not selective for dsRNA length.* RNA, 2009. **15**(3): p. 384-90.
85. Wilkins, C., et al., *RNA interference is an antiviral defence mechanism in Caenorhabditis elegans.* Nature, 2005. **436**(7053): p. 1044-7.
86. Zhou, K.M., et al., *PKA activation bypasses the requirement for UNC-31 in the docking of dense core vesicles from C. elegans neurons.* Neuron, 2007. **56**(4): p. 657-69.
87. Hirsh, D., D. Oppenheim, and M. Klass, *Development of the reproductive system of Caenorhabditis elegans.* Dev Biol, 1976. **49**(1): p. 200-19.
88. Sulston, J.E. and H.R. Horvitz, *Post-embryonic cell lineages of the nematode, Caenorhabditis elegans.* Dev Biol, 1977. **56**(1): p. 110-56.
89. Strange, K., *From genes to integrative physiology: ion channel and transporter biology in Caenorhabditis elegans.* Physiol Rev, 2003. **83**(2): p. 377-415.
90. Brockie, P.J., et al., *The C. elegans glutamate receptor subunit NMR-1 is required for slow NMDA-activated currents that regulate reversal frequency during locomotion.* Neuron, 2001. **31**(4): p. 617-30.
91. Nickell, W.T., et al., *Single ionic channels of two Caenorhabditis elegans chemosensory neurons in native membrane.* J Membr Biol, 2002. **189**(1): p. 55-66.
92. Richmond, J.E. and E.M. Jorgensen, *One GABA and two acetylcholine receptors function at the C. elegans neuromuscular junction.* Nat Neurosci, 1999. **2**(9): p. 791-7.
93. Teramoto, T. and K. Iwasaki, *Intestinal calcium waves coordinate a behavioral motor program in C. elegans.* Cell Calcium, 2006. **40**(3): p. 319-27.
94. Roy, P.J., et al., *Chromosomal clustering of muscle-expressed genes in Caenorhabditis elegans.* Nature, 2002. **418**(6901): p. 975-9.
95. Yang, Z., H.J. Edenberg, and R.L. Davis, *Isolation of mRNA from specific tissues of Drosophila by mRNA tagging.* Nucleic Acids Res, 2005. **33**(17): p. e148.
96. Page, A.P. and I.L. Johnstone, *The cuticle.* WormBook, 2007: p. 1-15.

97. Cox, G.N., M. Kusch, and R.S. Edgar, *Cuticle of Caenorhabditis elegans: its isolation and partial characterization.* J Cell Biol, 1981. **90**(1): p. 7-17.
98. Austin, J. and C. Kenyon, *Cell contact regulates neuroblast formation in the Caenorhabditis elegans lateral epidermis.* Development, 1994. **120**(2): p. 313-23.
99. Johnstone, I.L., *The cuticle of the nematode Caenorhabditis elegans: a complex collagen structure.* Bioessays, 1994. **16**(3): p. 171-8.
100. Cox, G.N., S. Staprans, and R.S. Edgar, *The cuticle of Caenorhabditis elegans. II. Stage-specific changes in ultrastructure and protein composition during postembryonic development.* Dev Biol, 1981. **86**(2): p. 456-70.
101. Papadopoulos, N.G., et al., *An improved fluorescence assay for the determination of lymphocyte-mediated cytotoxicity using flow cytometry.* J Immunol Methods, 1994. **177**(1-2): p. 101-11.
102. Szilagyi, M., et al., *Global Alterations in Gene Expression During Organophosphate Pesticide Intoxication and Recovery: Interim Report.* http://handle.dtic.mil/100.2/ADA469210, 2006.
103. Nass, R. and I. Hamza, *The Nematode C. elegans as an Animal Model to Explore Toxicology In Vivo: Solid and Axenic Growth Culture Conditions and Compound Exposure Parameters.* Curr Protocols in Toxicology, 2007: p. 1.9.1-1.9.18.
104. Honda, S. and H.F. Epstein, *Modulation of muscle gene expression in Caenorhabditis elegans: differential levels of transcripts, mRNAs, and polypeptides for thick filament proteins during nematode development.* Proc Natl Acad Sci U S A, 1990. **87**(3): p. 876-80.
105. Fire, A., et al., *Potent and specific genetic interference by double-stranded RNA in Caenorhabditis elegans.* Nature, 1998. **391**(6669): p. 806-11.
106. Maduro, M. and D. Pilgrim, *Identification and cloning of unc-119, a gene expressed in the Caenorhabditis elegans nervous system.* Genetics, 1995. **141**(3): p. 977-88.
107. Harfe, B.D., et al., *Analysis of a Caenorhabditis elegans Twist homolog identifies conserved and divergent aspects of mesodermal patterning.* Genes Dev, 1998. **12**(16): p. 2623-35.
108. Schachat, F., R.L. Garcea, and H.F. Epstein, *Myosins exist as homodimers of heavy chains: demonstration with specific antibody purified by nematode mutant myosin affinity chromatography.* Cell, 1978. **15**(2): p. 405-11.
109. Okkema, P.G., et al., *Sequence requirements for myosin gene expression and regulation in Caenorhabditis elegans.* Genetics, 1993. **135**(2): p. 385-404.
110. Ardizzi, J.P. and H.F. Epstein, *Immunochemical localization of myosin heavy chain isoforms and paramyosin in developmentally and structurally diverse muscle cell types of the nematode Caenorhabditis elegans.* J Cell Biol, 1987. **105**(6 Pt 1): p. 2763-70.
111. Miller, D.M., F.E. Stockdale, and J. Karn, *Immunological identification of the genes encoding the four myosin heavy chain isoforms of Caenorhabditis elegans.* Proc Natl Acad Sci U S A, 1986. **83**(8): p. 2305-9.
112. Miller, D.M., 3rd, et al., *Differential localization of two myosins within nematode thick filaments.* Cell, 1983. **34**(2): p. 477-90.
113. Altun, Z.F. and D.H. Hall, *Muscle system, somatic muscle.* WormAtlas, 2009.

114. Altun, Z.F. and D.H. Hall, *Nervous system, general description.* WormAtlas, 2009.
115. Durbin, R.M., *Studies on the Development and Organisation of the Nervous System of Caenorhabditis elegans.* PhD dissertation to the University of Cambridge, 1987.
116. Wang, J., R. Tokarz, and C. Savage-Dunn, *The expression of TGFbeta signal transducers in the hypodermis regulates body size in C. elegans.* Development, 2002. **129**(21): p. 4989-98.
117. Altun, Z.F. and D.H. Hall, *Introduction*, in *WormAtlas*, Z.F. Altun, et al., Editors. 2009.
118. Dixon, S.J. and P.J. Roy, *Muscle arm development in Caenorhabditis elegans.* Development, 2005. **132**(13): p. 3079-92.
119. Hedgecock, E.M. and J.G. White, *Polyploid tissues in the nematode Caenorhabditis elegans.* Dev Biol, 1985. **107**(1): p. 128-33.
120. Shemer, G. and B. Podbilewicz, *Fusomorphogenesis: cell fusion in organ formation.* Dev Dyn, 2000. **218**(1): p. 30-51.
121. Altun, Z.F. and D.H. Hall, *Epithelial system, seam cells.* WormAtlas, 2009.
122. Podbilewicz, B., *Cell fusion.* WormBook, 2006: p. 1-32.
123. Bianchi, L. and M. Driscoll, *Culture of embryonic C. elegans cells for electrophysiological and pharmacological analyses.* WormBook, 2006: p. 1-32.
124. Lin, S. and P. Talbot, *Methods for culturing mouse and human embryonic stem cells.* Methods Mol Biol, 2011. **690**: p. 31-56.
125. Moldaver, M.V. and Y.E. Yegorov, *Sparse plating increases the heterogeneity of proliferative potential of fibroblasts.* Mechanisms of Ageing and Development, 2009. **130**(5): p. 337-342.
126. Portela, V.M., G. Zamberlam, and C.A. Price, *Cell plating density alters the ratio of estrogenic to progestagenic enzyme gene expression in cultured granulosa cells.* Fertil Steril, 2010. **93**(6): p. 2050-5.
127. Pan, C., et al., *SNL fibroblast feeder layers support derivation and maintenance of human induced pluripotent stem cells.* J Genet Genomics, 2010. **37**(4): p. 241-8.
128. Merritt, C. and G. Seydoux, *Transgenic solutions for the germline.* WormBook, 2010: p. 1-21.
129. Prast, J., M. Gimona, and J.V. Small, *Immunofluorescence microscopy of the cytoskeleton: combination with green fluorescent protein tags.* In Cell Biology: A Laboratory Handbook (3rd ed.), JE Celis, ed. (Amsterdam; Boston: Elsevier Academic), 2006: p. pp. 557-61.
130. Ridley, A.J., et al., *Cell migration: integrating signals from front to back.* Science, 2003. **302**(5651): p. 1704-9.
131. Hall, A., *Rho GTPases and the actin cytoskeleton.* Science, 1998. **279**(5350): p. 509-14.
132. Chen, W., H.H. Lim, and L. Lim, *The CDC42 homologue from Caenorhabditis elegans. Complementation of yeast mutation.* J Biol Chem, 1993. **268**(18): p. 13280-5.
133. Paduch, M., F. Jelen, and J. Otlewski, *Structure of small G proteins and their regulators.* Acta Biochim Pol, 2001. **48**(4): p. 829-50.
134. Prior, I.A., P.D. Lewis, and C. Mattos, *A comprehensive survey of Ras mutations in cancer.* Cancer Res, 2012. **72**(10): p. 2457-67.

135. Kishore, R.S. and M.V. Sundaram, *ced-10 Rac and mig-2 function redundantly and act with unc-73 trio to control the orientation of vulval cell divisions and migrations in Caenorhabditis elegans.* Dev Biol, 2002. **241**(2): p. 339-48.
136. Chan, E. and J. Nance, *Mechanisms of CDC-42 activation during contact-induced cell polarization.* J Cell Sci, 2013. **126**(Pt 7): p. 1692-702.
137. Vartiainen, M.K. and L.M. Machesky, *The WASP-Arp2/3 pathway: genetic insights.* Curr Opin Cell Biol, 2004. **16**(2): p. 174-81.
138. Patel, F.B., et al., *The WAVE/SCAR complex promotes polarized cell movements and actin enrichment in epithelia during C. elegans embryogenesis.* Dev Biol, 2008. **324**(2): p. 297-309.
139. Roh-Johnson, M. and B. Goldstein, *In vivo roles for Arp2/3 in cortical actin organization during C. elegans gastrulation.* J Cell Sci, 2009. **122**(Pt 21): p. 3983-93.
140. Burkel, B.M., G. von Dassow, and W.M. Bement, *Versatile fluorescent probes for actin filaments based on the actin-binding domain of utrophin.* Cell Motil Cytoskeleton, 2007. **64**(11): p. 822-32.
141. Ji, L. and G. Danuser, *Tracking quasi-stationary flow of weak fluorescent signals by adaptive multi-frame correlation.* J Microsc, 2005. **220**(Pt 3): p. 150-67.
142. Gupta, B.P., W. Hanna-Rose, and P.W. Sternberg, *Morphogenesis of the vulva and the vulval-uterine connection.* WormBook, 2012: p. 1-20.
143. Asakura, T., et al., *Genes required for cellular UNC-6/netrin localization in Caenorhabditis elegans.* Genetics, 2010. **185**(2): p. 573-85.
144. Ziel, J.W. and D.R. Sherwood, *Roles for netrin signaling outside of axon guidance: a view from the worm.* Dev Dyn, 2010. **239**(5): p. 1296-305.
145. Levy-Strumpf, N. and J.G. Culotti, *VAB-8, UNC-73 and MIG-2 regulate axon polarity and cell migration functions of UNC-40 in C. elegans.* Nat Neurosci, 2007. **10**(2): p. 161-8.
146. Dalpe, G., et al., *Conversion of cell movement responses to Semaphorin-1 and Plexin-1 from attraction to repulsion by lowered levels of specific RAC GTPases in C. elegans.* Development, 2004. **131**(9): p. 2073-88.
147. Luo, L., *Rho GTPases in neuronal morphogenesis.* Nat Rev Neurosci, 2000. **1**(3): p. 173-80.
148. Brenner, S., *The genetics of Caenorhabditis elegans.* Genetics, 1974. **77**(1): p. 71-94.
149. Zhang, S. and J.R. Kuhn, *Cell isolation and culture.* WormBook, 2013: p. 1-39.
150. Harrison, R.G., et al., *Observations of the living developing nerve fiber.* The Anatomical Record, 1907. **1**(5): p. 116-128.
151. Wilson, H., *On some phenomena of coalescence and regeneration in sponges.* J. Exp. Zool., 1907. **5**(2): p. 245-258.
152. Klass, M.R. and D. Hirsh, *Sperm isolation and biochemical analysis of the major sperm protein from Caenorhabditis elegans.* Dev Biol, 1981. **84**(2): p. 299-312.
153. Laufer, J., P. Bazzicalupo, and W. Wood, *Segregation of Developmental Potential in Early Embryos of Caenorhabditis Elegans.* Cell, 1980. **19**(3): p. 569-577.
154. Laufer, J.S., *Cell Determination in Early Embryos of the Nematode Caenorhabditis elegans*, in *ProQuest Dissertations and Theses*1982, University of Colorado at Boulder: United States -- Colorado. p. 144 p.

155. Cowan, A.E. and J.R. McIntosh, *Mapping the distribution of differentiation potential for intestine, muscle, and hypodermis during early development in Caenorhabditis elegans.* Cell, 1985. **41**(3): p. 923-932.
156. Edgar, L.G. and J.D. McGhee, *DNA synthesis and the control of embryonic gene expression in C. elegans.* Cell, 1988. **53**(4): p. 589-599.
157. Bloom, L. and H.R. Horvitz, *Genetic and Molecular Analysis of Genes Required for Axon Outgrowth in Caenorhabditis elegans.* Ph.D. Thesis, 1993: p. 1-414.
158. Christensen, M. and K. Strange, *Developmental regulation of a novel outwardly rectifying mechanosensitive anion channel in Caenorhabditis elegans.* J Biol Chem, 2001. **276**(48): p. 45024-45030.
159. Christensen, M., et al., *A primary culture system for functional analysis of C. elegans neurons and muscle cells.* Neuron, 2002. **33**(4): p. 503-514.
160. Strange, K., M. Christensen, and R. Morrison, *Primary culture of Caenorhabditis elegans developing embryo cells for electrophysiological, cell biological and molecular studies.* Nat Protoc, 2007. **2**(4): p. 1003-1012.
161. Khan, F.R. and B.A. Mcfadden, *A Rapid Method of Synchronizing Developmental Stages of Caenorhabditis-Elegans.* Nematologica, 1980. **26**(2): p. 280-282.
162. Richmond, J.E. and E.M. Jorgensen, *One GABA and two acetylcholine receptors function at the C. elegans neuromuscular junction.* Nat Neurosci, 1999. **2**(9): p. 791-797.
163. Zhang, S., D. Banerjee, and J.R. Kuhn, *Isolation and Culture of Larval Cells from C. elegans.* PLoS ONE, 2011. **6**(4): p. e19505.
164. Clegg, E.D., et al. *Use of CeHR Axenic Medium for Exposure and Gene Expression Studies*. in *East Coast Worm Meeting*. 2002.
165. Nass, R. and I. Hamza, *The nematode C. elegans as an animal model to explore toxicology in vivo: solid and axenic growth culture conditions and compound exposure parameters.* Curr Protoc Toxicol, 2007. **Chapter 1**: p. Unit1.9.
166. Schlaeger, E.J., *Medium design for insect cell culture.* Cytotechnology, 1996. **20**(1): p. 57-70.
167. Choe, K.P. and K. Strange, *Genome-wide RNAi screen and in vivo protein aggregation reporters identify degradation of damaged proteins as an essential hypertonic stress response.* Am. J. Physiol., Cell Physiol., 2008. **295**(6): p. C1488-98.
168. Lamitina, S.T., et al., *Adaptation of the nematode Caenorhabditis elegans to extreme osmotic stress.* Am. J. Physiol., Cell Physiol., 2004. **286**(4): p. C785-91.
169. Edgar, L.G. and B. Goldstein, *Culture and manipulation of embryonic cells.* Methods Cell Biol, 2012. **107**: p. 151-175.
170. Kline, D., *Quantitative microinjection of mouse oocytes and eggs.* Methods Mol Biol, 2009. **518**: p. 135-156.
171. Lin, S. and P. Talbot, *Methods for culturing mouse and human embryonic stem cells.* Methods Mol Biol, 2011. **690**: p. 31-56.
172. Portela, V.M., G. Zamberlam, and C.A. Price, *Cell plating density alters the ratio of estrogenic to progestagenic enzyme gene expression in cultured granulosa cells.* Fertil. Steril., 2010. **93**(6): p. 2050-2055.
173. Moldaver, M.V. and Y.E. Yegorov, *Sparse plating increases the heterogeneity of proliferative potential of fibroblasts.* Mech. Ageing Dev., 2009. **130**(5): p. 337-342.

174. Spencer, W.C., et al., *A spatial and temporal map of C. elegans gene expression.* Genome Res, 2011. **21**(2): p. 325-341.
175. Von Stetina, S.E., et al., *Cell-specific microarray profiling experiments reveal a comprehensive picture of gene expression in the C. elegans nervous system.* Genome Biol, 2007. **8**(7): p. R135.
176. Fox, R.M., et al., *A gene expression fingerprint of C. elegans embryonic motor neurons.* BMC Genomics, 2005. **6**: p. 42.
177. Shim, Y.-H. and Y.-K. Paik, *Caenorhabditis elegans proteomics comes of age.* Proteomics, 2010. **10**(4): p. 846-857.
178. Husson, S.J., et al., *Comparative peptidomics of Caenorhabditis elegans versus C. briggsae by LC-MALDI-TOF MS.* Peptides, 2009. **30**(3): p. 449-457.
179. Kaji, H., et al., *Engineering systems for the generation of patterned co-cultures for controlling cell-cell interactions.* Biochim Biophys Acta, 2011. **1810**(3): p. 239-250.
180. Casbas-Hernandez, P., J.M. Fleming, and M.A. Troester, *Gene expression analysis of in vitro cocultures to study interactions between breast epithelium and stroma.* J. Biomed. Biotechnol., 2011. **2011**: p. 520987.
181. Fisher, J., et al., *Computational insights into Caenorhabditis elegans vulval development.* Proc Natl Acad Sci U S A, 2005. **102**(6): p. 1951-6.
182. Sternberg, P.W., *Vulval development.* WormBook, 2005: p. 1-28.
183. Quinn, C.C. and W.G. Wadsworth, *Axon guidance: asymmetric signaling orients polarized outgrowth.* Trends Cell Biol, 2008. **18**(12): p. 597-603.
184. Killeen, M.T. and S.S. Sybingco, *Netrin, Slit and Wnt receptors allow axons to choose the axis of migration.* Dev Biol, 2008. **323**(2): p. 143-151.
185. Hajduskova, M., et al., *Cell plasticity in Caenorhabditis elegans: from induced to natural cell reprogramming.* Genesis, 2012. **50**(1): p. 1-17.
186. Waters, K.A. and V. Reinke, *Extrinsic and intrinsic control of germ cell proliferation in Caenorhabditis elegans.* Mol Reprod Dev, 2011. **78**(3): p. 151-60.
187. Danuser, G. and C.M. Waterman-Storer, *Quantitative fluorescent speckle microscopy of cytoskeleton dynamics.* Annu Rev Biophys Biomol Struct, 2006. **35**: p. 361-387.
188. Axelrod, D., *Total internal reflection fluorescence microscopy in cell biology.* Traffic, 2001. **2**(11): p. 764-74.
189. Cox, G.N., S. Staprans, and R.S. Edgar, *The cuticle of Caenorhabditis elegans. II. Stage-specific changes in ultrastructure and protein composition during postembryonic development.* Dev Biol, 1981. **86**(2): p. 456-470.
190. Johnston, W.L. and J.W. Dennis, *The eggshell in the C. elegans oocyte-to-embryo transition.* Genesis, 2012. **50**(4): p. 333-349.
191. Hyenne, V., et al., *RAB-5 Controls the Cortical Organization and Dynamics of PAR Proteins to Maintain C. elegans Early Embryonic Polarity.* PLoS ONE, 2012. **7**(4): p. e35286.
192. Nemethova, M., S. Auinger, and J.V. Small, *Building the actin cytoskeleton: filopodia contribute to the construction of contractile bundles in the lamella.* J Cell Biol, 2008. **180**(6): p. 1233-1244.
193. Hu, K., et al., *Differential transmission of actin motion within focal adhesions.* Science, 2007. **315**(5808): p. 111-115.

194. Adams, M.C., et al., *Signal analysis of total internal reflection fluorescent speckle microscopy (TIR-FSM) and wide-field epi-fluorescence FSM of the actin cytoskeleton and focal adhesions in living cells.* J Microsc, 2004. **216**(Pt 2): p. 138-52.
195. Pasapera, A.M., et al., *Myosin II activity regulates vinculin recruitment to focal adhesions through FAK-mediated paxillin phosphorylation.* J Cell Biol, 2010. **188**(6): p. 877-890.
196. Lin, X.-G., et al., *UNC-31/CAPS docks and primes dense core vesicles in C. elegans neurons.* Biochem Biophys Res Commun, 2010. **397**(3): p. 526-531.
197. Rohrbach, A., *Observing secretory granules with a multiangle evanescent wave microscope.* Biophys J, 2000. **78**(5): p. 2641-2654.
198. Sund, S.E., J.A. Swanson, and D. Axelrod, *Cell membrane orientation visualized by polarized total internal reflection fluorescence.* Biophys J, 1999. **77**(4): p. 2266-2283.
199. Goodman, M.B., et al., *Active currents regulate sensitivity and dynamic range in C. elegans neurons.* Neuron, 1998. **20**(4): p. 763-772.
200. Bianchi, L. and M. Driscoll, *Culture of embryonic C. elegans cells for electrophysiological and pharmacological analyses.* WormBook, 2006: p. 1-15.
201. Sulston, J.E. and H.R. Horvitz, *Post-embryonic cell lineages of the nematode, Caenorhabditis elegans.* Dev Biol, 1977. **56**(1): p. 110-156.
202. White, J.G., et al., *The structure of the nervous system of the nematode Caenorhabditis elegans.* Philos Trans R Soc Lond B Biol Sci, 1986. **314**(1165): p. 1-340.
203. Varshney, L.R., et al., *Structural properties of the Caenorhabditis elegans neuronal network.* PLoS Comput Biol, 2011. **7**(2): p. e1001066.
204. Barker, K., *At The Bench: A Laboratory Navigator, Updated Edition*. 2004: Cold Spring Harbor Laboratory Press. 460.
205. Burkel, B.M., G. von Dassow, and W.M. Bement, *Versatile fluorescent probes for actin filaments based on the actin-binding domain of utrophin.* Cell Motil Cytoskeleton, 2007. **64**(11): p. 822-832.